COOPERATIVE SPECTRUM SENSING FOR COGNITIVE RADIO

A thesis submitted to the University of Manchester
for the degree of Doctor of Philosophy
in the Faculty of Engineering and Physical Sciences

2013

Warit Prawatmuang
School of Electrical and Electronic Engineering

Contents

Abstract **11**

Declaration **12**

Copyright Statement **13**

Acknowledgements **14**

Dedication **15**

List of Abbreviations **16**

List of Variables **17**

1 Introduction **19**

1.1 Wireless and Mobile Communications 19

1.2 Dynamic Spectrum Access and Cognitive Radio 20

1.3 Motivations 20

1.4 Lists of Contributions 21

1.5 Thesis Organization 22

1.6 List of Publications 23

2 Background Theory **25**

2.1 Wireless Communication Channel 25

2.2 Large-Scale Propagation 26

2.2.1 Path Loss 26

2.2.2 Shadowing 26

2.3 Small-Scale Propagation 27

2.3.1 Multipath Fading . . . 27
2.3.2 Doppler Shift . . . 27
2.4 Types of Small-Scale Fading . . . 28
2.4.1 Fading Effects due to Multipath Time Delay Spread . . . 28
2.4.2 Fading effects due to Doppler Spread . . . 29
2.5 Common Channel Models . . . 30
2.5.1 AWGN channel . . . 30
2.5.2 Rayleigh fading channel . . . 30
2.5.3 Rician fading channel . . . 31
2.5.4 Nakagami-m fading channel . . . 31
2.6 Quantization . . . 32
2.7 Time-Series Averaging Model . . . 33
2.7.1 Auto-Regressive Model . . . 33
2.7.2 Moving Average Model . . . 33
2.8 Statistical Distributions and Random Variables . . . 34
2.8.1 Gaussian Distribution . . . 34
2.8.2 Chi-Squared Distribution . . . 36
2.8.3 Non-Central Chi-Squared Distribution . . . 37
2.8.4 Summation of two Random Variables . . . 38
2.8.5 Central Limit Theorem . . . 39
2.9 Summary . . . 39

3 Cognitive Radio System **41**
3.1 Cognitive Radio Networks . . . 41
3.2 Cognitive Radio Architectures . . . 42
3.3 Cognitive Radio Characteristics . . . 43
3.3.1 Cognitive Capability . . . 43
3.3.2 Reconfigurability . . . 44
3.4 Spectrum Sharing . . . 45
3.5 Spectrum Sensing . . . 45
3.5.1 Transmitter Detection . . . 45
3.5.2 Cooperative Detection . . . 47

3.5.3 Interference-Based Detection . . . 47
3.6 IEEE 802.22 WRAN Standard . . . 48
3.7 Prior Works on Spectrum Sensing . . . 48
3.8 Summary . . . 50

4 Cooperative Spectrum Sensing 51
4.1 Energy Detection-Based Spectrum Sensing . . . 51
4.2 Related Mathematical Statistics . . . 52
4.2.1 Probability of False Alarm . . . 52
4.2.2 Probability of Detection . . . 53
4.2.3 Cumulative Density Function . . . 54
4.3 Statistical Approximation . . . 54
4.3.1 Probability of Detection . . . 55
4.3.2 Probability Density Function on H_1 . . . 56
4.4 Cooperative Spectrum Sensing . . . 57
4.4.1 Hard Decision Combining Rules . . . 57
4.4.2 Soft Decision Combining Rules . . . 58
4.5 Simulation Setup Scenario . . . 59
4.6 Summary . . . 60

5 EGC-SDC Cooperative Spectrum Sensing 61
5.1 Introduction . . . 61
5.2 EGC-SDC Sensing Procedures . . . 61
5.3 EGC-SDC Sensing Performance . . . 62
5.4 Analysis on EGC-SDC scheme . . . 63
5.4.1 EGC-SDC scheme under AWGN channel . . . 63
5.4.2 EGC-SDC scheme under Rayleigh fading channel . . . 64
5.4.3 EGC-SDC Analysis and Simulation Results . . . 65
5.5 Summary . . . 65

6 Quantized Cooperative Spectrum Sensing 68
6.1 Introduction . . . 68
6.2 Sensing Procedures . . . 69

6.3 Uniform Quantization 69
6.4 Non-uniform Quantization 70
6.5 Approximated Scheme 71
6.6 Simulation Results 72
6.7 Analysis on Quantized Cooperative Spectrum Sensing 74
6.8 Summary 76

7 Double Threshold Cooperative Spectrum Sensing 79
7.1 Introduction 79
7.2 Double Threshold Spectrum Sensing Procedures 80
7.2.1 Double Threshold Scheme 80
7.2.2 Double Threshold Scheme with Quantization 81
7.3 Double Threshold Analysis 82
7.3.1 Regions defined by Lower and Upper Threshold 82
7.3.2 Communication Overhead Requirement 83
7.3.3 Cooperative Probablility of False alarm and Detection 85
7.3.4 Bounds on Detection Performance 86
7.3.5 Q_f and Q_d for Two-User Double Threshold scheme 88
7.4 Simulation Results 93
7.4.1 Double Threshold Scheme 93
7.4.2 Double Threshold Scheme with Quantization 94
7.4.3 Simulation Results for Double Threshold Analysis 95
7.5 Summary 99

8 Sequential Cooperative Spectrum Sensing 100
8.1 Introduction 100
8.2 System Model 101
8.2.1 Time Varying Channel 101
8.2.2 Sensing Procedures 103
8.2.3 Primary User activity 103
8.3 Weighted SED 103
8.3.1 Sensing Procedures 104
8.3.2 Weight Vector for Static PU Activity 107

8.3.3 Weight Vector for Intermittent PU Activity 109
8.3.4 Simulation Results 109
8.4 Two-Stage SED 110
8.4.1 Two-Stage SED Sensing Procedures 110
8.5 Differential SED 111
8.6 SED Analysis 112
8.6.1 Primary User activity model 113
8.6.2 Weighted SED 114
8.6.3 Two-Stage SED 117
8.6.4 Two-Stage SED Approximation 122
8.6.5 Differential SED 122
8.7 Simulation Results 123
8.7.1 Weighted SED 124
8.7.2 Two-Stage SED 126
8.7.3 Differential SED 127
8.7.4 SNR requirement for IEEE 802.22 standard 128
8.7.5 Analysis for probability of false alarm and detection 129
8.8 Summary 130

9 Conclusions and Future Works **132**
9.1 Conclusions 132
9.2 Future Works 133

References **134**

Word count 37,378

List of Tables

3.1 Receiver Parameter for 802.22 WRAN 48

5.1 Comparison between system parameters used in Nakagami-m and EGC-SDC scheme 65

6.1 Quantization boundaries and quanta for Non-uniform scheme with 3-bit quantization 73

6.2 Quantization boundaries and quanta for Approximated scheme with 3-bit quantization 73

8.1 **S** : Set of PU's state 114

8.2 **D** : Set of CR's decision 117

8.3 **C** : Set of condition towards number of local observations in Differential SED 123

List of Figures

2.1 Types of Small-Scale Fading 28
2.2 Rayleigh and Rician Distribution 32
2.3 Autoregressive model 34
2.4 Moving Average model 35
2.5 Gaussian Distribution 36
2.6 Chi-Squared and Non-Central Chi-Squared Distribution 38

3.1 Cognitive Radio Concepts 42
3.2 Cognitive Cycle 44
3.3 Classification of spectrum sensing techniques 46

4.1 Probability density function of H_0 and H_1 52
4.2 Approximated and Exact Probability of Detection 56
4.3 Approximated and Exact Probability Density Function H_1 57
4.4 Simulation Setup Scenario 59

5.1 Detection Performance on EGC-SDC and OR-HDC scheme, SNR= 3dB 62
5.2 Detection Performance on EGC-SDC and OR-HDC scheme, SNR= 5dB 63
5.3 EGC-SDC Scheme : Probability of False Alarm and Detection with 3dB SNR 66
5.4 EGC-SDC Scheme : Probability of False Alarm and Detection with 5dB SNR 66

6.1 Detection performance for the proposed schemes with three-bit quantization 75
6.2 Detection performance for the proposed schemes with four-bit quantization 75

6.3 PMF for the quanta value at CR users when PU is active (H_1) 77
6.4 PMF for the quanta sum value at the fusion center when PU is active (H_1) 77
6.5 Quantized Cooperative Spectrum Sensing schemes: Probaility of false alarm and detection 78

7.1 Double Threshold Energy Detection Technique 80
7.2 Double Threshold Scheme : Three regions separated by λ_L and λ_U on H_0. 83
7.3 Double Threshold Scheme : Three regions separated by λ_L and λ_U on H_1. 84
7.4 Double Threshold Scheme : Frame structure for the forwarding process 84
7.5 Detection performance for Double Threshold Scheme with $\lambda_L = 7.841$ and $\lambda_U = 16.82$ 94
7.6 Detection performance for Double Threshold Scheme with $\lambda_L = 5.348$ and $\lambda_U = 16.82$ 95
7.7 Detection performance for Double Threshold Scheme with two and three bit quantization and $\lambda_L = 5.348$ and $\lambda_U = 16.82$ 96
7.8 Double Threshold Scheme : Probability of False Alarm $\lambda_L = 10$ and $\lambda_U = 15$. 96
7.9 Double Threshold Scheme : Probability of Detection $\lambda_L = 10$ and $\lambda_U = 15$. 97
7.10 Double Threshold Scheme : Probability of False Alarm $\lambda_L = 7$ and $\lambda_U = 17.5$. 98
7.11 Double Threshold Scheme : Probability of Detection $\lambda_L = 7$ and $\lambda_U = 17.5$. 98

8.1 Cooperative detection performance for energy detection for correlated and quasi-static channel 101
8.2 Real part of the channel gain in correlated channel with $f_d = 10$ Hz . . 102
8.3 Real part of the channel gain in correlated channel with $f_d = 50$ Hz . . 102
8.4 System model for correlated channel sensing framework 103
8.5 Two-state Markov chain on primary user's activity model 103

8.6 Energy distribution for weighted local observation with different number of previous observations taken 108
8.7 Detection performance for Weighted SED scheme with three previous observations on optimal H_0 and optimal H_1 weighting vector, when PU is static 125
8.8 Detection performance for Weighted SED scheme with static and intermittent PU activity in 50 Hz correlated channel 126
8.9 Detection performance for the Two-Stage SED scheme in 50 Hz correlated channel case 127
8.10 Detection performance for the Differential SED scheme in 50 Hz correlated channel case 128
8.11 Minimum required SNR for target probability of detection and false alarm 129
8.12 Probability of false alarm and detection in Weighted SED scheme . . . 130
8.13 Probability of false alarm and detection in Two-Stage SED scheme . . . 131

The University of Manchester

Warit Prawatmuang
Doctor of Philosophy
Cooperative Spectrum Sensing for Cognitive Radio
September 2, 2013

Cognitive Radio (CR) aims to access the wireless spectrum in an opportunistic manner while the licensed user is not using it. To accurately determine the licensed user's existence, spectrum sensing procedure is vital to CR system. Energy detection-based spectrum sensing techniques is favourable due to its simplicity and low complexity. In addition, to improve the detection performance, cooperative spectrum sensing technique exploits multi-user diversity and mitigates detection uncertainty. In this thesis, we investigate several energy detection based cooperative spectrum sensing techniques.

First, the closed-form analysis for the Equal Gain Combining based Soft Decision Combining (EGC-SDC) scheme, in which all CR users forward its observation to the fusion center, is derived. In order to reduce the communication overhead between CR users and the fusion center, we proposed quantized cooperative spectrum sensing technique, in which CR users quantize its local observation before forwarding to the fusion center. Next, the Double Threshold scheme, where some users only forward its local decision while other users forward its observation, is considered and analyzed. To further reduce the communication overhead, we also proposed that quantization is applied to the users who forward its observation. Later on, three sequential cooperative spectrum sensing schemes in time-varying channel are considered. By aggregating past local observations from previous sensing slots, CR users can improve the detection performance. The Weighted Sequential Energy Detector (SED) scheme simply takes fixed number of past local observations, while the other two schemes, Two-Stage SED and Differential SED, adaptively determine the number of observations, based on its decision towards primary user's existence.

Simulation results show that the analysis on EGC-SDC scheme is accurate and the quantized cooperative spectrum sensing technique can improve the performance and approach the detection performance of EGC-SDC scheme with much less bandwidth requirement. Also, the Double Threshold scheme can help improve the detection performance over the conventional technique. Furthermore, the analysis on Double Threshold provides a closed-form for the probability of false alarm and detection. Additionally, the sequential spectrum sensing schemes are shown to improve the detection performance and enable CR system to work in scenarios that the conventional technique can not accommodate.

Declaration

No portion of the work referred to in the thesis has been submitted in support of an application for another degree or qualification of this or any other university or other institute of learning.

Copyright Statement

i. The author of this thesis (including any appendices and/or schedules to this thesis) owns certain copyright or related rights in it (the "Copyright") and s/he has given The University of Manchester certain rights to use such Copyright, including for administrative purposes.

ii. Copies of this thesis, either in full or in extracts and whether in hard or electronic copy, may be made **only** in accordance with the Copyright, Designs and Patents Act 1988 (as amended) and regulations issued under it or, where appropriate, in accordance with licensing agreements which the University has from time to time. This page must form part of any such copies made.

iii. The ownership of certain Copyright, patents, designs, trade marks and other intellectual property (the "Intellectual Property") and any reproductions of copyright works in the thesis, for example graphs and tables ("Reproductions"), which may be described in this thesis, may not be owned by the author and may be owned by third parties. Such Intellectual Property and Reproductions cannot and must not be made available for use without the prior written permission of the owner(s) of the relevant Intellectual Property and/or Reproductions.

iv. Further information on the conditions under which disclosure, publication and commercialisation of this thesis, the Copyright and any Intellectual Property and/or Reproductions described in it may take place is available in the University IP Policy (see http://documents.manchester.ac.uk/DocuInfo.aspx?DocID=487), in any relevant Thesis restriction declarations deposited in the University Library, The University Library's regulations (see http://www.manchester.ac.uk/library/aboutus/regulations) and in The University's Policy on Presentation of Theses.

Acknowledgements

I would like to thank my supervisor Dr. Daniel K. C. So for his guidance, advices and encouragement over the years. I would also like to thank all academics and colleagues within the research group.

Finally, I wholeheartedly thank my parents, my sister and my lovely family for their encouragement, understanding and support.

Dedication

To my parents, my sister, my lovely family and my teachers.

List of Abbreviations

AMPS	Advanced mobile phone system
CCDF	Complementary cumulative distribution function
CDF	Cumulative density function
CR	Cognitive radio
EGC-SDC	Equal gain combining based SDC
HDC	Hard decision combining
i.i.d.	Independent and identically distributed
ISI	Intersymbol interference
LTE-A	Long term evolution-advanced
MSE	Mean-squared error
OFDMA	Orthogonal frequency division multiple access
OR-HDC	OR-rule based HDC
PDF	Probability density function
PU	Primary user
ROC	Receiver operating characteristic
RV	Random variable
SDC	Soft decision combining
SED	Sequential energy detection
SNR	Signal-to-noise ratio
WCDMA	Wideband code division multiple access
WRAN	Wireless regional area network

List of Variables

$1F_1(\cdot;\cdot;\cdot)$	Confluent hypergeometric function
α	PU activity factor when changing from active to idle
β	PU activity factor when changing from idle to active
B_c	Coherence bandwidth
B_D	Doppler spread
B_i	Quantization boundaries
B_s	Bandwidth of the signal
d	CR's local decision
$\mathbf{D}$	Set of CR's decision
D_i	CR's forwarded decision (Double Threshold)
η	Path loss exponent
f_d	Doppler frequency
f_s	Sampling frequency
g	Nakagami parameter
G_r	Antenna gain for the receiver
G_t	Antenna gain for the transmitter
γ	Instantaneous SNR
$\bar{\gamma}$	Average SNR
h	Channel gain
H_0	Hypothesis that PU is idle
H_1	Hypothesis that PU is active
$I_0(\cdot)$	Modified Bessel function of the first kind and zero-order
k	Degree of freedom
L_0	Path loss at a reference distance d_0
$L_n(\cdot)$	Laguerre polynomial of degree n

λ	Wavelength
λ_f	Fusion decision threshold
λ_L	Lower threshold (Double Threshold)
λ_U	Upper threshold (Double Threshold)
λ_{nc}	Noncentrality parameter (Non-Central Chi-Squared distribution)
m	time-bandwidth product
M	Number of quantization regions
μ	Mean of a Gaussian Distribution
$\mathcal{N}$	Gaussian Distribution
P_d	Probability of detection
P_f	Probability of false alarm
P_t	Transmit power
Q_α	α^{th} quantization region
q_α	α^{th} quanta value
Q_d	Cooperative probability of detection
Q_f	Cooperative probability of false alarm
$Q_m(\cdot,\cdot)$	Marcum-Q function
s	PU's signal
$\mathbf{S}$	Set of PU's state
$\mathbf{S_{active}}$	Subset of $\mathbf{S}$ where PU is active
$\mathbf{S_{idle}}$	Subset of $\mathbf{S}$ where PU is idle
σ^2	Variance of a Gaussian Distribution
σ_T	RMS delay spread of the channel
T_s	Symbol period
T_c	Coherence time
v	Speed of movement
$\mathbf{W}$	Weighting vector
x	Distance between transmitter and receiver
y	Received signal
$\mathbf{Y}$	Received signal vector

Chapter 1

Introduction

1.1 Wireless and Mobile Communications

Over the years from the beginning of wireless communications, many aspects of the personal mobile phone and wireless communications have changed and evolved in order to cope with ever-increasing high demands and popularity. These aspects are such as the move from analog to digital communications, from voice-centric to data-centric systems [1]. Especially in recent decades, there has been rapid growing need for the anytime, anywhere and always-connected communication [2]. With the number of mobile subscribers grows exponentially from less than a hundred million subscribers in 1996 to more than five billions in 2010 [3], wireless networks have evolved over the year since the first generation Advanced mobile phone system (AMPS) to the current fourth generation Long Term Evolution (LTE) [4]. For each generation of wireless and mobile communications, many technologies have been improved and enabled higher data rates, better spectral efficiency. The move from analog to digital communication occurs in the transition from first generation (1G) to second generation (2G). With spread spectrum technologies, Wideband Code Division Multiple Access (WCDMA) becomes dominant in the third generation (3G) mobile communication. With Orthogonal Frequency Division Multiple Access (OFDMA), current 4G system supports higher data rates and better spectral efficiency over existing 3G system.

In order to further cope with an increasing demand, a new paradigm and technologies that can enhance spectral efficiency and improve spectrum utilization are needed

for the next generation beyond 4G mobile networks. The concept for the fifth generation (5G) are highlighted in [5] such that the 5G terminals will be equipped with various technologies, able to combine different technologies and adapt itself to the environment. Cognitive Radio (CR) is proposed and designed to tackle these challenges [6] and it is one of the enabling technologies and solutions for the future 5G mobile networks.

1.2 Dynamic Spectrum Access and Cognitive Radio

Currently, spectrum assignment policy is fixed in terms of frequency band. As a result, the spectrum usage is limited to a certain part of the frequency spectrum. With the high and increasing demand of mobile services and current studies mentioning that the rest of the spectrum remains under-utilized [7], dynamically accessing the spectrum can help improve the spectrum utilization. CR is proposed and designed to sense and learn from the environment in order to perform the best services to users [8]. By opportunistically accessing the licensed spectrum without interfering the licensed user, CR can improve the efficiency of spectrum usage [9]. Further details on CR will be summarized in Chapter 3.

1.3 Motivations

CR aims to improve spectrum utilization and efficiency of spectrum usage by opportunistically accessing the licensed spectrum without interfering the licensed users [9]. To avoid using the spectrum at the same time with the licensed users, CR has to determine the existence of primary user (PU) by sensing the wireless spectrum. It can communicate to its receiver if the spectrum is vacant. However, when PUs retransmit again, CR users should stop their transmission immediately to avoid creating interference to the PUs. Hence, spectrum sensing is vital for CR. The better CR knows about the PU's existence, the better it can communicate and utilize the spectrum. There are several types of spectrum sensing techniques for CR such as Energy Detection,

Matched-Filtered Detection, Cyclostationary Detection [10]. In this thesis, we investigate several energy detection based spectrum sensing techniques due to its simplicity, low computational and implementation costs as well as its wider applicability as it works irrespective of the signal format to be detected [11]. With the aim of improving the detection performance, we have proposed several new techniques in this thesis.

1.4 Lists of Contributions

In this thesis, several energy detection based cooperative spectrum sensing techniques have been investigated. The performance of these schemes have been improved over existing schemes, not only on the detection performance aspects but also on the communication overhead among the CR system. The main contributions of this thesis are summarized as follows.

1. The approximation of statistical distribution related to the energy detection based spectrum sensing as well as the approximated inverse probability of detection under Rayleigh fading channel is proposed.

2. The closed-form analysis for Equal gain combining based SDC (EGC-SDC) Cooperative spectrum sensing is derived, under both AWGN and Rayleigh fading channels.

3. The quantization-based cooperative spectrum sensing is studied. Various quantization techniques are applied to the CR's observation before forwarding to the fusion center. The simulation results show that these schemes provide comparable detection performance to EGC-SDC, while requiring less communication bandwidth.

4. The Double Threshold energy detection scheme is evaluated and analysed. To improve the performance in terms of communication overhead, quantization is applied towards the Double Threshold scheme. Simulation results show that the Double Threshold scheme provides better detection performance as compared to the conventional scheme. Moreover, the analysis on the detection performance is provided.

5. Sequential cooperative spectrum sensing is investigated. The PU activity is considered as static and intermittent and the communication channel is modelled as time-varying one. First, a Weighted SED, which is a fixed scheme, is studied. Then, two adaptive schemes, namely Two-Stage SED and Differential SED, are investigated to further improve the detection performance. Simulation results show that the adaptive schemes provide better performance than the Weighted SED scheme. In addition, the related probabilities are derived and the closed-form analysis for the probability of false alarm and detection probability for Weighted SED and Two-Stage SED scheme is provided.

1.5 Thesis Organization

This thesis consists of nine chapters. Introduction, motivation and description of technical contributions in the thesis are presented in the first chapter.

In Chapter 2, background theories on wireless communications and its characteristics are presented. Both large-scale and small-scale propagation are discussed along with common channel models. Backgrounds of quantization, averaging models and random variables are also presented.

Then, fundamentals of CR are presented in Chapter 3. This chapter covers the CR architecture as well as background on spectrum sensing techniques. The brief introduction on IEEE 802.22 WRAN standard is also presented. An overview on energy detection based spectrum sensing technique is presented in Chapter 4. The same chapter also presents the statistics related to energy detection as well as its approximation. Cooperative spectrum sensing is also presented.

In Chapter 5, a soft decision combining rule based spectrum sensing technique, namely the EGC-SDC scheme, is discussed. Its detection performance as well as the closed-form analysis is presented.

The cooperative spectrum sensing scheme with quantization is discussed in Chapter 6. In order to reduce the communication overhead among cognitive radio system, while retaining good detection performance, quantization is applied towards conventional EGC-SDC scheme. Various quantization techniques are considered here. Simulation results as well as the analysis on the detection performance are presented.

In Chapter 7, the Double Threshold spectrum sensing scheme is discussed. First the simple Double Threshold scheme is presented. Then, quantization is applied towards this technique. Simulation results on the detection performance for these techniques are shown. Finally, the closed-form analysis on its detection performance is presented.

Next, our previously proposed sequential cooperative spectrum sensing techniques are presented in Chapter 8. First, the Weighted SED scheme which takes fixed number of past observations is presented. Then, Two-Stage and Differential SED schemes which adaptively determine the number of past observations are shown. The mathematical analysis on probability of false alarm and detection for the Weighted and Two-Stage SED is presented.

Finally, conclusions are drawn and possible future works are outlined in Chapter 9.

1.6 List of Publications

Relevant Journal Publications

1. Warit Prawatmuang, Daniel K.C. So and Emad Alsusa, Sequential Cooperative Spectrum Sensing Technique in Time Varying Channel, *IEEE Transactions on Wireless Communications*. (Under submission)

Relevant Conference Publications

1. Warit Prawatmuang and Daniel K.C. So, Sequential cooperative spectrum sensing technique for cognitive radio system in correlated channel, in *IEEE Vehicular Technology Conference (VTC Spring)*, 2012.

2. Warit Prawatmuang and Daniel. K.C. So, Adaptive sequential cooperative spectrum sensing technique in time varying channel, in *IEEE 23rd International Symposium on Personal Indoor and Mobile Radio Communications (PIMRC)*, 2012.

3. Warit Prawatmuang and Daniel K.C. So, Quantized Cooperative Spectrum Sensing for Cognitive Radio, *IEEE 24th International Symposium on Personal Indoor and Mobile Radio Communications (PIMRC)*, 2013. (Accepted for publication)

Relevant Conference Presentations

1. Warit Prawatmuang and Daniel. K.C. So, Sequential cooperative spectrum sensing technique for cognitive radio system in correlated channel, in *EEE PGR Conference, The University of Manchester, UK.*, 2011.

Other Publications

1. Antonis Phasouliotis, Daniel K.C. So and Warit Prawatmuang, Energy-efficient user grouping algorithms for power minimisation in multi-carrier code division multiple access systems, *IET Communications*, 2011.

2. Imran Rashid, Warit Prawatmuang and Daniel K.C. So, Energy Efficient Parallel HARQ Schemes for MIMO Relay Systems, *IEEE Transactions on Communications*. (In preparation)

3. Edwin Mugume, Warit Prawatmuang and Daniel K.C. So, Cooperative Spectrum Sensing for Green Cognitive Femtocell Network, *IEEE 24th International Symposium on Personal Indoor and Mobile Radio Communications (PIMRC)*, 2013. (Accepted for publication)

Chapter 2

Background Theory

In this chapter, relevant background theory of wireless communications is presented. First, wireless communication channel modellings, both large-scale and small-scale propagations are described. Quantization and time-series averaging models are presented in Section 2.6 and 2.7 respectively. Then, statistical distributions and random variables are discussed in Section 2.8.

2.1 Wireless Communication Channel

Wireless communication operates through the media which is the air interface. The transmitted signal will travel along the transmission path from the transmitter to the receiver. This path can be obstructed not only by objects in the line-of-sight between them, but also objects that cause changes in the electromagnetic field at the receiver [12]. As a result, the received signal will degrade and become different to the transmitted signal. As the wireless channels are random, the wireless channel modelling is typically done in a statistical way [13].

Wireless channel modelling is classified upon the variation in the channel. The variation due to path Loss and shadowing occurring over relatively large distances is referred as the *large-scale propagation*. On the contrary, the variation due to rapid fluctuations and fading over a short distance or time is referred as the *small-scale propagation* [14].

2.2 Large-Scale Propagation

Large-scale propagation can be classified into two models; path loss and shadowing. These models are used to predict the average received signal strength at large transmitter-receiver distance [13].

2.2.1 Path Loss

Path loss is used to model the attenuation of the signal which travels from the transmitter to the receiver. The further the signal travels, the more attenuation it experiences. Hence, path loss increases exponentially with the increasing distance.

The propagation model for path loss at the distance x is given as

$$\frac{P_r}{P_t} = \frac{L_0}{x^\eta} \tag{2.1}$$

where η is path loss exponent which is different and dependent on the propagation environment, for instance, it is 2 for free-space propagation and 4 to 6 under shadowed urban cellular radio. P_r and P_t are respectively the received and transmitted power. L_0 is the path loss at a reference distance d_0, which is given as [13]

$$L_0 = \frac{(4\pi d_0)^2}{\lambda^2 G_t G_r} \tag{2.2}$$

$$L_0(dB) = 10\log_{10}\left(\frac{(4\pi d_0)^2}{\lambda^2 G_t G_r}\right) \tag{2.3}$$

where λ is the wavelength, G_t and G_r are the antenna gains for the transmitter and receiver respectively.

2.2.2 Shadowing

Shadowing is an effect of the variation in terrain and presence of obstacles. This affects the received power at different locations with a fixed distance x and is modelled as log-normal distribution. The effect of shadowing can be expressed as [15]

$$L\ (dB) = L_0(dB) + 10\eta\log_{10}\left(\frac{x}{d_0}\right) + X_\sigma \tag{2.4}$$

where the summation for first two terms (L_0 and the $\log_{10}$ terms) are the path loss at distance d and X_σ, which is a zero-mean Gaussian distributed random variable in log-scale, represents log-normal shadowing effect.

2.3 Small-Scale Propagation

Small-scale propagation is to characterize rapid fluctuations over short distance or time. There are various factors which influence small-scale fading such as multipath propagation, speed of the mobile, speed of surrounding objects, and the transmission bandwidth of the signal.

2.3.1 Multipath Fading

Multipath fading occurs when signal arrives at the receiver through different paths, as a result of reflection, diffraction or scattering. This creates many replicas of the transmitted signal as each path can arrive with different gains, phases and delays. Mathematically, the multipath channel with N number of multipath components can be modelled as [13]

$$h(t,\tau) = \sum_{i=0}^{N-1} a_i(t,\tau) \exp\left[j\theta_i(t,\tau)\right] \delta(\tau - \tau_i(t)) \tag{2.5}$$

where $h(t,\tau)$ is tap-filter representing multipath channel, $a_i(t,\tau), \theta_i(t,\tau), \tau_i(t)$ is gain, phase and path excess delay respectively. There are two time-related variables in this equation as t is time variation due to motion and τ is time variation due to multipath delay.

2.3.2 Doppler Shift

Doppler shift is the shift in the received signal frequency due to the relative motion of transmitter and receiver. This shift can influence small-scale fading and it depends on the velocity and direction of motion of the mobile. The Doppler shift f_d can be expressed as

$$f_d = \frac{v}{\lambda} \cos\psi \tag{2.6}$$

where v, λ, ψ is the speed of movement, the wavelength and the angle between the direction of motion and the wave's arrival path.

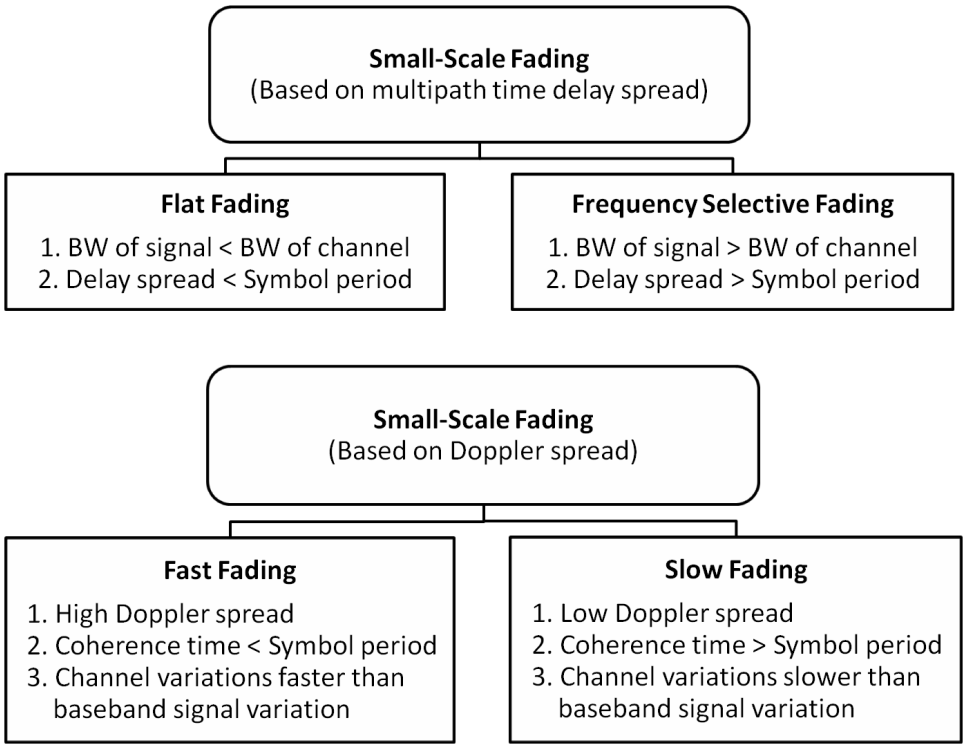

Figure 2.1: Types of Small-Scale Fading

2.4 Types of Small-Scale Fading

There are two types of small-scale fading. One is based on multipath time delay spread, while the other is based on Doppler spread. However, these two types of fading are not mutually exclusive. Fig. 2.1 summarizes small-scale fading based on multipath time delay spread and Doppler spread [13].

2.4.1 Fading Effects due to Multipath Time Delay Spread

Signals can experience either flat fading and frequency selective fading, depending on the Multipath time delay spread.

Flat Fading

Signal undergoes flat fading when coherence bandwidth, over which the mobile radio channel has a constant gain and linear phase response, is greater than the bandwidth of the signal, and the delay spread is smaller than the symbol period.

Flat fading can be summarized as

$$B_s << B_C \tag{2.7}$$

and

$$T_S >> \sigma_T \tag{2.8}$$

where B_s, B_c, T_S, σ_T is respectively the bandwidth of the signal, the coherence bandwidth, symbol period and the rms delay spread of the channel.

Frequency Selective Fading

Signals undergo frequency selective fading when coherence bandwidth is smaller than the bandwidth of the signal and the delay spread is greater than the symbol period. In this case, the received signal is distorted because of multiple waveforms and channel induces intersymbol interference (ISI) to the signal.

Frequency selective fading can be summarized as

$$B_s > B_C \tag{2.9}$$

and

$$T_S < \sigma_T. \tag{2.10}$$

2.4.2 Fading effects due to Doppler Spread

This type of fading is subject to the change of the channel due to motion. Channel can be classified as fast fading or slow fading based on the symbol duration and the change of channel.

Fast Fading

In fast fading, the channel impulse response changes rapidly within the symbol duration. In other words, coherence time, which is time duration that the fading parameters remain fairly constant, is smaller than the symbol period. Fast fading is also called *time selective fading.*

Fast fading can be summarized as

$$T_S > T_C \tag{2.11}$$

and

$$B_s > B_D \tag{2.12}$$

where T_C, B_D is the coherence time and the measure of spectral broadening caused by the time variation of the channel. B_D is defined as the range of frequencies where the received Doppler spectrum is non-zero.

Slow Fading

In slow fading, the channel impulse response changes much slower than the transmitted baseband signal. In other words, coherence time is greater than the symbol period. The channel can be assumed to be static over one or several bandwidth intervals.

Slow fading can be summarized as

$$T_S << T_C \tag{2.13}$$

and

$$B_s >> B_D. \tag{2.14}$$

2.5 Common Channel Models

In this section, four common channel models are presented; AWGN channel, Rayleigh, Rician and Nakagami-m fading channel.

2.5.1 AWGN channel

The additive white Gaussian noise (AWGN) channel model is an ideal channel model as it merely adds the white Gaussian noise linearly into the signal. Being the non-fading channel model, the phenomenon of fading is not taken into account for this channel type, where the channel gain is always 1.

2.5.2 Rayleigh fading channel

Rayleigh fading channel model is normally used to describe the time-varying nature of the received envelope of a flat fading channel. This model is based on assumptions

that there are infinite arrival paths at the same time at all angles, all paths have zero mean and similar variance, which means there is no dominant path and all path gains are statistically independent. By taking central limit theorem, I (In-phase) and Q (Quadrature) components of the Rayleigh fading channel are Gaussian distributed.

In Rayleigh fading channel, the instantaneous SNR follows the probability density function (PDF) given by

$$f_\gamma(\gamma) = \begin{cases} \frac{1}{\bar{\gamma}} \exp\left(-\frac{\gamma}{\bar{\gamma}}\right) & , \gamma \geq 0 \\ 0 & , \text{otherwise} \end{cases} \tag{2.15}$$

where γ and $\bar{\gamma}$ is respectively the instantaneous and average SNR [16].

2.5.3 Rician fading channel

Rician fading channel is used to model propagation paths between the transmitter and the receiver, when there is a dominant line-of-sight path and many weaker multipaths. Channel fading statistics in this case is Rician distributed as follows [17]

$$f_\gamma(\gamma) = \begin{cases} \frac{\gamma}{\sigma^2} \exp\left(-\frac{(\gamma^2 + A^2)}{2\sigma^2}\right) I_0\left(\frac{A\gamma}{\sigma^2}\right) & , A \geq 0, \gamma \geq 0 \\ 0 & , \text{otherwise} \end{cases} \tag{2.16}$$

where A denotes the peak amplitude of the dominant signal and $I_0(\cdot)$ is the modified Bessel function of the first kind and zero-order.

The Rician distribution is also described in terms of a parameter K, which is the ratio between the deterministic signal power and the variance of the multipath.

$$K = \frac{A^2}{2\sigma^2}$$
$$K(dB) = 10 \log_{10} \frac{A^2}{2\sigma^2} \text{ dB}. \tag{2.17}$$

The Rayleigh distribution is a special case for Rician distribution where K approaches 0 or $-\infty$ dB. Fig. 2.2 shows the distribution for Rayleigh and Rician fading channel.

2.5.4 Nakagami-m fading channel

In Nakagami-m fading channel, the instantaneous SNR follows the PDF given by

$$f_\gamma(\gamma) = \frac{m^m \gamma^{m-1}}{\bar{\gamma}^m \Gamma(m)} \exp\left(-\frac{m\gamma}{\bar{\gamma}}\right), \quad \gamma \geq 0 \tag{2.18}$$

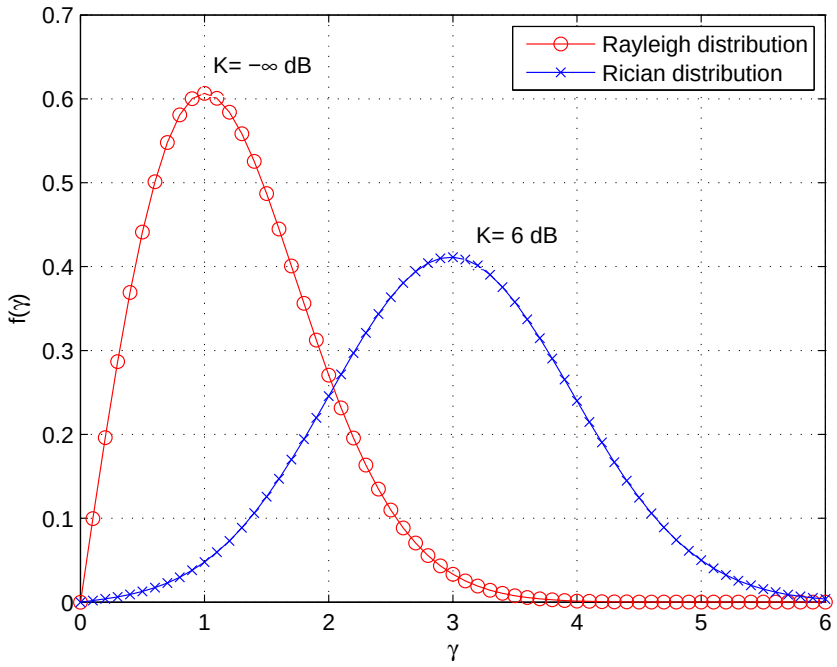

Figure 2.2: Rayleigh and Rician Distribution

where m is the Nakagami-m parameter [18].

Rayleigh fading channel is a special case for Nakagami-m fading channel where m equals to 1. Also, in the limit where $m \to +\infty$, Nakagami-m fading channel converges to an AWGN channel [16].

2.6 Quantization

Quantization is the process to represent a range of values using one quantum value. As a result, an information is split into various regions, each of which is represented by its corresponding quantum value. Its resolution or number of quantization regions is defined by the number of quantization bits. If n-bit quantization is applied, this can represent 2^n quantization regions.

Quantization can be classified into two groups: uniform and non-uniform quantization. In uniform quantization, each quantization region is equally spaced and has the same width, whereas the width is different for the non-uniform one. The overall distortion for a quantizer can be measured using the Mean-Squared Error (MSE),

given in [19] as

$$\text{MSE} = \int_{Q_\alpha} (y - q_\alpha)^2 \, p(y) \, dy \tag{2.19}$$

where Q_α represents each quantization region, q_α is the quanta for the α region, y is input to the quantizer and $p(y)$ is the PDF of the random variable $\mathbf{Y}$.

By optimizing the quantizer characteristic and its associated quantization regions, MSE can be minimized [19, 20]. The uniform quantization is optimal only for the uniformly distributed random variable, while the non-uniform quantization is optimal for the rest [21].

2.7 Time-Series Averaging Model

The averaging model is mainly used in time series to smoothen the data and remove short-term fluctuations. This can be applied in CR spectrum sensing techniques such that short-term fluctutations such as noise can be removed. There are two types of averaging model; the autoregressive and moving average model.

2.7.1 Auto-Regressive Model

The autoregressive model can be written mathematically as [22]

$$y[n] = x[n] - \sum_{k=1}^{N} a[k] \cdot y[n-k]. \tag{2.20}$$

This model is similar to the IIR filter, which takes the previous output into the summation for the current one. The diagram for autoregressive model is shown in Fig. 2.3. In terms of sensing and sequential detection, Auto-Regressive model was utilized in [22, 23].

2.7.2 Moving Average Model

The moving average model can be written mathematically as

$$y[n] = \sum_{k=0}^{N} b[k] \cdot x[n-k]. \tag{2.21}$$

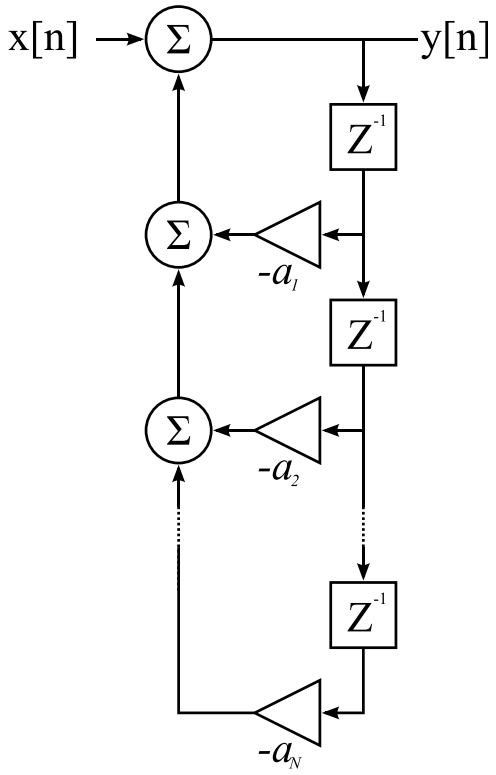

Figure 2.3: Autoregressive model

This model is similar to the FIR filter, which takes the previous input into the summation for the current output. The output comes from the summation of the weighted input value [24]. The diagram for moving average model is shown in Fig. 2.4. Later in this thesis, Moving-Average model is applied towards CR's observations in Chapter 8, where we investigate sequential cooperative spectrum sensing.

2.8 Statistical Distributions and Random Variables

A random variable (RV) is a variable whose value depends on the randomness and is statistically modelled by the distribution or the PDF it follows. In this section, commonly used statistical distributions in wireless communication are presented, along with its PDF and cumulative density function (CDF).

2.8.1 Gaussian Distribution

If a RV follows a Gaussian or Normal distribution, its PDF is defined by

$$f(y) = \frac{1}{\sqrt{2\pi}\sqrt{\sigma^2}} e^{-(y-\mu)^2/2\sigma^2} \quad , -\infty < y < \infty \tag{2.22}$$

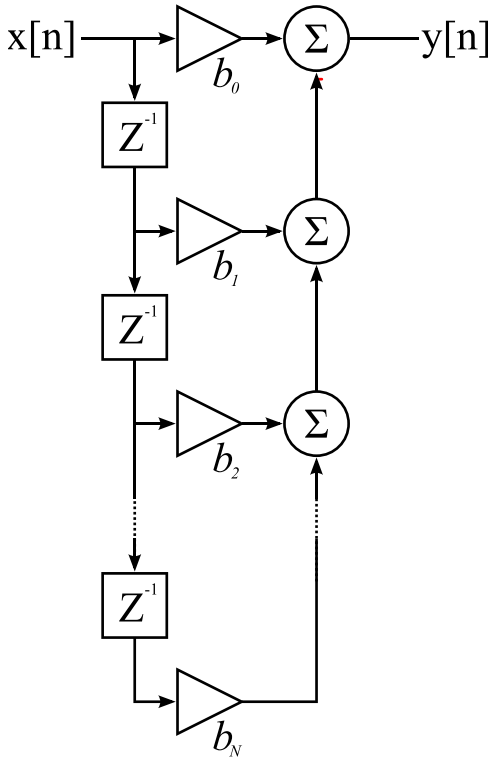

Figure 2.4: Moving Average model

where μ, σ^2 is the mean and variance [25]. The notation $y \sim \mathcal{N}(\mu, \sigma^2)$ means that a random variable y is Gaussian-distributed, with mean μ and variance σ^2. Its CDF is defined as

$$\begin{aligned} F(y) &= P(Y \leq y) \\ &= \int_{-\infty}^{y} f(y)\, dy \\ &= \frac{1}{2}\left[1 + \operatorname{erf}\left(\frac{x-\mu}{\sqrt{2\sigma^2}}\right)\right]. \end{aligned} \tag{2.23}$$

Moreover, its complementary cumulative density function (CCDF) is defined as

$$\begin{aligned} \text{CCDF}(y) &= P(Y > y) \\ &= 1 - F(y) \\ &= \frac{1}{2}\operatorname{erfc}\left(\frac{x-\mu}{\sqrt{2\sigma^2}}\right). \end{aligned} \tag{2.24}$$

Fig. 2.5 shows PDF for two RVs following Gaussian distribution, with different mean and variance.

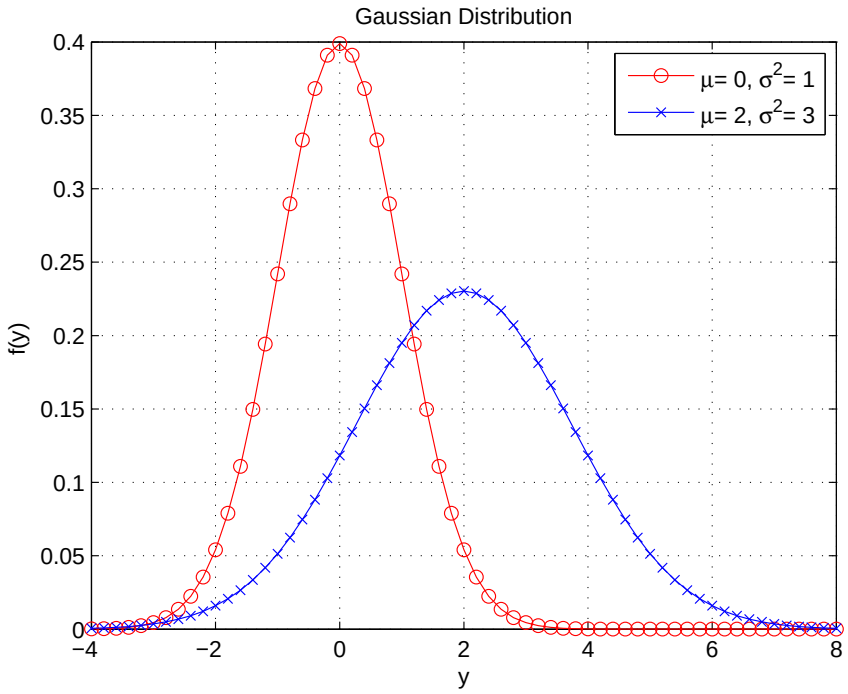

Figure 2.5: Gaussian Distribution

2.8.2 Chi-Squared Distribution

A Chi-Squared or a central Chi-Squared distribution is defined as a summation of squares of independent standard normal RVs, Y, with zero mean and unit variance. A RV Z is

$$Z = \sum_{i=1}^{k} Y_i^2 \tag{2.25}$$

and it is distributed according to the Chi-Squared distribution with k degrees of freedom. It is also denoted as $z \sim \mathcal{X}_k^2$.

The PDF for the Chi-Squared distribution is

$$f(y) = \begin{cases} \dfrac{1}{2^{\frac{k}{2}}\Gamma(k/2)} y^{\frac{k}{2}-1} e^{-\frac{y}{2}} & , 0 \leq y < \infty \\ 0 & , \text{otherwise.} \end{cases} \tag{2.26}$$

Its CDF is defined as

$$\begin{aligned} F(y) &= P\left(Y \leq y\right) \\ &= \int_0^y f(y)\, dy \\ &= \frac{1}{\Gamma(k/2)} \gamma\left(\frac{k}{2}, \frac{y}{2}\right) \qquad , 0 \leq y < \infty \end{aligned} \tag{2.27}$$

and its CCDF is defined as

$$\begin{aligned} \text{CCDF}(y) &= P\left(Y > y\right) \\ &= 1 - F(y) \\ &= \frac{1}{\Gamma(k/2)}\Gamma\left(\frac{k}{2}, \frac{y}{2}\right) \quad , 0 \leq y < \infty. \end{aligned} \tag{2.28}$$

Fig. 2.5 shows PDF for two RVs following Gaussian distribution, with different mean and variance.

2.8.3 Non-Central Chi-Squared Distribution

A Non-Central Chi-Squared Distribution is defined as a summation of squares of independent normal RVs, Y, with mean μ and variance σ^2. A RV Z is

$$Z = \sum_{i=1}^{k} \left(\frac{Y_i}{\sigma_i}\right)^2 \tag{2.29}$$

and it is distributed according to the Non-central Chi-Squared distribution with k degrees of freedom and the non-centrality parameter λ_{nc}, which is defined as

$$\lambda_{nc} = \sum_{i=1}^{k} \left(\frac{\mu_i}{\sigma_i}\right)^2. \tag{2.30}$$

The PDF for Non-Central Chi-Squared distribution is

$$f(y) = \begin{cases} \frac{1}{2} e^{-(y+\lambda_{nc})/2} \left(\frac{y}{\lambda_{nc}}\right)^{k/4-1/2} I_{k/2-1}\left(\sqrt{\lambda_{nc} y}\right) & , 0 \leq y < \infty \\ 0 & , \text{otherwise} \end{cases} \tag{2.31}$$

and its CDF is defined as

$$F(y) = 1 - Q_{\frac{k}{2}}\left(\sqrt{\lambda_{nc}}, \sqrt{y}\right) \quad , 0 \leq y < \infty \tag{2.32}$$

where $Q_M(a, b)$ is Marcum-Q function.

Fig. 2.6 shows PDF for two RVs following Chi-Squared and Non-central Chi-Squared Distributions. The Chi-Squared distributed RV is with $k = 4$ and the Non-central Chi-Squared distributed one is with $k = 4$ and $\lambda = 6$.

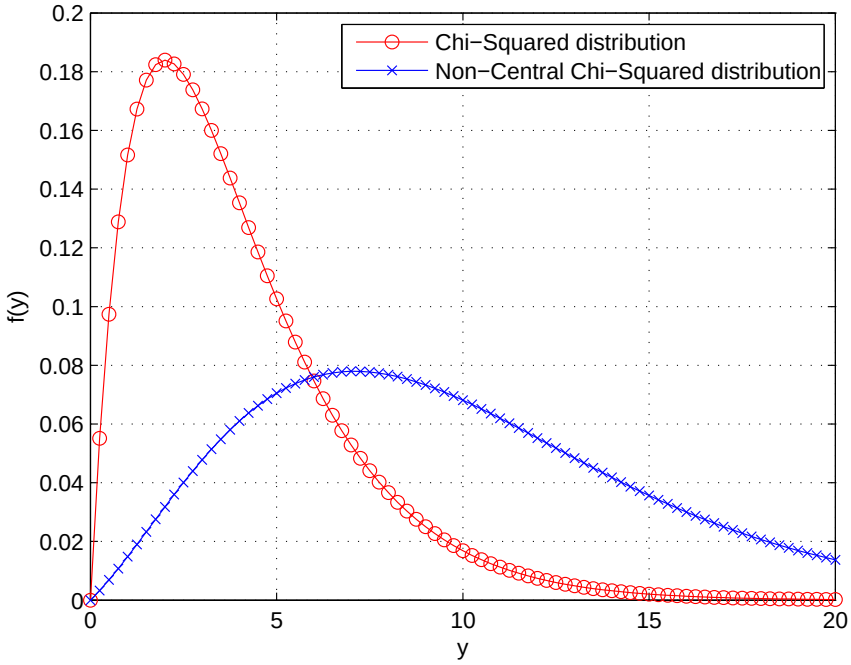

Figure 2.6: Chi-Squared and Non-Central Chi-Squared Distribution

2.8.4 Summation of two Random Variables

Let X and Y be independent RVs with the PDF of $f_X(x)$ and $f_Y(y)$. The summation of these two independent RVs are $Z = X + Y$. The PDF of Z is given by

$$\begin{aligned} f_Z(z) &= f_X(x) * f_Y(y) \\ &= \int_{-\infty}^{\infty} f_X(x) \cdot f_Y(z-x)\, dx. \end{aligned} \tag{2.33}$$

In other words, $f_Z(z)$ is the convolution of $f_X(x)$ and $f_Y(y)$ [26].

For instance, let Z be the summation of two independent Gaussian distributed X and Y, with μ_x, σ_x^2, μ_y and σ_y^2. The PDF of X can be written according to (2.22) as

$$f_X(x) = \frac{1}{\sqrt{2\pi}\sqrt{\sigma_x^2}} e^{-(x-\mu_x)^2/2\sigma_x^2} \tag{2.34}$$

and similarly the PDF of Y is

$$f_Y(y) = \frac{1}{\sqrt{2\pi}\sqrt{\sigma_y^2}} e^{-(y-\mu_y)^2/2\sigma_y^2} \tag{2.35}$$

The PDF of Z, which is $Z = X + Y$, becomes

$$\begin{aligned} f_Z(z) &= f_X(x) * f_Y(y) \\ &= \int_{-\infty}^{\infty} f_X(x) \cdot f_Y(z-x)\, dx \\ &= \int_{-\infty}^{\infty} \frac{1}{\sqrt{2\pi}\sqrt{\sigma_x^2}} e^{-(x-\mu_x)^2/2\sigma_x^2} \cdot \frac{1}{\sqrt{2\pi}\sqrt{\sigma_y^2}} e^{-(z-x-\mu_y)^2/2\sigma_y^2}\, dx. \end{aligned} \tag{2.36}$$

After some derivations, we have

$$f_Z(z) = \frac{1}{\sqrt{2\pi(\sigma_x^2+\sigma_y^2)}} \exp\left[\frac{-(z-(\mu_x+\mu_y))^2}{2(\sigma_x^2+\sigma_y^2)}\right]. \tag{2.37}$$

This derivation shows that if X and Y are independent Gaussian distributed RVs such that

$$\begin{aligned} X &\sim \mathcal{N}(\mu_x, \sigma_x^2) \\ Y &\sim \mathcal{N}(\mu_y, \sigma_y^2) \end{aligned} \tag{2.38}$$

then, Z which is a summation of X and Y, $Z = X + Y$ is distributed as

$$Z \sim \mathcal{N}(\mu_x + \mu_y, \sigma_x^2 + \sigma_y^2). \tag{2.39}$$

2.8.5 Central Limit Theorem

The Central Limit Theorem is defined that a sum of n independent, identically distributed (i.i.d.) RVs can be approximated as a normal distribution when there is a large number of RVs and the contribution for each of them is small compared to the total.

For instance, let $X_1, X_2, ...X_n$ be i.i.d. RVs with mean μ and variance σ^2 and let $S_n = Y_1 + Y_2 + ... + Y_n$, then

$$\lim_{n\to\infty} P\left(\frac{S_n - n\mu}{\sqrt{n\sigma^2}} \le y\right) = F(y) \tag{2.40}$$

where $F(\cdot)$ is the CDF for Gaussian distribution as in (2.23) [27].

2.9 Summary

In this chapter, relevant background theories of wireless communications are presented. First, large-scale propagation including path loss and shadowing is discussed. Then,

small-scale propagation including flat and frequency-selective fading, fast and slow fading is summarized. Commonly used channel model such as AWGN, Rayleigh and Rician fading channel as well as its related statistics are presented. Then, background of quantizataion and the time-series averaging model is shown. Finally, fundamentals of random variables along with Central limit theorem are summarized.

Chapter 3

Cognitive Radio System

In this chapter, we present Cognitive Radio (CR) networks, its architectures and characteristics. Various aspects of spectrum sensing is discussed in Section 3.5. Then, IEEE 802.22 WRAN Standard and prior works on spectrum sensing are presented in Section 3.6 and 3.7.

3.1 Cognitive Radio Networks

Wireless networks are now based on fixed spectrum allocation policy. Spectrum can be under-utilized in some area or some period of time, while some frequencies are highly-utilized [7]. To maximize the frequency spectrum usage, some under-utilized wireless spectrum should be exploited. CR aims to opportunistically access the spectrum as the secondary-tier networks. CR user utilizes the spectrum while the licensed users or primary users (PUs) are not using it, in order to maximize the spectrum utilization [9]. As a secondary-tier user, CR user needs to vacate the spectrum whenever PU retransmits again. CR is defined as a radio that can change its transmission parameters based on interaction with the environment in which it operates [7]. CR enables its users to

1. determine which portion of the spectrum is available and detect the presence of licensed users when a user operates in a licensed band.

2. select the best available channel.

3. coordinate access to this channel with others.

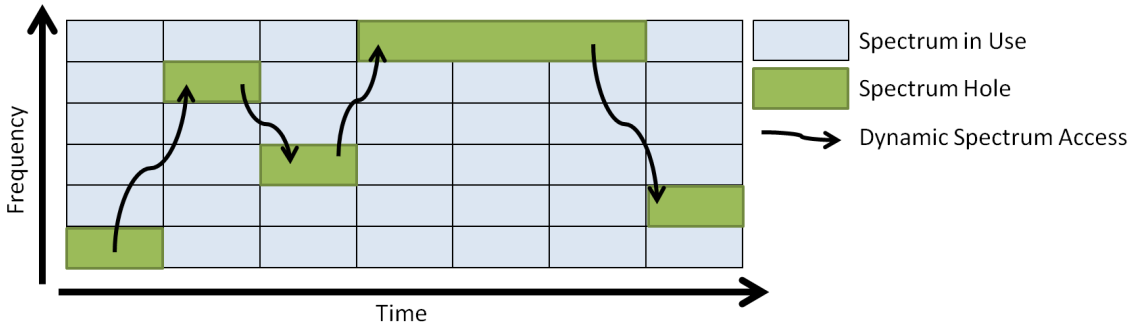

Figure 3.1: Cognitive Radio Concepts

4. vacate the channel when PU is detected.

Fig. 3.1 shows the concept of CR and Dynamic Spectrum Access. CR user dynamically and opportunistically accesses the spectrum hole or the white space, while avoiding an access to the spectrum which is currently in use by the PUs.

3.2 Cognitive Radio Architectures

Cognitive Radio network architecture can be categorized into two groups, the primary network and the cognitive radio network [7].

The primary network is an existing infrastructure which has an exclusive right over a certain spectrum band, for example, the cellular networks and TV broadcast networks. The components of the primary networks are

- Primary User (licensed user): a user which has a license to operate in a licensed band. The PU operation should not be affected by the operations of CR users.
- Primary Base-Station (licensed base-station): a fixed infrastructure network component with spectrum license.

The CR network does not have license to operate in a licensed band and its spectrum access is allowed opportunistically. The components of the cognitive radio networks are

- Cognitive Radio User (unlicensed user): a user who has no license over the spectrum. CR user can access the spectrum opportunistically only when PU is not present and CR user must vacate the channel immediately when the PU is detected

- Cognitive Radio Base-Station (unlicensed base-station): a fixed infrastructure component with CR capabilities, providing a single-hop connection to CR users. In cooperative spectrum sensing, the CR Base-Station also serves as a fusion center to gather the information from cooperative users and make the final spectrum sensing decision.

- Spectrum Broker (scheduling server): a central network entity that controls spectrum resource sharing among the CR users.

3.3 Cognitive Radio Characteristics

There are two main characteristics of cognitive radio, Cognitive Capability and Reconfigurability.

3.3.1 Cognitive Capability

CR's cognitive capability allows CR to capture or sense the information from its radio environment. This task is functioned in three steps, which are referred as the cognitive cycle, shown in Fig. 3.2 [14].

- Spectrum Sensing: The radio environment and the available spectrum band are monitored. Their information is captured and spectrum holes are detected.

- Spectrum Analysis: The characteristics of the spectrum holes detected are estimated.

- Spectrum Decision: The appropriate spectrum band is chosen according to the spectrum analysis and characteristics and user requirements: data rate, bandwidth, and transmission mode.

Fig. 3.2 shows the cognitive cycle [7]. First, the CR user needs to sense the radio environment once it wants to access the spectrum. In this step, spectrum sensing captures the information and detects the spectrum holes. Afterwards, for the spectrum analysis, the characteristics of the spectrum holes are estimated. Then, for the spectrum decision, CR determines the characteristics such as the data rate, the transmission mode and the bandwidth of the trasmission. Then, once CR user starts to

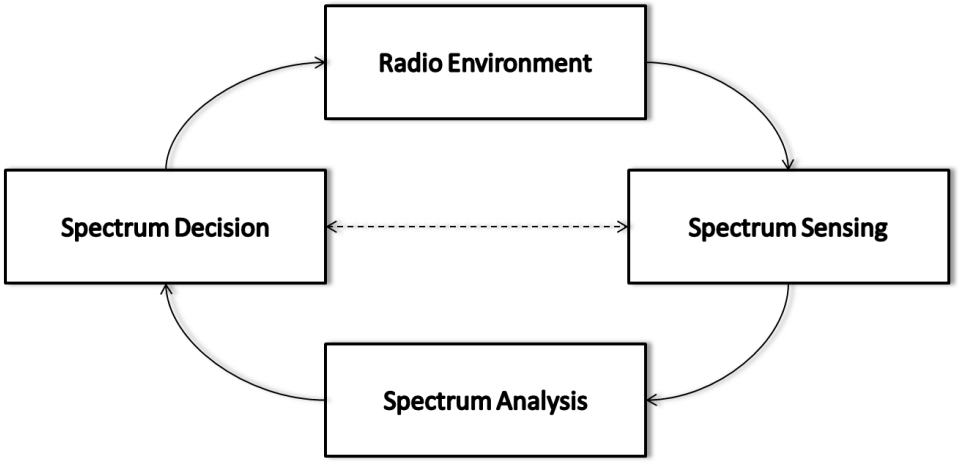

Figure 3.2: Cognitive Cycle

operate in determined spectrum band, it should keep track of the changes in the radio environment, as the radio environment can change over time and space. When the current spectrum band becomes unavailable, CR user needs to stop utilizing that channel immediately to avoid interference to the PU.

3.3.2 Reconfigurability

CR's reconfigurability enables CR to be dynamically programmed according to the radio environment, to transmit or to receive on a variety of frequency and different transmission access. The configurable parameters in CR system are

- Operating frequency: CR user can change its operating frequency depending on radio environment
- Modulation: CR user can adapt its modulation scheme to user requirements and channel conditions
- Transmission Power: CR user can reduce it transmission power to a lower level to allow more users to share the same channel and to decrease the interference.
- Communication Technology: CR user can provide interoperability among different communication systems

3.4 Spectrum Sharing

Based on the access technology, spectrum sharing can be classified as [7]

- **Overlay spectrum sharing**: In this spectrum sharing technique, a portion of the spectrum that is not used by the licensed user is accessed by the CR users. As a result, interference to the PU is minimized.

- **Underlay spectrum sharing**: This spectrum access technique exploits the spread spectrum techniques developed for cellular networks. CR user begins communication at the certain portion of the spectrum allocated by a spectrum allocation map with transmission power regarded as noise by the licensed user. This technique can utilize increased bandwidth compared to the overlay technique.

3.5 Spectrum Sensing

CR user can access spectrum band only when the licensed user does not exist and it needs to vacate the channel immediately when the PU comes back. As a result, spectrum hole detection plays an important role in the CR system. There are various ways to detect the spectrum holes: transmitter detection, cooperative detection and interference based detection. Fig. 3.3 shows the classification of spectrum sensing techniques [7]. In this section, three different aspects for spectrum sensing techniques are discussed.

3.5.1 Transmitter Detection

First, the transmitter detection is to detect spectrum holes, which CR can access and utilize [28]. The transmitter detection detects the spectrum holes by detecting whether any PU transmitter is operating or not. The basic hypothesis model here is that if PU exists, the received signal at the CR user would consist of the PU's signal and noise. Otherwise, it would be noise only in case that PU does not exist. There are three techniques generally used for transmitter detection in CR networks

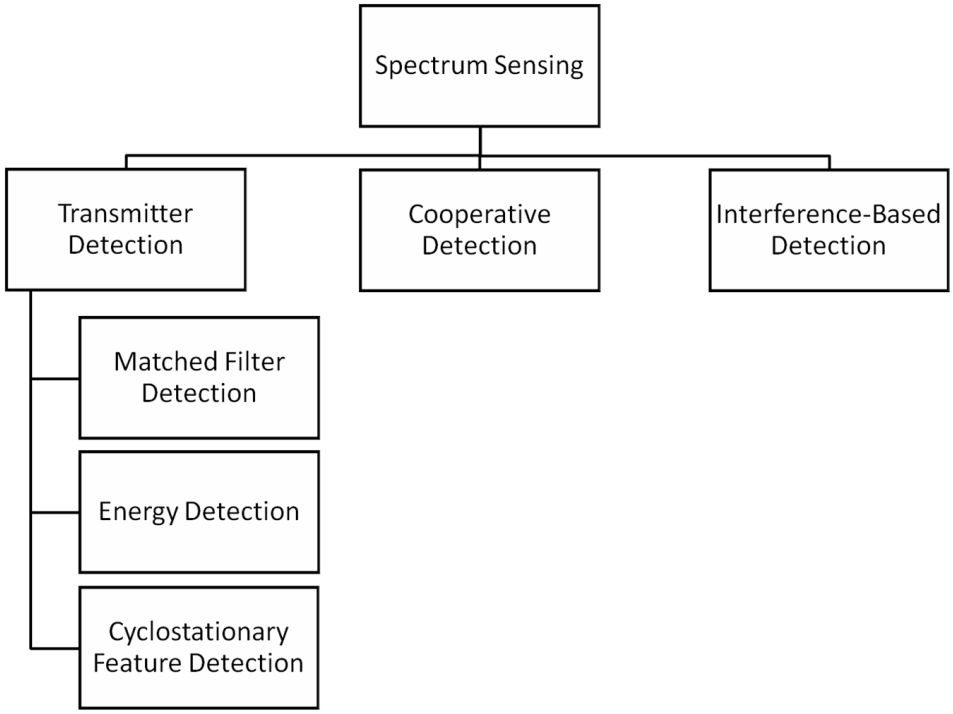

Figure 3.3: Classification of spectrum sensing techniques

Matched Filter Detection

In stationary Gaussian noise, the matched filter detection is optimal as it maximizes signal-to-noise ratio (SNR). However, this technique requires an *a priori* knowledge of the PU such as the modulation type and order, the pulse shape, and the packet format [7]. An inaccuracy in this information can lead to poor performance. Nonetheless, pilot, preambles, synchronization, or spreading codes can be used for this coherent detection. Matched filter detection is robust to noise uncertainty and delivers good performance under low SNR scenario [29].

Energy Detection

In this technique, energy of the received signal is compared to the threshold value to decide whether the PU exists or not. This technique is simple to implement [14] and does not require prior knowledge on PU. However, it cannot distinguish signal types but can only determine the existence of signal. More details on Energy detection-based spectrum sensing will be covered in Chapter 4.

Cyclostationary Feature Detection

This technique differentiates noise energy from the modulated signal energy using the fact that the noise is wide-sense stationary with no correlation, while modulated signals are cyclostationary with spectral correlation due to the embedded redundancy of signal periodicity [30]. This technique is robust in low SNR scenario and is also robust to the interference. However, it requires partial information on PU and high computational cost.

3.5.2 Cooperative Detection

The hidden terminal problem occurs in conventional energy detection as the CR can experience deep fade and not be able to detect the PU. Furthermore, there is still a chance when the CR user has a line-of-sight to the primary user but cannot detect the PU's existence due to shadowing uncertainty. When CR user experiences hidden terminal problem or shadowing uncertainty, the transmitter detection cannot detect the PU's presence. As a result, cooperation among CR users can reduce an uncertainty caused by the single user's detection. Using multiple sensing nodes, cooperative sensing can exploit spatial diversity and mitigate multipath fading and shadowing effects, which are the main factors that deteriorate performance of single user's detection.

The cooperative detection can provide more accurate performance [14]. However, it requires additional operations and overhead traffic to communicate among CR users. As a result, there can be an effect on the performance of resource-constrained networks.

3.5.3 Interference-Based Detection

In this technique, the interference level at the PU receivers is measured in order to protect them from interference. CR user can access the spectrum bands as long as its interference at the primary receiver does not exceed PU's *interference temperature limit*, which is the maximum amount of interference that the receiver can tolerate.

The interference temperature T_I is defined as

$$T_I(f_c, B) = \frac{P_I(f_c, B)}{kB} \tag{3.1}$$

where $P_I(f_c, B)$ is the average interference power in Watts centered at f_c, covering bandwidth B and k is Boltzmann's constant of 1.38×10^{-23} J/K [31].

Parameter	Analog TV	Digital TV	Wireless Microphone
Probability of Detection	90%	90%	90%
Probability of False Alarm	10%	10%	10%
Channel Detection Time	≤ 2 s	≤ 2 s	≤ 2 s

Table 3.1: Receiver Parameter for 802.22 WRAN

3.6 IEEE 802.22 WRAN Standard

IEEE 802.22 Wireless regional area network (WRAN) is the standard based on the CR technology. It focuses on utilizing and enabling un-licensed use on the UHF/VHF TV bands (54-862MHz) [7]. Spectrum sensing is an important component for CR to operate without interfering the PU system. The standard's requirement on the receiver parameters for 802.22 WRAN is shown in Table 3.1 [32]. It is shown that signals are classified into three types; analog TV, digital TV and wireless microphone. However, the requirements for probability of false alarm and detection are the same for all three signals types. In later chapters, the simulation will consider the probability of false alarm and detection as provided in Table 3.1.

3.7 Prior Works on Spectrum Sensing

With the aim to improve the detection performance in cooperative spectrum sensing, many novel techniques have been investigated and proposed. Various aspects and algorithms as well as the challenges for spectrum sensing are summarized in [33–35].

Cooperative detection with distributed sensors has been studied in [36, 37]. A theory and application on detection of abrupt changes has been investigated in [38]. However, in terms of CR, cooperative spectrum sensing and its algorithms have been proposed in [8] for two-user network and in [39] for multi-user network. Cooperative spectrum sensing under fading channel as well as effect of shadowing is considered in [40–42]. These works show that cooperation helps improve the overall performance of the network. In [43], an energy detector based cooperative spectrum sensing is improved under multiple antenna scenario.

In [44], a linear optimization is applied at fusion center for each local test statistics

from individual CR user. The linear network coding is applied to the cooperative spectrum sensing in [45]. In [46], final decision is formed based on the result of a weighted summation of the neighboring results. Variable weighting factors are considered here such as the distance to neighboring nodes, influence of positive results and influence of a node's own result. In [47], weighting decision fusion scheme is also considered. A spectrum sensing technique based on a Neyman-Pearson criterion is studied in [48]. Also, the detection techniques related to Log-likelihood based detector are proposed in [49–51].

Apart from the above-mentioned spectrum sensing schemes, various different techniques have been proposed. The quickest spectrum sensing is presented in [52]. Sequential spectrum sensing techniques are considered in [53–55]. Minimum-delay spectrum sensing considering both fixed sample size and sequential sensing algorithms are investigated and developed in [56]. Adaptive sensing techniques are proposed in [57] to maximize spectrum utilization such that CR performs channel sensing when it is needed only. Hence, the unnecessary sensing can be avoided. In [58], the protoypes and protocols are tested and built equipped with cooperative sensing, interference alerting and frequency management. A cooperative sensing, in Heterogeneous Network (HetNet) with Joint sensing and belief propagation is proposed in [59]. Cyclostationary sensing is considered in [60]. An advanced technique using OFDM-based MIMO is proposed in [61] and is shown that it improves the detection performance. Spectrum sensing of OFDM signals in known and unknown noise variance is considered in [50]. Imperfect reporting channel between CR and the fusion center as well as the error it induces is studied in [34, 62]. In [63], local oscillator leakage power is exploited and help to locate receivers. In [64], linear composite hypothesis in the case, where knowledge on PU and channel statistics is incomplete, is proposed. An improvement on blind spectrum sensing technique is proposed in [65]. A probability-based scheme for combination of spectrum sensing information collected from cooperative cognitive radio users is proposed in [66]. In [67], a technique in which PU helps with spectrum sensing is proposed.

3.8 Summary

In this chapter, fundamentals and backgrounds of CR networks along with its architectures and characteristics are presented. Being secondary-tier users, CR user needs to be aware of the PU's state and by dynamically accessing the under-utilized spectrum, CR could improve the spectrum utilization. Hence, spectrum sensing procedure is essential in order to determine whether the spectrum is available for CR's access or not. Various aspects of spectrum sensing are summarised in this chapter as well as the IEEE 802.22 WRAN standard and various prior research works on spectrum sensing.

Chapter 4

Cooperative Spectrum Sensing

An energy detection-based spectrum sensing is discussed in Section 4.1. Related mathematical statistics is presented and approximated in Section 4.2 and 4.3. Then, Section 4.4 discusses the cooperative spectrum sensing.

4.1 Energy Detection-Based Spectrum Sensing

The energy detection technique is a simple and effective spectrum sensing approach whereby the received signal energy is compared to a detection threshold to determine the existence of PUs [68]. The received signal energy (y) at the CR user can be expressed as

$$y = \begin{cases} \sum_{i=1}^{m} |n_i|^2 & H_0 \\ \sum_{i=1}^{m} |h_i s_i + n_i|^2 & H_1 \end{cases} \tag{4.1}$$

where m is the time-bandwidth product, h_i, s_i and n_i is the channel gain between PU and CR, PU's signal and noise in the i^{th} time slot respectively. H_0 and H_1 represents the case when PU is idle and active respectively.

The received signal energy is compared to the detection threshold (λ). A decision saying that PU is idle (H_0) is made if it is less than the threshold. Otherwise CR thinks that PU is active (H_1).

$$d = \begin{cases} H_0 & \text{, if } y < \lambda \\ H_1 & \text{, otherwise .} \end{cases} \tag{4.2}$$

Fig. 4.1 shows the distribution for received signal energy and its corresponding probabilities. $P(H_i|H_j)$ defines the probability that CR decides that PU is in H_i state

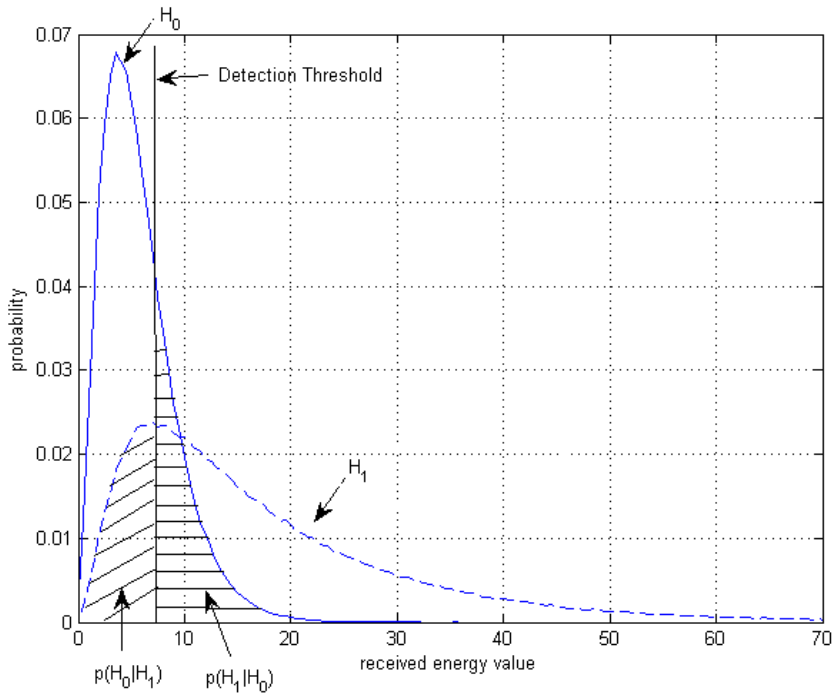

Figure 4.1: Probability density function of H_0 and H_1

while PU is in H_j state. The CR's detection performance is commonly measured by the probability of false alarm (P_f) and detection (P_d), which are defined as the probability of locally detecting H_1, given that PU is idle and active respectively

$$\begin{aligned} P_f(\lambda) &= P(H_1|H_0) \\ &= P(y > \lambda|H_0) \\ P_d(\lambda) &= P(H_1|H_1) \\ &= P(y > \lambda|H_1). \end{aligned} \tag{4.3}$$

4.2 Related Mathematical Statistics

4.2.1 Probability of False Alarm

When PU is idle (H_0), the received signal energy at the CR follows the Central Chi-Squared distribution with $2m$ degree of freedom. Its PDF can be written as [42]

$$f(y|H_0) = \frac{y^{m-1}e^{-y/2}}{\Gamma(m) \cdot 2^m} \tag{4.4}$$

where $\Gamma(.)$ is the gamma function.

As there is only noise in the received signal, when PU is idle (H_0) as in (4.1), the probability of false alarm is independent of the channel and can be given as [42]

$$\begin{aligned} P_f(\lambda) &= \int_{\lambda}^{\infty} f(y|H_0)\, dy \\ &= \frac{\Gamma(m, \lambda/2)}{\Gamma(m)}. \end{aligned} \tag{4.5}$$

4.2.2 Probability of Detection

On the contrary, when PU is active (H_1) as in (4.1), the received signal energy is dependent on the channel type. The received signal energy for a particular instantaneous SNR follows the Non-Central Chi-Squared distribution with degree of freedom of $2m$ and non-centrality parameter of $2m\gamma$, where γ is the instantaneous SNR. Its PDF can be written as [42]

$$f(y, \gamma|H_1) = \frac{y^{m-1}e^{-(y+2m\gamma)/2}}{2^m \cdot \Gamma(m)} {}_0F_1(m, \frac{m\gamma y}{2}) \tag{4.6}$$

where ${}_0F_1(.,.)$ is the confluent hypergeometric limit function [69].

In an AWGN Channel, the instantaneous SNR at the CR user is constant at $\bar{\gamma}$. The PDF for the received signal energy is

$$f(y|H_1) = \frac{y^{m-1}e^{-(y+2m\bar{\gamma})/2}}{2^m \cdot \Gamma(m)} {}_0F_1(m, \frac{m\bar{\gamma} y}{2}). \tag{4.7}$$

Hence, similarly to the P_f in (4.5), probability of detection (P_d) is

$$\begin{aligned} P_d(\lambda) &= \int_{\lambda}^{\infty} f(y|H_1)\, dy \\ &= Q_m(\sqrt{2m\bar{\gamma}}, \sqrt{\lambda}). \end{aligned} \tag{4.8}$$

In fading channel, however, the instantaneous SNR at the CR user is random. Assuming Rayleigh fading with a PDF of $f_h(\gamma)$, the PDF for the received signal energy can be obtained by

$$\begin{aligned} f(y|H_1) &= \int_0^{\infty} f(y, \gamma|H_1) \cdot f_h(\gamma)\, d\gamma \\ &= \int_0^{\infty} \frac{y^{m-1}e^{-(y+2m\gamma)/2}}{2^m \cdot \Gamma(m)} {}_0F_1(m, \frac{m\gamma y}{2}) \cdot \frac{1}{\bar{\gamma}} e^{-\frac{\gamma}{\bar{\gamma}}}\, d\gamma. \end{aligned} \tag{4.9}$$

After some derivations, we obtain

$$f(y|H_1) = \frac{e^{-\frac{1}{2(1+m\bar{\gamma})}y} \times \left[\Gamma(m-1) - \Gamma(m-1, \frac{m\bar{\gamma}y}{2+2m\bar{\gamma}})\right]}{2 \cdot (1+m\bar{\gamma}) \cdot (\frac{m\bar{\gamma}}{1+m\bar{\gamma}})^{m-1} \cdot \Gamma(m-1)} \tag{4.10}$$

where $\bar{\gamma}$ is the average SNR received at the CR user.

Hence, in Rayleigh fading channel, the probability of detection (P_d) is

$$\begin{aligned} P_d(\lambda) &= \int_{\lambda}^{\infty} f(y|H_1)\, dy \\ &= \frac{\Gamma(m-1, \lambda/2)}{\Gamma(m-1)} \\ &\quad + \; e^{-\frac{\lambda}{2(1+m\bar{\gamma})}} \times \left(1 + \frac{1}{m\bar{\gamma}}\right)^{m-1} \times \left[1 - \frac{\Gamma(m-1, \frac{\lambda m\bar{\gamma}}{2(1+m\bar{\gamma})})}{\Gamma(m-1)}\right]. \end{aligned} \tag{4.11}$$

While in the Nakagami fading channel, the derivation for P_d is presented in [41] and as follows.

$$\begin{aligned} P_{d,Nak}(g, m, \bar{\gamma}, \lambda) &= \alpha \left[G_1 + \beta \sum_{n=1}^{m-1} \frac{(\lambda/2)^n}{2(n!)} \, {}_1F_1\Big(g; n+1; \frac{\lambda}{2}\frac{\bar{\gamma}}{g+\bar{\gamma}}\Big)\right] \\ \alpha &= \frac{1}{\Gamma(g) 2^{g-1}} \left(\frac{g}{\bar{\gamma}}\right)^g \\ \beta &= \Gamma(g)\Big(\frac{2\bar{\gamma}}{g+\bar{\gamma}}\Big)^g e^{-\lambda/2} \\ G_1 &= \frac{2^{g-1}(g-1)!}{(\frac{g}{\bar{\gamma}})^g} \frac{\bar{\gamma}}{g+\bar{\gamma}} e^{\frac{-\lambda}{2}\frac{g}{g+\bar{\gamma}}} \left[\Big(1 + \frac{g}{\bar{\gamma}}\Big)\Big(\frac{g}{g+\bar{\gamma}}\Big)^{g-1} \right. \\ &\quad \left. \times L_{g-1}\Big(-\frac{\lambda}{2}\frac{\bar{\gamma}}{g+\bar{\gamma}}\Big) + \sum_{n=0}^{g-2} \Big(\frac{g}{g+\bar{\gamma}}\Big)^n L_n\Big(-\frac{\lambda}{2}\frac{\bar{\gamma}}{g+\bar{\gamma}}\Big)\right] \end{aligned} \tag{4.12}$$

where ${}_1F_1(.;.;.)$, $L_n(.)$, g, m is the confluent hypergeometric function, Laguerre polynomial of degree n, Nakagami parameter and time-bandwidth product respectively [69].

4.2.3 Cumulative Density Function

As CDF is the probability that a random variable is smaller than a particular level, the CDF under H_0 and H_1 case can be defined as

$$\text{CDF } (\lambda) = \begin{cases} 1 - P_f(\lambda) & , H_0 \\ 1 - P_d(\lambda) & , H_1. \end{cases} \tag{4.13}$$

4.3 Statistical Approximation

Here, we propose a statistical approximation for the P_d and PDF of H_1 in (4.11) and (4.10) respectively. The approximation is useful in the case that the closed-form is

difficult to use such that derivation for inverse of P_d. The approximation on P_d will be used in Chapter 6, while that of PDF of H_1 will be in Chapter 7 and 8.

4.3.1 Probability of Detection

The incomplete gamma function is given by [69] as

$$\frac{\Gamma(s,x)}{\Gamma(s)} = e^{-x}\sum_{k=0}^{s-1}\frac{x^k}{k!}\ . \tag{4.14}$$

When x is sufficiently large and s is small, this function will approach zero, due to the dominance of e^{-x} over the summation term. Consider the two incomplete gamma functions in the first and last term of (4.11). In case that λ is large and $m-1$ is small, these two incomplete gamma functions will tend to zero.

$$\begin{aligned}\frac{\Gamma(m-1,\lambda/2)}{\Gamma(m-1)} &\approx 0\\ \frac{\Gamma(m-1,\frac{\lambda m\bar{\gamma}}{2(1+m\bar{\gamma})})}{\Gamma(m-1)} &\approx 0.\end{aligned} \tag{4.15}$$

Hence, the approximated probability of detection ($\tilde{P}_d$) in Rayleigh fading channel becomes

$$\begin{aligned}P_d(\lambda) &= \frac{\Gamma(m-1,\lambda/2)}{\Gamma(m-1)}\\ &\quad + \ e^{-\frac{\lambda}{2(1+m\bar{\gamma})}}\times\left(1+\frac{1}{m\bar{\gamma}}\right)^{m-1}\times\left[1-\frac{\Gamma(m-1,\frac{\lambda m\bar{\gamma}}{2(1+m\bar{\gamma})})}{\Gamma(m-1)}\right].\\ \tilde{P}_d(\lambda) &= 0 + e^{-\frac{\lambda}{2(1+m\bar{\gamma})}}\times\left(1+\frac{1}{m\bar{\gamma}}\right)^{m-1}[1-0]\\ \tilde{P}_d(\lambda) &= e^{-\frac{\lambda}{2(1+m\bar{\gamma})}}\times\left(1+\frac{1}{m\bar{\gamma}}\right)^{m-1}.\end{aligned} \tag{4.16}$$

Given that the time-bandwidth product in CR is usually a small integer, the approximation will be valid if the detection threshold is high. Fig. 4.2 compares this approximation to the exact value of P_d, when m is set to 3 and PU's SNR is 5dB. The approximation is very accurate when λ is large while a slight error occurs when λ is small.

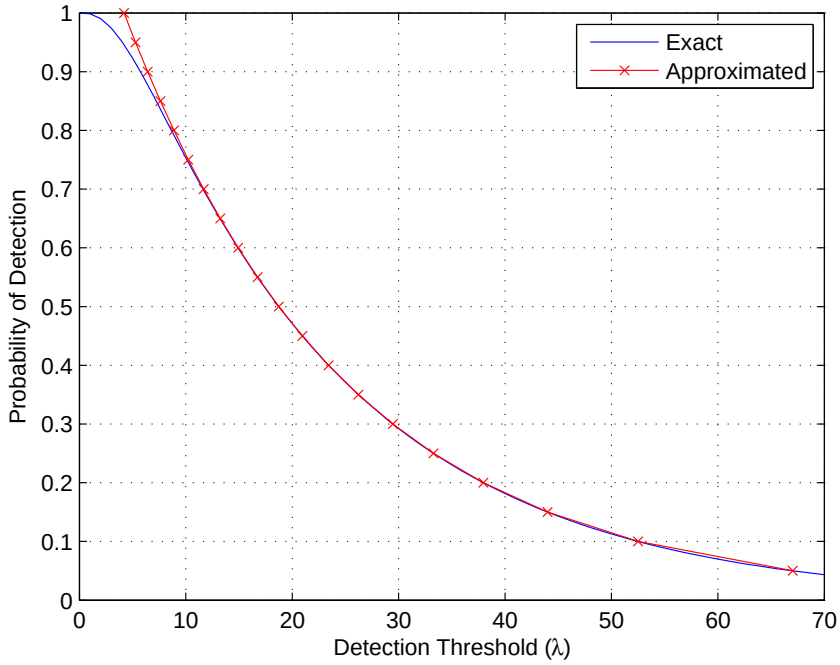

Figure 4.2: Approximated and Exact Probability of Detection

4.3.2 Probability Density Function on H_1

Similarly to P_d approximation, the incomplete gamma function terms in (4.10) could be approximated to zero.

$$\frac{\Gamma(m-1, \frac{m\bar{\gamma}y}{2+2m\bar{\gamma}})}{\Gamma(m-1)} \approx 0. \tag{4.17}$$

And the PDF of H_1 under Rayleigh fading channel is approximated as

$$\begin{aligned} f(y|H_1) &= \frac{e^{-\frac{1}{2(1+m\bar{\gamma})}y} \times}{2 \cdot (1+m\bar{\gamma}) \cdot (\frac{m\bar{\gamma}}{1+m\bar{\gamma}})^{m-1}} \left[1 - \frac{\Gamma(m-1, \frac{m\bar{\gamma}y}{2+2m\bar{\gamma}})}{\Gamma(m-1)}\right] \\ \tilde{f}(y|H_1) &= \frac{e^{-\frac{1}{2(1+m\bar{\gamma})}y} \times}{2 \cdot (1+m\bar{\gamma}) \cdot (\frac{m\bar{\gamma}}{1+m\bar{\gamma}})^{m-1}} [1-0] \\ &= \frac{e^{-\frac{1}{2(1+m\bar{\gamma})}y}}{2 \cdot (1+m\bar{\gamma}) \cdot (\frac{m\bar{\gamma}}{1+m\bar{\gamma}})^{m-1}}. \end{aligned} \tag{4.18}$$

Fig. 4.3 compares this approximation to the exact PDF, when m is set to 3 and PU's SNR is 5dB. The simulation result also proves that the approximation is very accurate when λ is large while an error occurs when λ is small.

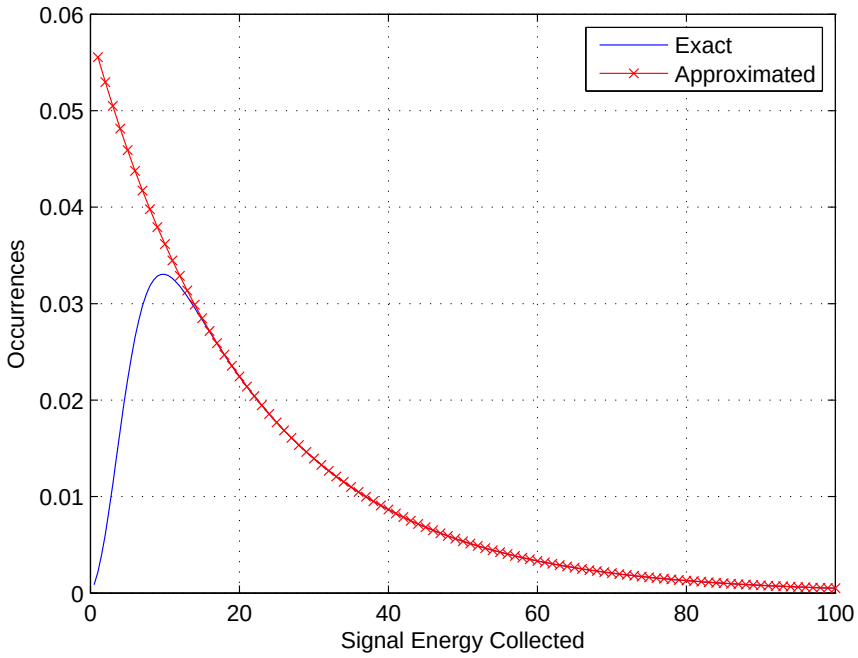

Figure 4.3: Approximated and Exact Probability Density Function H_1

4.4 Cooperative Spectrum Sensing

Detection performance metrics in cooperative spectrum sensing are the cooperative probability of false alarm (Q_f) and detection (Q_d). Being a cooperative system, a final decision needs to be made from various local information. Hence, decision combining rule plays an important role here. Cooperative spectrum sensing can be classified into Hard Decision Combining (HDC) and and Soft Decision Combining (SDC). For HDC, only local decision from sensing nodes is forwarded to the fusion center, while the local observation is forwarded for SDC.

4.4.1 Hard Decision Combining Rules

In HDC rules based cooperative spectrum sensing, CR users forward its local decision to the fusion center to make a final decision. Assuming that the energy observations at each CR user is independent and identically distributed (i.i.d.), the Q_f and Q_d can be expressed according to the combining rules as follows [42, 70].

OR Rule

In OR-rule based HDC, the final decision of H_1 is made when at least one CR user reports H_1 local decision. The Q_f and Q_d is given as

$$\begin{aligned} Q_f(\lambda) &= 1 - (1 - P_f(\lambda))^N \\ Q_d(\lambda) &= 1 - (1 - P_d(\lambda))^N \end{aligned} \tag{4.19}$$

where N is the number of cooperative CR users.

AND Rule

In AND-rule based HDC, the final decision of H_1 is made only when all CR users report H_1 local decision. The Q_f and Q_d is given as

$$\begin{aligned} Q_f(\lambda) &= (P_f(\lambda))^N \\ Q_d(\lambda) &= (P_d(\lambda))^N . \end{aligned} \tag{4.20}$$

k-out-of-n Rule

In k-out-of-n-rule based HDC, the final decision of H_1 is made only at least k CR users report H_1 local decision. The Q_f and Q_d is given as

$$\begin{aligned} Q_f(\lambda) &= \sum_{l=k}^{n} \binom{n}{l} (P_f(\lambda))^l (1 - P_f(\lambda))^{n-l} \\ Q_d(\lambda) &= \sum_{l=k}^{n} \binom{n}{l} (P_d(\lambda))^l (1 - P_d(\lambda))^{n-l} . \end{aligned} \tag{4.21}$$

4.4.2 Soft Decision Combining Rules

In SDC rules based cooperative spectrum sensing, CR users forward its local observation to the fusion center to make a final decision. The fusion center then combines the forwarded observations and compares the aggregated energy value to the fusion threshold. The Q_f and Q_d can be expressed as follows

$$\begin{aligned} Q_f(\lambda_f) &= P\{T > \lambda_f | H_0\} \\ Q_d(\lambda_f) &= P\{T > \lambda_f | H_1\} \end{aligned} \tag{4.22}$$

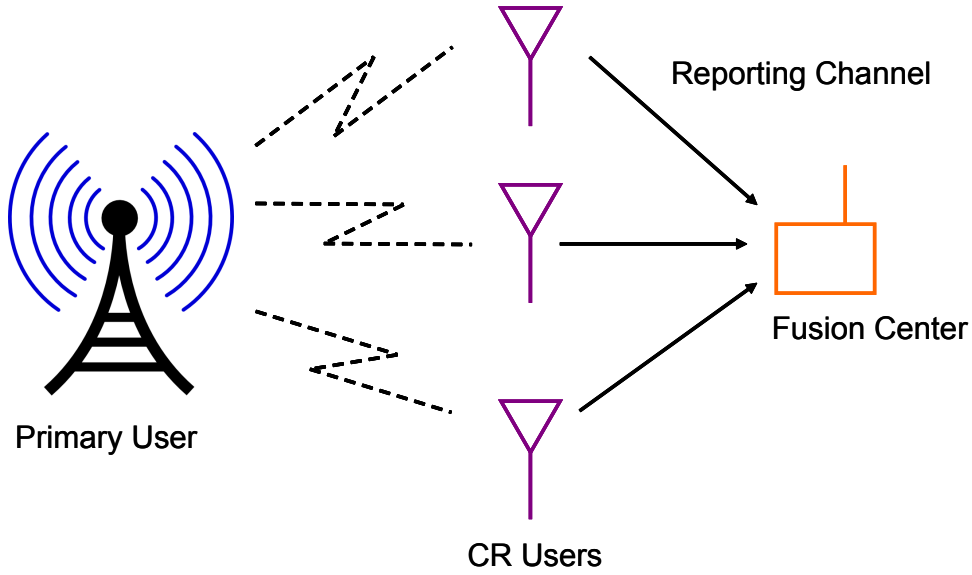

Figure 4.4: Simulation Setup Scenario

where $T = \mathbf{WY} = \sum_{i=1}^{N} w_i y_i$, $\mathbf{W}$ is weighting vector and λ_f is the fusion center detection threshold.

If the fusion center equally weighs and aggregates the forwarded observations, it is called Equal Gain Combining based SDC (EGC-SDC) approach. More detail on the EGC-SDC will be presented in Chapter 5.

4.5 Simulation Setup Scenario

Along this thesis, we assume that the simulation scenario is set up as illustrated in Fig. 4.4. We adopt the energy detection based transmitter detection technique to detect whether PU is transmitting or not. It is assumed that CR users are separately placed. The sensing procedure is that the CR users locally sense the PU. Then, they collaboratively forward either its decision or observation to the fusion center. In this step, we assume that the reporting channel is error-free such that the fusion center receives exactly the same information as sent. Finally, the fusion center makes final decision and inform all CR users.

Later in this thesis, OR rule is chosen at the fusion center where hard decision is forwarded to the fusion center. This is due to the PU's protection property of OR rule such that all CR users will stop its transmission as long as only at least one CR user reports the PU's existence. Moreover, OR rule was shown to deliver a better

performance over the other rules for many cases of practical interest [42].

4.6 Summary

In this chapter, an energy detection-based spectrum sensing was discussed. First, related mathematical statistics including probability of false alarm and detection under AWGN, Rayleigh and Nakagami fading channel was presented. Then, the PDF and probability of detection under Rayleigh fading channel were approximated. Both HDC and SDC-based cooperative spectrum sensing were discussed. Finally, the cooperative spectrum sensing scenario is illustrated.

Chapter 5

EGC-SDC Cooperative Spectrum Sensing

5.1 Introduction

In this chapter, we present the EGC-SDC cooperative spectrum sensing scheme, where all cooperating CR users forward its received signal energy to the fusion center. The forwarded signal energy are then equally combined for decision making. First, we present the detailed sensing procedures for EGC-SDC scheme and its sensing performance. Then, we derive and present the analysis for the closed-form of probability of false alarm and detection under AWGN and Rayleigh fading channel in Section 5.4.

5.2 EGC-SDC Sensing Procedures

As briefly mentioned in Chapter 4, the detailed sensing procedures for EGC-SDC scheme are as follows.

1. First, every CR user gathers its information using energy detection technique and then forwards its local observation to the fusion center.

2. The fusion center equally weighs the forwarded observation and aggregate all of them.

3. Then, the aggregated value (T) is compared to the fusion center decision threshold (λ_f).

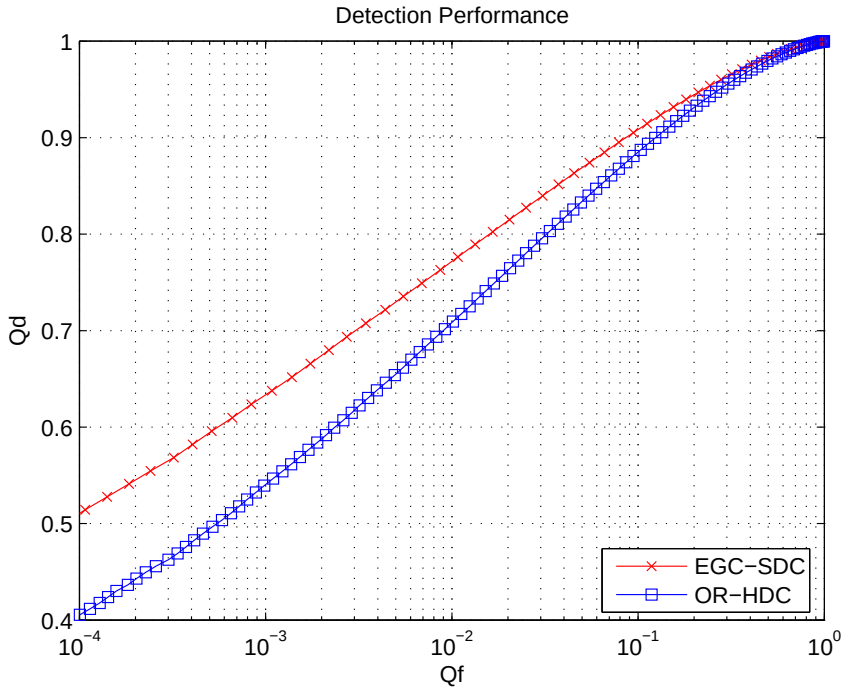

Figure 5.1: Detection Performance on EGC-SDC and OR-HDC scheme, SNR= 3dB

4. The final decision H_0 is made, if T is less than λ_f, otherwise final decision H_1 is made.

$$d = \begin{cases} H_0 & \text{, if } T < \lambda_f \\ H_1 & \text{, otherwise .} \end{cases} \tag{5.1}$$

5. Then, the final decision, either H_0 or H_1, is sent back to inform all CR users whether to transmit on the spectrum or not.

5.3 EGC-SDC Sensing Performance

The detection performance for EGC-SDC spectrum sensing scheme is shown in Fig. 5.1 and 5.2 and compared with that of OR-HDC scheme. The simulation parameters are three cooperative CR users with time-bandwidth product m of 3 and SNR of 3dB and 5dB respectively. Simulation results show that EGC-SDC scheme achieves good performance by equally combining the local observations from the sensing nodes and especially, the detection performance achieved by EGC-SDC scheme is much better than that of OR-HDC under the same scenario.

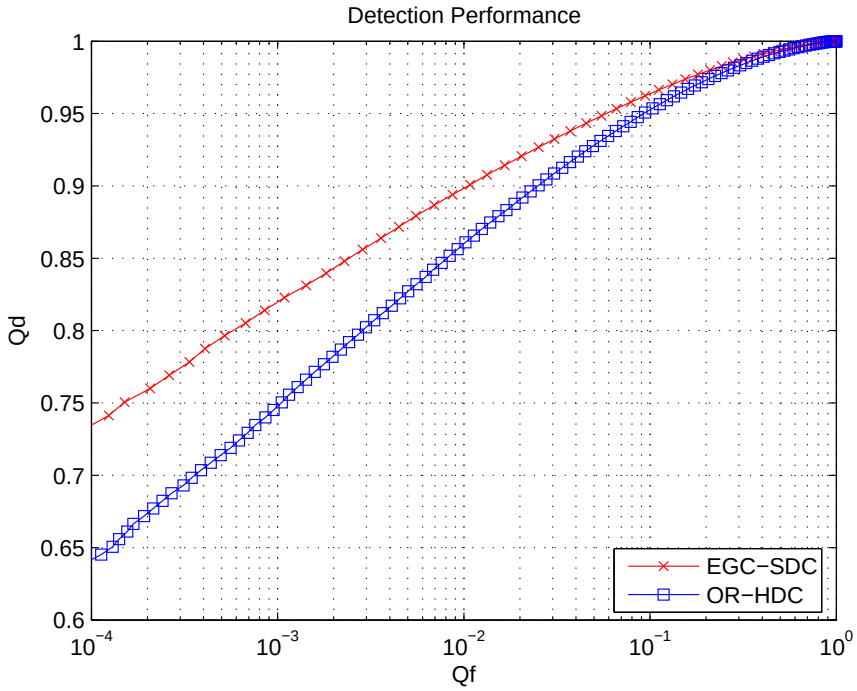

Figure 5.2: Detection Performance on EGC-SDC and OR-HDC scheme, SNR= 5dB

5.4 Analysis on EGC-SDC scheme

In this section, we provide the analysis for the probability of false alarm and detection for the EGC-SDC scheme. First, the detection performance under AWGN channel is considered. Then, the detection performance under Rayleigh fading channel is investigated. As local observations are forwarded to the fusion center, the closed-form for both Q_f and Q_d can serve as the upper bound performance for the CR's spectrum sensing.

5.4.1 EGC-SDC scheme under AWGN channel

The analysis on EGC-SDC scheme under AWGN channel was presented in [42] and the probability of false alarm and detection were given conditioned on the SNR of fading channel. Here, we presented the closed-form analysis for the probability of false alarm and detection under AWGN channel.

As previously mentioned in the EGC-SDC sensing procedures, the fusion center simply weighs and aggregates the forwarded observation from CR users [71]. When PU is idle (H_0), the local observation at CR user is Central Chi-Squared distribution with $2m$ degree of freedom [72]. Hence, at the fusion center, the equally weighed and

aggregated energy value comes from N cooperative users. Hence, the distribution here becomes Central Chi-Squared distribution with $2Nm$ degree of freedom, with a scaling factor of $\frac{1}{N}$ on the energy value as all forwarded observation is equally weighed.

Similarly, when PU is active (H_1), the local observation at CR user is Non-Central Chi-Squared distribution with $2m$ degree of freedom and non-centrality parameter of $2m\bar{\gamma}$. Hence, similarly to the false alarm, the aggregated distribution at the fusion center becomes Non-Central Chi-Squared distribution with with $2Nm$ degree of freedom and non-centrality parameter of $2Nm\bar{\gamma}$, with a scaling factor of $\frac{1}{N}$ on the energy value.

Hence, the closed-form of Q_f and Q_d for EGC-SDC channel under AWGN channel is as follows.

$$\begin{aligned} Q_f(\lambda_f) &= \frac{\Gamma(Nm, N\lambda_f/2)}{\Gamma(Nm)}. \\ Q_d(\lambda_f) &= Q_{Nm}(\sqrt{2Nm\bar{\gamma}}, \sqrt{N\lambda_f}). \end{aligned} \tag{5.2}$$

Note that the detection threshold (λ_f) here needs a scaling factor of N as fusion center equally weighs forwarded local observations, while the theoretical distribution considers simple aggegration.

5.4.2 EGC-SDC scheme under Rayleigh fading channel

In Rayleigh fading channel, Q_f is simple and exactly the same with the one in AWGN channel in (5.2), as there is only noise in H_0 and the received energy is channel-independent.

$$Q_f(\lambda_f) = \frac{\Gamma(Nm, N\lambda_f/2)}{\Gamma(Nm)}. \tag{5.3}$$

In order to consider the Q_d here, P_d in Nakagami channel, presented in (4.12), are revisited. The sum of multiple i.i.d. Rayleigh faded signals is Nakagami distributed [73,74]. Hence, the aggregated value at the fusion center is also Nakagami distributed. Here, the formula for $P_{d,Nak}$ presented in (4.12) is adopted and modified in terms of the system parameters to create a closed-form Q_d for EGC-SDC scheme.

First, consider $P_{d,Nak}(g, m, \bar{\gamma}, \lambda)$ as a function of Nakagami parameter, time-bandwidth product, average SNR and decision threshold. Then, for parameter adjustments, Table 5.1 shows comparison between system parameters used in Nakagami-m and EGC-SDC

Table 5.1: Comparison between system parameters used in Nakagami-m and EGC-SDC scheme

	Nakagami-m		EGC-SDC
Diversity	g		N
Time-bandwidth product	m		Nm
Average SNR	$\bar{\gamma}$		$Nm\bar{\gamma}$
Detection Threshold	λ		$N\lambda_f$

scheme. Hence, a closed-form for Q_d in EGC-SDC scheme becomes a function of $P_{d,Nak}$ in (4.12) with the modified parameters as

$$Q_{d,Rayl}(N, m, \bar{\gamma}, \lambda_f) = P_{d,Nak}(N, Nm, Nm\bar{\gamma}, N\lambda_f). \tag{5.4}$$

5.4.3 EGC-SDC Analysis and Simulation Results

Fig. 5.3 compares Q_f and Q_d, obtained from the simulation and the closed-form analysis. The simulation parameters are three cooperative CR users with time-bandwidth product m=3 and SNR= 3dB under Rayleigh fading channel. The result shows that the closed-form analysis perfectly matches with the simulation results.

Fig. 5.4 compares Q_f and Q_d, obtained from the simulation and the closed-form analysis. Apart from SNR being 5dB here, other simulation parameters are set exactly the same with the previous simulation. Similarly here, the figure also shows that the closed-form analysis perfectly matches with the simulation results.

5.5 Summary

In this chapter, a closed-form analysis for the Q_f and Q_d in EGC-SDC cooperative spectrum sensing scheme is provided. By knowing that a sum of Central Chi-Squared distributed RVs is also a Central Chi-Squared distributed RV with higher degree of freedom. Also, sum of Non-Central Chi-Squared distributed RVs is also Non-Central Chi-Squared distributed. Q_f and Q_d under AWGN channel is derived. Similarly, by knowing that a sum of i.i.d. Rayleigh distributed RVs is Nakagami distributed, and by modifying the P_d formula in Nakagami fading channel, the closed-form of EGC-SDC

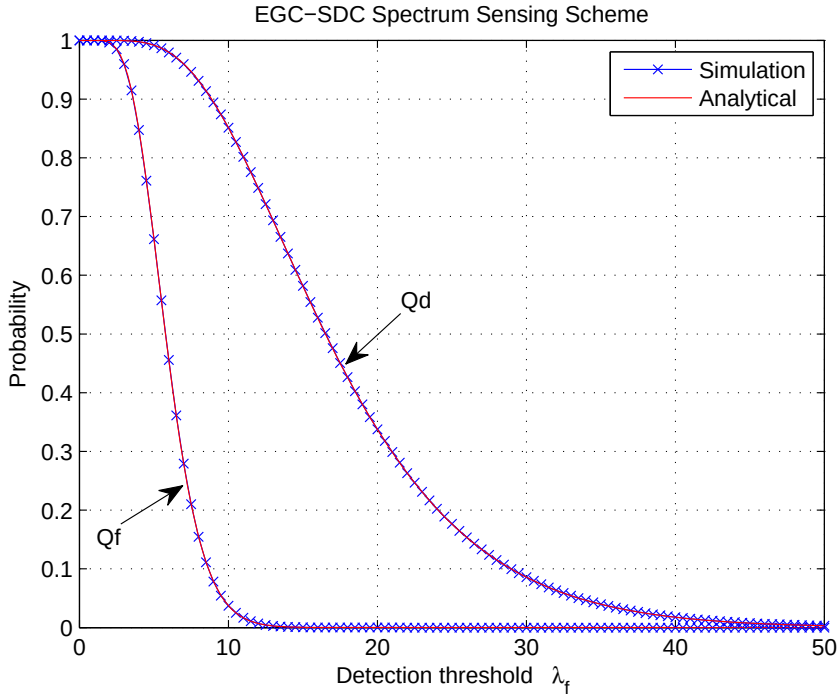

Figure 5.3: EGC-SDC Scheme : Probability of False Alarm and Detection with 3dB SNR

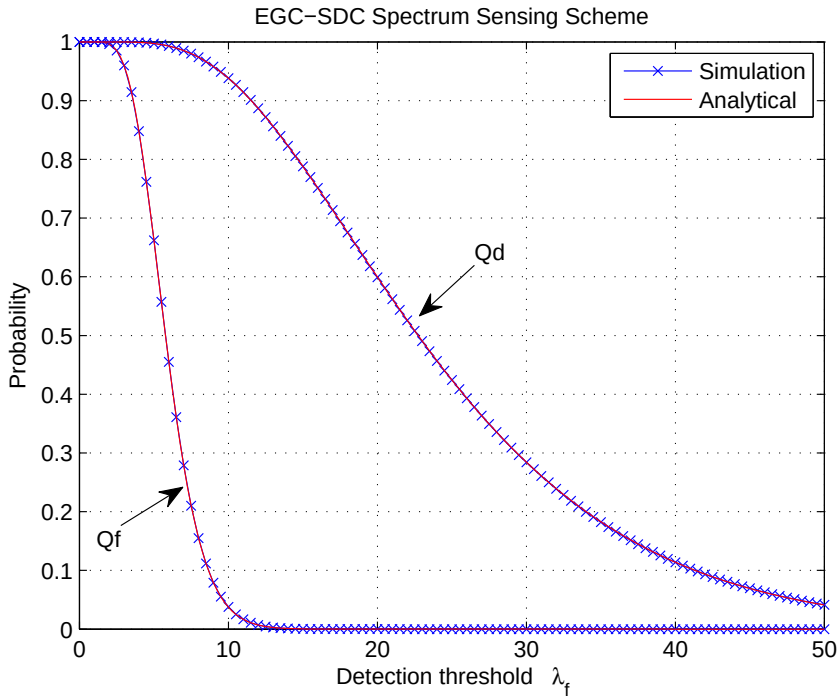

Figure 5.4: EGC-SDC Scheme : Probability of False Alarm and Detection with 5dB SNR

scheme under Rayleigh fading channel is achieved. The simulation results shown under different scenarios prove that the closed-form analysis of EGC-SDC spectrum sensing scheme is accurate.

Chapter 6

Quantized Cooperative Spectrum Sensing

6.1 Introduction

As mentioned in Chapter 4, the hidden terminal problem occurs in conventional energy detection as the CR user can experience deep fade and not be able to detect the PU. Using multiple sensing nodes, cooperative sensing can exploit spatial diversity and mitigate this problem. EGC-SDC cooperative scheme achieves good performance by equally combining the local observations from the sensing nodes. However, forwarding those observations require large feedback overheads. In order to reduce the communication overheads among CR users, quantization is applied to reduce these overheads. Applying quantization towards the observations under multisensor detection was previously proposed in various literatures such as those in [75–81].

In this chapter, we propose and investigate three quantized cooperative spectrum sensing schemes. Instead of sending the received signal energy values as in conventional SDC schemes, the CRs quantize their observations according to their received signal energy and the quantization boundaries. Then, the quantized level is forwarded to the fusion centre, which sums up all the received quantum it re-creates and compares to the fusion threshold. First the optimization for both uniform and non-uniform quantization for cooperative spectrum sensing is considered. Then, the low complexity quantized approach using an approximated CDF on H_1 is investigated. In these schemes, the optimization is based only on H_1 in order to minimize the quantization

uncertainty for the PU's signal, and hence improve the detection probability.

6.2 Sensing Procedures

The sensing procedures for the Quantized cooperative spectrum sensing scheme are as follows.

1. First, every CR user gathers its information using energy detection technique then quantizes its local observation, depending on the quantization scheme it uses.

2. Being aware of the quantization scheme including the quantization boundaries and the quanta, the fusion center then recreates the forwarded quantized energy and aggregates all of them.

3. Then, the aggregated value (T) is compared to the fusion center decition threshold (λ).

4. The final decision H_0 is made, if T is less than λ, otherwise final decision H_1 is made.

$$d = \begin{cases} H_0 & \text{, if } T < \lambda \\ H_1 & \text{, otherwise .} \end{cases} \tag{6.1}$$

5. Then, the final decision, either H_0 or H_1, is sent back to inform all CR users whether to transmit on the spectrum or not.

6.3 Uniform Quantization

For uniform quantization, the quanta for each region lies midway between its boundaries such that

$$q_i = \frac{(2i-1)\cdot Q}{2} \qquad \text{for } i = 1, 2, ..., M \tag{6.2}$$

where Q represents the width of each quantization region, M is number of quantization regions which equals to 2^n with n being the number of quantization bits.

The overall distortion for a quantizer can be measured using the MSE, given in (2.19) as

$$\text{MSE} = \int_{Q_\alpha} (y - q_\alpha)^2 \, p(y) \, dy. \tag{6.3}$$

When PU is active (H_1), the MSE of quantizing the local observations is

$$\begin{aligned} \text{MSE}(Q) = \sum_{i=1}^{M-1} \int_{(i-1)Q}^{iQ} \left[y - \frac{(2i-1)\cdot Q}{2} \right]^2 f(y|H_1)\, dy \\ + \int_{(M-1)Q}^{\infty} \left[y - \frac{(2M-1)\cdot Q}{2} \right]^2 f(y|H_1)\, dy. \end{aligned} \tag{6.4}$$

The optimal width of each quantization boundaries, i.e. the optimal Q, is the one that minimizes the MSE in (6.4). Hence, it can be derived by solving

$$\frac{d\,\text{MSE}(Q)}{dQ} = 0. \tag{6.5}$$

However, due to the complexity of $f(y|H_1)$ in (4.10), a closed-form solution is not available for (6.5). Hence, a numerical solution is required to obtain the optimal Q.

6.4 Non-uniform Quantization

The uniform quantization is optimal only for uniformly distributed RVs, while the non-uniform quantization is optimal for all the others [21]. Thus, we consider a non-uniform quantization approach that optimizes the quantization level based on the CDF of H_1. The quantization boundaries are set to equally split the CDF of signal distribution in the H_1 case, such that each region has similar probability of occurrences. In other words, this scheme applies quantization boundaries according to the percentiles of PU's signal distribution. The quantization boundaries, B_i, are defined as a quantile function or an inverse CDF function such that

$$B_i = \text{CDF}^{-1}(\frac{i}{M}), \text{ for } i = 1, 2, ..., M-1. \tag{6.6}$$

For instance, if 2-bit quantization is used, there are 4 quantization levels, and 3 quantization boundaries. The quantization boundaries are at $25^{th}, 50^{th}$ and 75^{th} percentile of PU's signal distribution respectively.

Due to the non-uniformity here, the quanta for each region is represented by the centre of mass, which can be obtained using

$$q_\alpha = \frac{\int_{Q_\alpha} y \cdot f(y|H_1)\, dy}{\int_{Q_\alpha} f(y|H_1)\, dy} \quad \text{for } \alpha = 1, 2, ..., N. \tag{6.7}$$

In order to compute the closed-form solutions for quantization boundaries in this scheme, an inverse CDF function is needed. However as the inverse CDF function cannot be analytically obtained, a numerical solution is used to find the quantization boundaries as well as the quanta.

6.5 Approximated Scheme

In Section 6.6, it will be shown that the Non-uniform scheme performs close to the non quantized EGC-SDC scheme, presented in Chapter 5. However, a numerical solution is required to obtain the quantization boundaries, which has high computational complexity. Here, consider an approximated scheme, which makes use of P_d approximation so that an approximated inverse CDF can be obtained. As presented in (4.16), the approximated probability of detection is

$$\tilde{P}_d(\lambda) = e^{-\frac{\lambda}{2(1+m\bar{\gamma})}} \times \left(1 + \frac{1}{m\bar{\gamma}}\right)^{m-1}. \tag{6.8}$$

Hence, the approximated inverse CDF function can be obtained as

$$\begin{aligned} \lambda &= \text{CDF}^{-1}(x) \\ &= -2(1+m\bar{\gamma}) \times \log_e\big[(1-x)\cdot(1+\frac{1}{m\bar{\gamma}})^{1-m}\big]. \end{aligned} \tag{6.9}$$

Since the approximation is accurate when λ is large, it is used to determine the quantization boundaries in high quantization levels, but not those where λ is small. Specifically, the approximated inverse CDF function is used for boundaries above the 50^{th} percentile. For the lower λ region, uniform quantization is used such that all the levels are equally spaced. The quantization boundaries are therefore defined as

$$B_i = \begin{cases} \frac{2i}{M} \cdot \text{CDF}^{-1}(\frac{1}{2}) & , i = 1, 2, .., \frac{M}{2} - 1 \\ \text{CDF}^{-1}(\frac{i}{M}) & , i = \frac{M}{2}, \frac{M}{2} + 1, .., M - 1. \end{cases} \tag{6.10}$$

For implementation simplicity, it is assumed that the quanta for each region lies midway between its boundaries. For the last region, since the upper limit is infinity, this

approach cannot be used. In order to maintain the low complexity of this scheme, the same spacing is kept between the quanta and the boundary of the previous region (i.e., $B_{M-1} - q_{M-1}$, which equals to $^{(B_{M-1}-B_{M-2})}/_{2}$) for this region. Therefore, the quanta are computed by

$$q_i = \begin{cases} \frac{B_{i-1}+B_i}{2} & , i = 1, 2, .., M-1 \\ \frac{3B_{M-1}-B_{M-2}}{2} & , i = M \end{cases} \tag{6.11}$$

where $B_0 = 0$. The rest of the sensing procedures are similar with two previously mentioned techniques.

6.6 Simulation Results

Here, the three schemes are evaluated using computer simulation. Three spatially separated users are considered for cooperative spectrum sensing. The time-bandwidth product is set to 3 for each observation. The PU's SNR is 5dB and the channel is modelled as Rayleigh fading channel and the communication channels between CR users and the fusion center is assumed error-free.

The detection performance for these proposed schemes are evaluated and compared to the OR-HDC and EGC-SDC scheme. Both schemes serve as the lower bound and upper bound performance of the proposed quantized approaches. In the Uniform and Non-uniform scheme, the width of each quantization boundaries needs to be numerically optimized. The optimal Q is found to be 14.56 in 3-bit Uniform scheme for current simulation parameters. In the Non-uniform scheme, the optimal quantization boundaries and quanta are numerically obtained according to (6.6) and (6.7). In the Approximated scheme, the quantization boundaries and quanta are calculated according to (6.10) and (6.11). The quantization boundaries and quanta for the Non-uniform and Approximated scheme are shown in Table 6.1 and Table 6.2 respectively. It is shown that the approximation is accurate in the region where the detection threshold is high, i.e. 4^{th} region onwards, as the approximated quantization boundaries are very close to those in the Non-uniform scheme.

Fig. 6.1 and 6.2 show the detection performance for the proposed schemes with three and four quantization bits respectively. Simulation results show that with the same number of quantization levels, the Non-uniform and Approximated scheme

Region	Boundaries	Quanta
1^{st}	0 to 6.483	4.315
2^{nd}	6.483 to 10.103	8.292
3^{rd}	10.103 to 14.032	12.021
4^{th}	14.032 to 18.737	16.301
5^{th}	18.737 to 24.775	21.612
6^{th}	24.775 to 33.279	28.740
7^{th}	33.279 to 47.817	39.715
8^{th}	47.817 onwards	68.791

Table 6.1: Quantization boundaries and quanta for Non-uniform scheme with 3-bit quantization

Region	Boundaries	Quanta
1^{st}	0 to 4.685	2.342
2^{nd}	4.685 to 9.371	7.028
3^{rd}	9.371 to 14.056	11.713
4^{th}	14.056 to 18.742	16.399
5^{th}	18.742 to 24.775	21.758
6^{th}	24.775 to 33.279	29.027
7^{th}	33.279 to 47.817	40.548
8^{th}	47.817 onwards	55.086

Table 6.2: Quantization boundaries and quanta for Approximated scheme with 3-bit quantization

achieve better performance than the Uniform scheme. This verifies that for non-uniform distribution, uniform quantization is not a suitable approach. Both figures show that the detection performance achieved by the Approximated scheme is very close to that of the Non-uniform scheme, which is numerically optimized. In particular, the detection performance for 4-bit Non-uniform and Approximated scheme closely approaches that of EGC-SDC.

The Uniform and Non-uniform schemes require numerical calculation for quantization boundaries and quanta, which are complex. These issues can be solved by an offline calculation and CR users only need to store the values for the particular cases. Another approach is for the fusion centre to provide these values to the CR users and update their quantization boundaries and quanta. Nevertheless, these schemes place high computational burden on CR system.

On the contrary, the Approximated scheme is simple to implement and the quantization boundaries can be computed at the CR users. With a close performance to the Non-uniform and EGC-SDC scheme, the approximated approach is highly beneficial for cooperative spectrum sensing. Moreover, in terms of the communication overheads, only three or four bits are required in this scheme to achieve the performance close to that of EGC-SDC scheme.

6.7 Analysis on Quantized Cooperative Spectrum Sensing

The generic form for the probability of false alarm and detection, Q_f and Q_d for this quantized cooperative spectrum sensing scheme is analysed in this section. In fact, both Q_f and Q_d are the probability mass function (PMF) summation of the discrete CR's forwarded quanta value, where the summation is larger than the detection threshold. It can be formulated as

$$\begin{aligned} Q_f &= \sum_{\forall i,\, qs_i > \lambda_f} p_i | H_0 \\ Q_d &= \sum_{\forall i,\, qs_i > \lambda_f} p_i | H_1 \end{aligned} \tag{6.12}$$

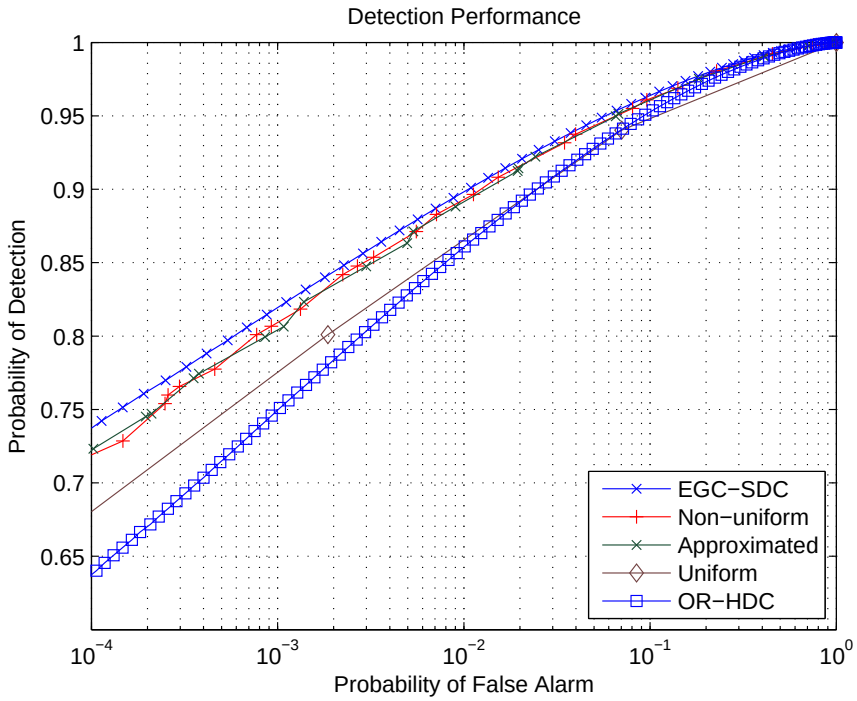

Figure 6.1: Detection performance for the proposed schemes with three-bit quantization

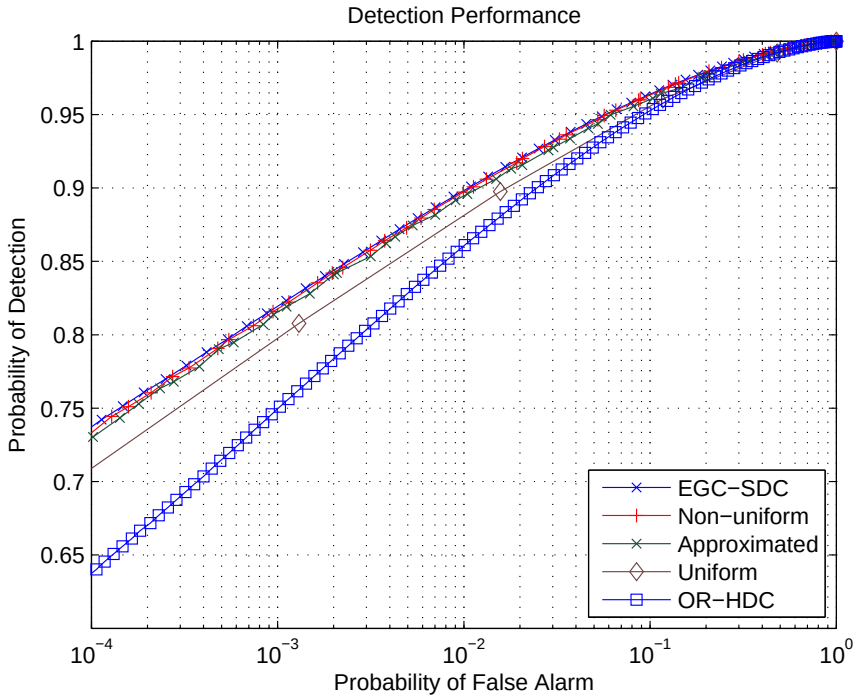

Figure 6.2: Detection performance for the proposed schemes with four-bit quantization

where p_i and qs_i represents the PMF and the value for the i^{th} quanta sum at the fusion center.

For illustration, we assume that two-bit quantization is applied to two cooperative users. First, the probability of occurence of the area under curve, where the quantization boundaries split, is defined. The probability of having each quanta representing the received energy when PU is active (H_1) is as follows.

$$\begin{aligned}\gamma_1 &= 1 - P_d(B_1) \\ \gamma_2 &= P_d(B_1) - P_d(B_2) \\ \gamma_3 &= P_d(B_2) - P_d(B_3) \\ \gamma_4 &= P_d(B_3)\end{aligned} \tag{6.13}$$

where γ_i represents the probability that CR user quantizes its received energy as q_i. For the Non-uniform scheme, where the received energy is equally split under the case when PU is active (H_1), the value for each γ_i is the same. Then, at the fusion center, the sum of quanta which are forwarded from each user are also discrete. Q_f and Q_d can be obtained by the summation of all p_i where the corresponding qs_i is larger than the detection threshold, as shown in (6.12).

Fig. 6.3 shows the PMF for quanta value at the local CR user when Non-uniform scheme with two-bit quantization is applied. The PU's SNR is 5dB with time-bandwidth of 3. Fig. 6.4 shows the PMF for quanta value at the fusion center under the same scenario. Note that the first quanta sum value is similar to the first quanta at CR users, since the quanta sum are weighted by the number of cooperative CR users. Finally, Fig. 6.5 compares Q_f and Q_d from this analysis with the simulated results, and shows that the analytical Q_f and Q_d closely match with the simulated results

6.8 Summary

In this chapter, the quantization-based cooperative spectrum sensing techniques were investigated. By applying quantization to local observations, the communication overhead among CR users are reduced while retaining a good detection performance. Simulation results showed that the proposed schemes can achieve good detection performance. In particular, the detection performance of the Non-uniform scheme almost

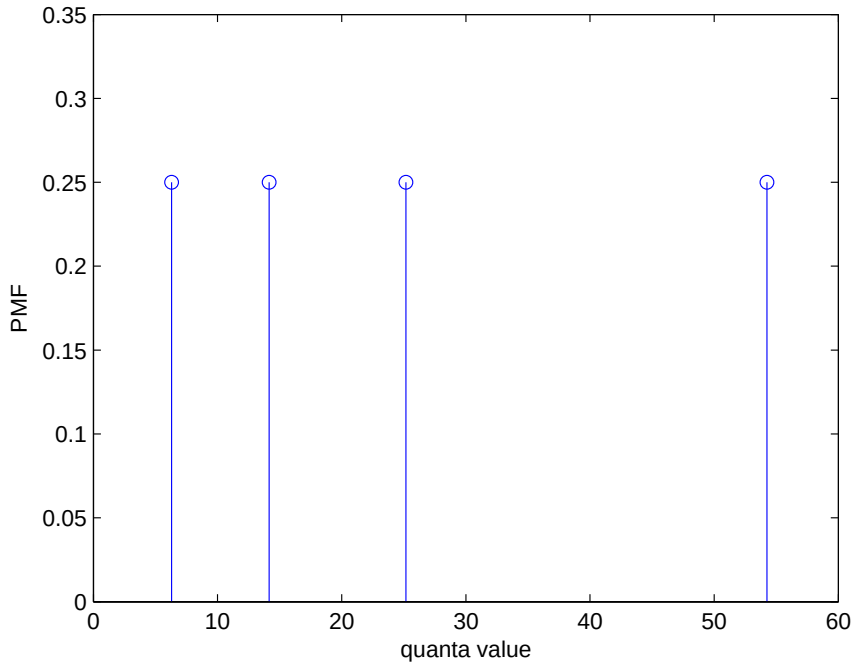

Figure 6.3: PMF for the quanta value at CR users when PU is active (H_1)

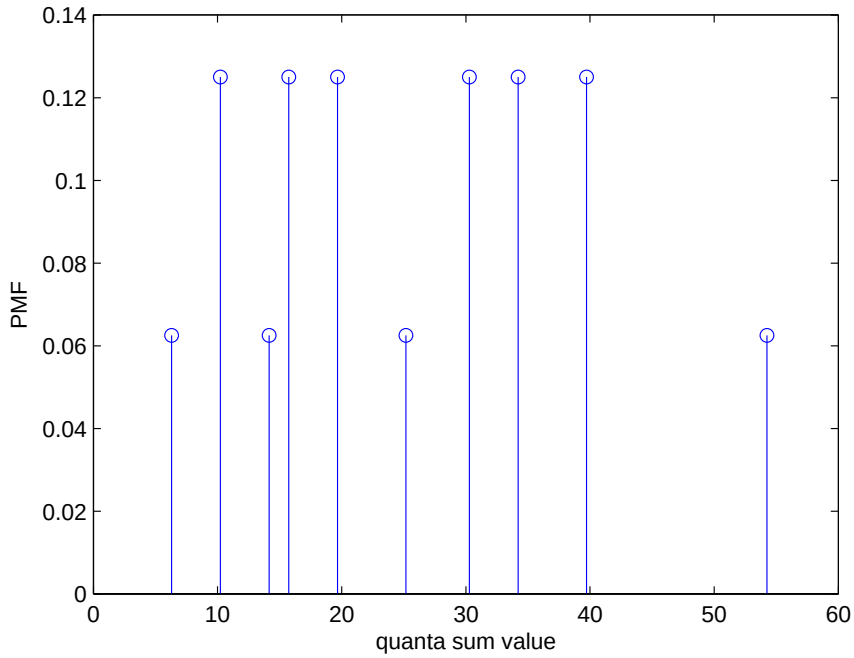

Figure 6.4: PMF for the quanta sum value at the fusion center when PU is active (H_1)

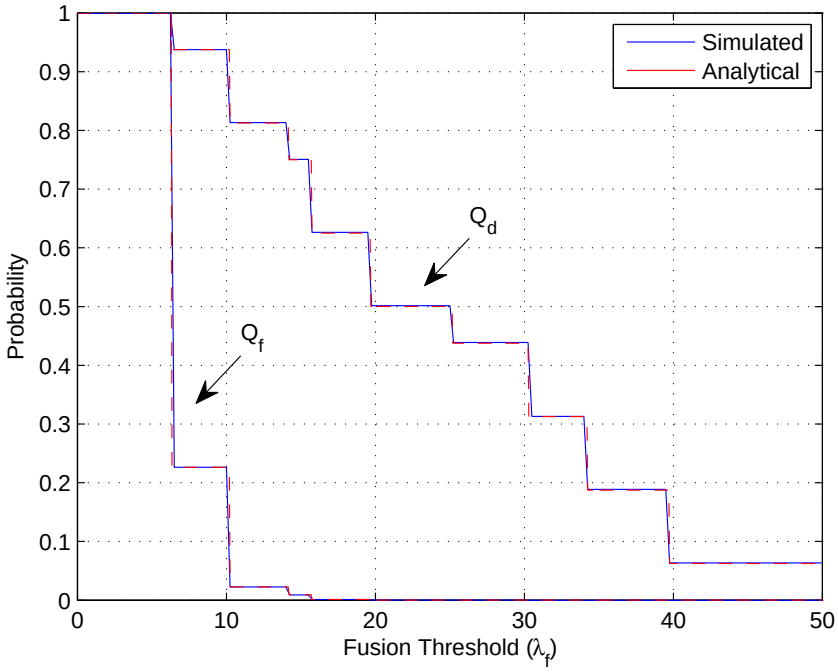

Figure 6.5: Quantized Cooperative Spectrum Sensing schemes: Probaility of false alarm and detection

matches that of the EGC-SDC scheme. By applying an approximation to the CDF of H_1, the computational complexity is significantly reduced while retaining similar detection performance to the numerically optimized non-uniform scheme. This Approximated scheme allows CR users to adapt its sensing parameters with very low complexity and make it suitable for real-time cooperative spectrum sensing. The generic analysis for Quantized Cooperative spectrum sensing scheme is also derived. An illustratation on the analysis under Non-uniform scheme is also provided.

Chapter 7

Double Threshold Cooperative Spectrum Sensing

7.1 Introduction

The main difference for the Double Threshold Energy Detection scheme to SDC and HDC scheme is the type of data which is forwarded to the fusion centre. In SDC scheme, local observation is forwarded to the fusion centre. In HDC scheme, one-bit local decision is forwarded, while, in Double Threshold scheme, information which is forwarded to the fusion centre could be either local observation or local decision.

Various techniques, related to the Double Threshold scheme, have been previously proposed. Censoring method on the uncertain area is considered in [82–85] in order to decrease the bandwidth constraints and average number of sensing bits. Any CR user, with local observation falling in uncertain area, will stay silent and send nothing to the fusion centre, as its own observation is not reliable enough. If all CR users stay silent, it will cause a fail sensing problem. This scheme can greatly help decrease the average number of sensing bits to the fusion centre with only little loss in performance. Also in [86], neither local observation or decision is sent to the fusion centre, if the local observation falls in the uncertain area. However, fail sensing can occur when no CR reports its decision. This scheme aims to solve the fail sensing problem by applying the reputation score. If fail sensing occurs, the fusion centre will ask the CR user with the highest reputation to make a local decision based on the conventional single threshold method. Instead of leaving the uncertain area out, the work proposed in [87] makes

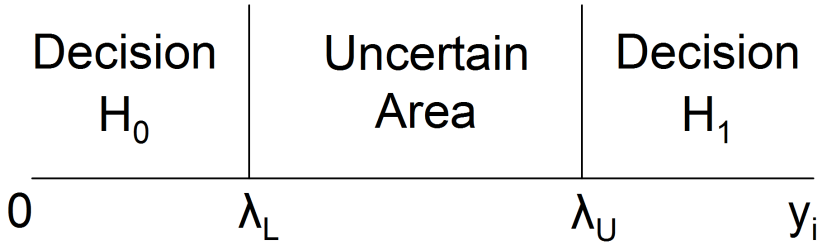

Figure 7.1: Double Threshold Energy Detection Technique

use of the uncertain area. The local observation, in the uncertain area, is forwarded to the fusion centre. This method can improve the overall detection performance for the CR system. However, AWGN channel is considered here and both lower and upper threshold are defined using the area between two thresholds without defining where both thresholds are. Throughput benefit of using double threshold is illustrated in [88]. In [89], the Double threshold scheme is proposed to tackle untrusted nodes with malicious effects such as always reporting PU's absence or existence.

In this chapter, we investigate the scheme proposed in [87] and propose a modified version of that technique in terms of the detection scheme and sensing procedures.

7.2 Double Threshold Spectrum Sensing Procedures

Here, sensing procedures for Double Threshold schemes are presented. First, in Section 7.2.1, sensing procedure for the simple Double Threshold scheme is covered. Then, in Section 7.2.2, the procedures for the Double Threshold scheme with quantization applied to the forwarded local observations are presented.

7.2.1 Double Threshold Scheme

In Double Threshold energy detection scheme, the local observation at CR users is divided into three regions by two thresholds, which are the lower threshold and upper threshold λ_L and λ_U respectively as shown in Fig 7.1. Local decision is made when received energy signal falls into the region below λ_L or above λ_U. Otherwise, it is not sufficient for making a local decision as the local observation falls in the uncertain area.

The detailed sensing procedures for Double Threshold scheme are as follows.

1. First, the local energy observation is compared to λ_L and λ_U. CR user makes a local decision of H_0, if the observation is less than λ_L. However, if it is more than λ_U, the local decision of H_1 is made. Otherwise, the local decision is not made as the CR is uncertain about its observation.

$$D_i = \begin{cases} H_0 & \text{for } y_i < \lambda_L \\ H_1 & \text{for } y_i > \lambda_U \\ \text{no decision made and } L_i \text{ is forwarded} & \text{otherwise} \end{cases} \tag{7.1}$$

   where D_i is the forwarded local decision.

2. Then, either local decision or observation is forwarded to the fusion center.

3. At the fusion center, all forwarded local observations (L_i) are aggregated and compared to the fusion threshold λ_f to make a fusion decision.

$$\text{fusion decision} = \begin{cases} H_0 & \text{for } \sum L_i < \lambda_f \\ H_1 & \text{otherwise} \end{cases} \tag{7.2}$$

   where L_i is the forwarded local observation.

4. Finally, all forwarded decision (D_i) and the fusion decision are combined using the OR-rule to make the final decision.

$$\text{final decision} = \begin{cases} H_0 & \text{if all } D_i \text{ and fusion decision is } H_0 \\ H_1 & \text{otherwise} \end{cases} \tag{7.3}$$

7.2.2 Double Threshold Scheme with Quantization

In the previous section, it is assumed that the local observation forwarded to the fusion centre is non-quantized such that there is no distortion between the local observation at CR user and the one received at the fusion centre. Here, to reduce the communication overhead between CR users and the fusion center, we proposed that quantization is applied to the forwarding process for the uncertain users, i.e. users forwarding its local observation. Hence, the only difference here to the scheme mentioned above are the additional quantization process. The rest of the sensing procedures are similar to the Double Threshold scheme. On the quantization scheme, the uniform quantization is very simple on how to define the quantization boundaries and the quanta. Hence, for this reason, we only apply the uniform quantization to the uncertain area and do not consider the non-uniform one, which we considered in Chapter 6.

The details of quantization procedures are as follows

1. A uniform quantization is applied to the local observation in the unknown area. The area between lower and upper threshold are divided into a number of areas, depending on number of quantization-bit.

2. Then, CR user forwards the quantized value of local observation to the fusion centre.

3. As the fusion center is aware of the quantization, it re-creates the local observation to the quantum value for each region. We assume that the quantum for each region lies midway between its quantization boundaries. The fusion center then sums all the quantum up and compares to fusion threshold to make fusion decision, as shown in (7.2).

7.3 Double Threshold Analysis

In this section, an analysis on the Double Threshold scheme is provided. An analytical closed-form for cooperative probability of false alarm and detection as well as the bandwidth requirement is given.

7.3.1 Regions defined by Lower and Upper Threshold

In order to analyze the detection performance on the Double Threshold scheme, the related fundamental statistics need to be defined first. Here, parameters α, β, γ, illustrated in Fig. 7.2 and 7.3 respectively for H_0 and H_1, define the probability that the local observation is less or more than a particular threshold, conditioned on the PU's state, such that

$$\begin{aligned} \alpha_i &= P\{y < \lambda_L | H_i\} \\ \beta_i &= P\{\lambda_L < y < \lambda_U | H_i\} \\ \gamma_i &= P\{y > \lambda_U | H_i\} \\ \alpha_i + \beta_i + \gamma_i &= 1 \end{aligned} \tag{7.4}$$

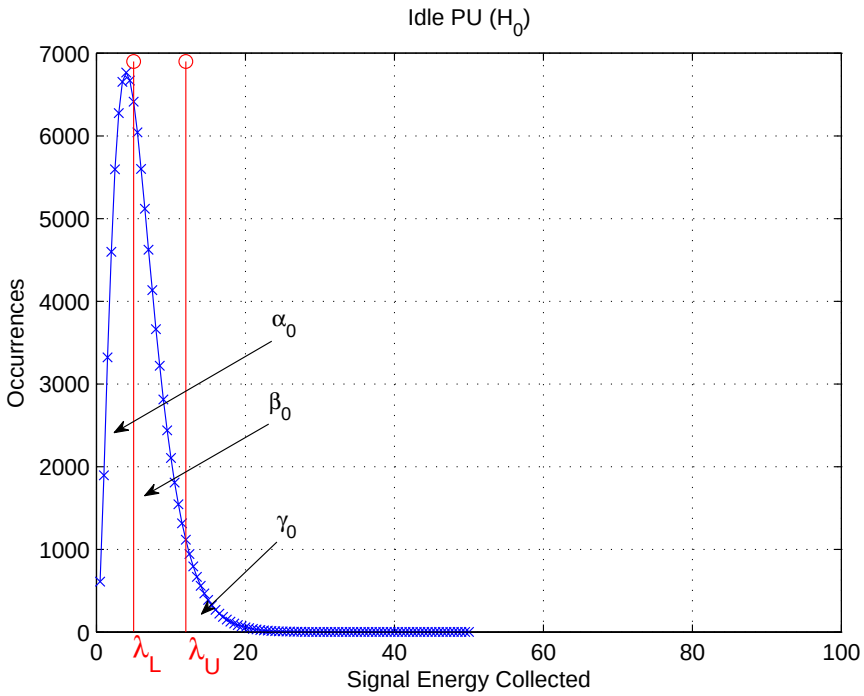

Figure 7.2: Double Threshold Scheme : Three regions separated by λ_L and λ_U on H_0.

In case that PU is idle (H_0), these parameters are statistically given as

$$\begin{aligned} \alpha_0 &= 1 - P_f(\lambda_L) \\ \beta_0 &= P_f(\lambda_L) - P_f(\lambda_U) \\ \gamma_0 &= P_f(\lambda_U) \\ \alpha_0 + \beta_0 + \gamma_0 &= 1. \end{aligned} \tag{7.5}$$

Similarly, when PU is active (H_1), they are given as

$$\begin{aligned} \alpha_1 &= 1 - P_d(\lambda_L) \\ \beta_1 &= P_d(\lambda_L) - P_d(\lambda_U) \\ \gamma_1 &= P_d(\lambda_U) \\ \alpha_1 + \beta_1 + \gamma_1 &= 1. \end{aligned} \tag{7.6}$$

7.3.2 Communication Overhead Requirement

In Double Threshold scheme, either local decision or local observation is sent to the fusion center. Hence, the communication overhead requirement is defined by whether and how often a CR user forwards its decision or observation.

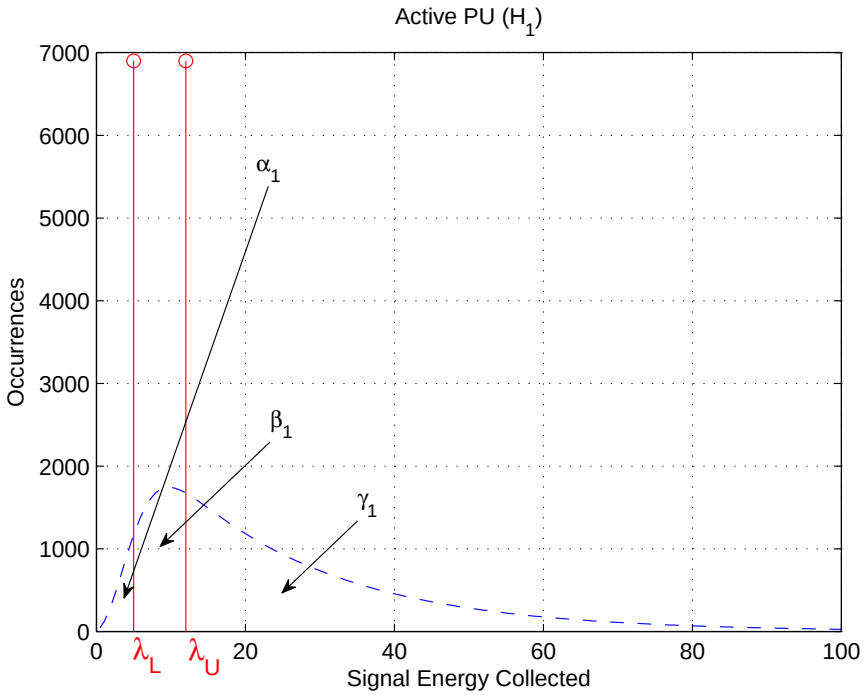

Figure 7.3: Double Threshold Scheme : Three regions separated by λ_L and λ_U on H_1.

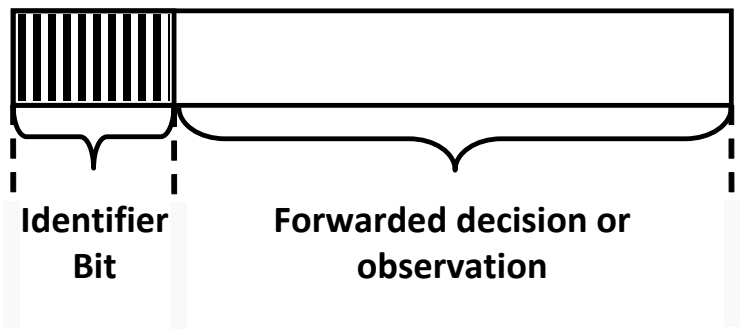

Figure 7.4: Double Threshold Scheme : Frame structure for the forwarding process

First, a frame structure for the forwarding process is modelled and illustrated here in Fig.7.4. For completeness of the scheme to identify whether either local decision or observation is forwarded, the first one-bit identifier is used to inform the fusion center about the following data. Then, either local observation or one-bit decision follows. If the local observation forwarded is quantized, then n quantization bits are required. However, if local observation forwarded is non-quantized, 16 bits are required assuming that binary16, IEEE754 half precision floating-point format [90] is adopted.

Then, to consider bandwidth requirement, the probability that the received signal falls within uncertain area and CR user forwards its local observation is defined as follows.

$$P\{\text{local observation is forwarded}\} = \begin{cases} \beta_0 & \text{, PU is idle} \\ \beta_1 & \text{, PU is active} \end{cases} \tag{7.7}$$

In case that PU is idle (H_0), the communication overhead requirement is

$$\text{required bits} = [(1+1)\cdot(1-\beta_0) + (1+n)\cdot\beta_0] \tag{7.8}$$

assuming that n bits are required for forwarding the observation.

Similarly, when PU is active (H_1), it is

$$\text{required bits} = [(1+1)\cdot(1-\beta_1) + (1+n)\cdot\beta_1]\,. \tag{7.9}$$

Hence, an average bandwidth requirement is given as

$$\begin{aligned} \text{average bits} &= P(H_0) * [(1+1)\cdot(1-\beta_0) + (1+n)\cdot\beta_0] \\ &\quad + P(H_1) * [(1+1)\cdot(1-\beta_1) + (1+n)\cdot\beta_1] \\ &= 2 + (n-1)\cdot[P(H_0)\cdot\beta_0 + P(H_1)\cdot\beta_1]\,. \end{aligned} \tag{7.10}$$

7.3.3 Cooperative Probablility of False alarm and Detection

In this section, an analysis on cooperative probability of false alarm and detection is presented. First, the generic form for Q_f and Q_d is investigated in this section. Then, the detection performance bounds are considered in Section 7.3.4. Finally, the analytical Q_f and Q_d is compared to the simulation results in Section 7.4.3.

The probability of correct rejection, Q_{cr} is defined as the probability that CR correctly decides that PU is idle. In other words, it is the probability that the final

decision (F) is H_0, while PU is idle (H_0). First, let N be the number of all cooperating users, k is the number of certain users reporting local decision, L is the forwarded local observation and D is the forwarded local decision.

$$\begin{aligned} Q_{cr} &= P\{F=0\} \\ &= P\{F=0, k\neq N\} + P\{F=0, k=N\} \\ &= P\{\sum L_i = 0, k\neq N\} \cdot P\{D=0, k\neq N\} \\ &\quad + P\{\sum L_i = 0, k=N\} \cdot P\{D=0, k=N\} \\ &= \left[\sum_{k=0}^{N-1} \begin{pmatrix} N \\ k \end{pmatrix} \cdot \alpha_0^k \cdot \beta_0^{N-k} \cdot P\{\sum_{i=1}^{N-k} F_i < \lambda_f\}\right] + \left[\alpha_0^N \cdot (1)\right]. \end{aligned} \tag{7.11}$$

Then, Q_f is

$$Q_f = 1 - Q_{cr}. \tag{7.12}$$

The probability of missed detection, Q_m can be derived, similarly with the derivation of Q_{cr} in (7.11), as

$$Q_m = \left[\sum_{k=0}^{N-1} \begin{pmatrix} N \\ k \end{pmatrix} \cdot \alpha_1^k \cdot \beta_1^{N-k} \cdot P\{\sum_{i=1}^{N-k} F_i < \lambda_f\}\right] + \left[\alpha_1^N \cdot (1)\right]. \tag{7.13}$$

Then, Q_d is

$$Q_d = 1 - Q_m. \tag{7.14}$$

7.3.4 Bounds on Detection Performance

In this section, the detection performance bounds of this scheme are investigated. The lower and upper bounds on both Q_f and Q_d are analyzed.

Lower Bound on Q_f and Q_d

The lower bound occurs when the fusion decision is always H_0 such that

$$P\{\sum_{i=1}^{N-k} F_i > \lambda_f\} = 0 \tag{7.15}$$

or

$$P\{\sum_{i=1}^{N-k} F_i < \lambda_f\} = 1. \tag{7.16}$$

Hence, considering (7.11), Q_{cr} becomes

$$\begin{aligned} Q_{cr} &= \left[\sum_{k=0}^{N-1} \begin{pmatrix} N \\ k \end{pmatrix} \cdot \alpha_0^k \cdot \beta_0^{N-k} \cdot P\{\sum_{i=1}^{N-k} F_i < \lambda_f\}\right] + \left[\alpha_0^N \cdot (1)\right] \\ &= \left[\sum_{k=0}^{N-1} \begin{pmatrix} N \\ k \end{pmatrix} \cdot \alpha_0^k \cdot \beta_0^{N-k} \cdot (1)\right] + \left[\alpha_0^N \cdot (1)\right] \\ &= \left[\sum_{k=0}^{N} \begin{pmatrix} N \\ k \end{pmatrix} \cdot \alpha_0^k \cdot \beta_0^{N-k} \cdot (1)\right] \\ &= (\alpha_0 + \beta_0)^N \end{aligned} \tag{7.17}$$

Hence, lower bound on Q_f is

$$\begin{aligned} Q_f &= 1 - (\alpha_0 + \beta_0)^N \\ &= 1 - (1 - \gamma_0)^N \end{aligned} \tag{7.18}$$

Applying similar derivation in (7.17) and (7.18) to (7.13), the lower bound on Q_d is

$$\begin{aligned} Q_d &= 1 - (\alpha_1 + \beta_1)^N \\ &= 1 - (1 - \gamma_1)^N \end{aligned} \tag{7.19}$$

This lower bound is equivalent to the detection performance obtained from the OR-HDC scheme with the local detection threshold of λ_U.

Upper Bound on Q_f and Q_d

The upper bound occurs when the fusion decision is always H_1 such that

$$P\{\sum_{i=1}^{N-k} F_i > \lambda_f\} = 1 \tag{7.20}$$

or

$$P\{\sum_{i=1}^{N-k} F_i < \lambda_f\} = 0. \tag{7.21}$$

Hence, considering (7.13), Q_{cr} becomes

$$\begin{aligned} Q_{cr} &= \left[\sum_{k=0}^{N-1} \begin{pmatrix} N \\ k \end{pmatrix} \cdot \alpha_0^k \cdot \beta_0^{N-k} \cdot P\{\sum_{i=1}^{N-k} F_i < \lambda_f\}\right] + \left[\alpha_0^N \cdot (1)\right] \\ &= \left[\sum_{k=0}^{N-1} \begin{pmatrix} N \\ k \end{pmatrix} \cdot \alpha_0^k \cdot \beta_0^{N-k} \cdot (0)\right] + \left[\alpha_0^N \cdot (1)\right] \\ &= (\alpha_0)^N \end{aligned} \tag{7.22}$$

Hence, upper bound on Q_f becomes

$$Q_f = 1 - (\alpha_0)^N \tag{7.23}$$

Applying similar derivation in (7.22) and (7.23) to (7.13), upper bound on Q_d is

$$Q_d = 1 - (\alpha_1)^N \tag{7.24}$$

Similarly to the lower bound, this upper bound is equivalent to the detection performance obtained from the OR-HDC scheme with the local detection threshold of λ_L. This relationship explains why Receiver Operating Characteristic (ROC) curve for Double Threshold scheme adjoins with that of OR-HDC in Fig.7.5, 7.6 and 7.7.

7.3.5 Q_f and Q_d for Two-User Double Threshold scheme

In this section, the closed-form of Q_f and Q_d for this Double Threshold scheme is considered for the case with two cooperating users. Refering to (7.11) to (7.14), the closed-form of Q_f and Q_d is dependent on the probability of fusion decision, $P\{\sum_{i=1}^{N-k} F_i < \lambda_f\}$. As this term is the linear summation of the forwarded observation from each uncertain user, $\sum_{i=1}^{N-k} F_i$ becomes a joint distribution. Hence, the Q_f and Q_d analysis are dependent on the number of users reporting local observations. It was shown in previous section that λ_L and λ_U define the lower and upper bounds of Q_f and Q_d. Here, we consider the case when at least one CR user has its received signal energy falling within the uncertain region, i.e. between λ_L and λ_U. First, it is considered when only one uncertain user reports its local observation. Then, two uncertain users case is considered. We do not further proceed to consider the three users case, as the summation of three independent RVs is much more complicated and makes the analysis more difficult. Moreover, later in this section, it will be shown that the summation of RVs in two user

cases is complicated and we resolve this by approximating the PDF of received signal energy.

One uncertain user

Here, the term $P\{\sum_{i=1}^{N-k} F_i < \lambda_f\}$, when only one user reports local observation, is considered. CR user only reports local observation when it is between λ_L and λ_U. As PU could be either idle or active, the probability is separately considered.

First, consider when PU is active (H_1). Let z represents the forwarded observation received at the fusion center.

$$z = \begin{cases} y_{\text{user1}} & \text{, for } \lambda_L < y_{\text{user1}} < \lambda_U \\ 0 & \text{, otherwise} \end{cases} \tag{7.25}$$

where y_{user1} is the forwarded local observation from CR user 1.

As a result, z becomes a truncated RV for which the PDF is the normalised and truncated version of the PDF when PU is active as shown in (4.10) and is given as

$$f_z(z|H_1) = \begin{cases} {}^{f(y|H_1)}/_{\beta_1} & \text{, for } \lambda_L < z < \lambda_U \\ 0 & \text{, otherwise .} \end{cases} \tag{7.26}$$

Therefore, the CDF of z or $P\{\sum_{i=1}^{1} F_i < \lambda_f|H_1\}$ becomes

$$P\{\sum_{i=1}^{1} F_i < \lambda_f|H_1\} = \begin{cases} 0 & \text{, for } 0 < \lambda_f < \lambda_L \\ \dfrac{P_d(\lambda_L) - P_d(\lambda_f)}{\beta_1} & \text{, for } \lambda_L < \lambda_f < \lambda_U \\ 1 & \text{for } \lambda_f > \lambda_U \text{ .} \end{cases} \tag{7.27}$$

Then, similar to the above, when PU is idle (H_0), the PDF of z is given as

$$f_z(z|H_0) = \begin{cases} {}^{f(y|H_0)}/_{\beta_0} & \text{, for } \lambda_L < z < \lambda_U \\ 0 & \text{, otherwise} \end{cases} \tag{7.28}$$

and the CDF of z or $P\{\sum_{i=1}^{1} F_i < \lambda_f|H_0\}$ becomes

$$P\{\sum_{i=1}^{1} F_i < \lambda_f|H_0\} = \begin{cases} 0 & \text{, for } 0 < \lambda_f < \lambda_L \\ \dfrac{P_f(\lambda_L) - P_f(\lambda_f)}{\beta_0} & \text{, for } \lambda_L < \lambda_f < \lambda_U \\ 1 & \text{, for } \lambda_f > \lambda_U \text{ .} \end{cases} \tag{7.29}$$

Two uncertain users

Here, consider the case that there are two uncertain users reporting its local observation. Hence, z becomes

$$z = \begin{cases} y_{\text{user1}} + y_{\text{user2}} & \text{, for } \lambda_L < y_{\text{user1}} < \lambda_U \text{ and } \lambda_L < y_{\text{user2}} < \lambda_U \\ 0 & \text{, otherwise .} \end{cases} \tag{7.30}$$

which is a RV of a distribution which follows a summation of two truncated distributions.

First, consider when PU is active (H_1). Both PDFs of y_{user1} and y_{user2} become a truncated PDF of (4.10) as

$$f_{trun,y}(y|H_1) = \begin{cases} f_y(y|H_1)/\beta_1 & \text{, for } \lambda_L < y < \lambda_U \\ 0 & \text{, otherwise .} \end{cases} \tag{7.31}$$

However, as mentioned in Section 4.3 that the PDF $f_y(y|H_1)$ is complicated, the approximated version $\tilde{f}(y|H_1)$, presented in (4.18), is adopted here for simplicity purpose.

$$\tilde{f}(y|H_1) = \frac{e^{-\frac{1}{2(1+m\bar{\gamma})}y}}{2 \cdot (1+m\bar{\gamma}) \cdot (\frac{m\bar{\gamma}}{1+m\bar{\gamma}})^{m-1}}. \tag{7.32}$$

Hence (7.31) becomes

$$f_{trun,y}(y|H_1) = \begin{cases} \dfrac{\tilde{f}_y(y|H_1)}{\beta_1} & \text{, for } \lambda_L < y < \lambda_U \\ 0 & \text{, otherwise .} \end{cases} \tag{7.33}$$

or

$$f_{trun,y}(y|H_1) = \begin{cases} \dfrac{e^{-\frac{1}{2(1+m\bar{\gamma})}y}}{A_1 \cdot \beta_1} & \text{, for } \lambda_L < y < \lambda_U \\ 0 & \text{, otherwise .} \end{cases} \tag{7.34}$$

where

$$A_1 = 2 \cdot (1+m\bar{\gamma}) \cdot (\frac{m\bar{\gamma}}{1+m\bar{\gamma}})^{m-1}. \tag{7.35}$$

Consequently, PDF for a summation z is obtained by integrating the PDF of both RVs such that

$$f_z(z|H_1) = \int_{-\infty}^{\infty} f_{trun,y}(z-y|H_1)\, f_{trun,y}(y|H_1)\, dy. \tag{7.36}$$

As $f_{trun,y}$ is a truncated distribution, an integration region for both y and $z-y$ needs to be considered. $f_{trun,y}(y|H_1)$ and $f_{trun,y}(z-y|H_1)$ has value or is not zero only when

$$\lambda_L \leq y \leq \lambda_U \tag{7.37}$$

for $f_{trun,y}(y|H_1)$.

Whereas for $f_{trun,y}(z-y|H_1)$, the relevant y is

$$\begin{aligned} \lambda_L \leq z-y \leq \lambda_U \\ \lambda_L - z \leq -y \leq \lambda_U - z \\ z-\lambda_U \leq y \leq z-\lambda_L. \end{aligned} \tag{7.38}$$

Hence, the integration region needs to be restricted according to (7.37) and (7.38). For this reason, integration region are splitted into two cases, $2\lambda_L < z < \lambda_L + \lambda_U$ and $\lambda_L + \lambda_U < z < 2\lambda_U$.

After some derivations, $f_z(z|H_1)$, when $2\lambda_L < z < \lambda_L + \lambda_U$, is

$$\begin{aligned} f_z(z|H_1) &= \int_{\lambda_L}^{z-\lambda_L} \tilde{f}(z-y|H_1)\tilde{f}(y|H_1)dy \\ &= \int_{\lambda_L}^{z-\lambda_L} \frac{e^{-\frac{1}{2(1+m\bar{\gamma})}(z-y)}}{A_1 \cdot \beta_1} \cdot \frac{e^{-\frac{1}{2(1+m\bar{\gamma})}y}}{A_1 \cdot \beta_1} dy \\ &= \frac{1}{A_1^2\beta_1^2}\left(z-2\lambda_L\right) e^{-\frac{1}{2(1+m\bar{\gamma})}z} \end{aligned} \tag{7.39}$$

and $f_z(z|H_1)$, when $\lambda_L + \lambda_U < z < 2\lambda_U$, is

$$\begin{aligned} f_z(z|H_1) &= \int_{z-\lambda_U}^{\lambda_U} \tilde{f}(z-y|H_1)\tilde{f}(y|H_1)dy \\ &= \int_{z-\lambda_U}^{\lambda_U} \frac{e^{-\frac{1}{2(1+m\bar{\gamma})}(z-y)}}{A_1 \cdot \beta_1} \cdot \frac{e^{-\frac{1}{2(1+m\bar{\gamma})}y}}{A_1 \cdot \beta_1} dy \\ &= \frac{1}{A_1^2\beta_1^2}\left(2\lambda_U - z\right) e^{-\frac{1}{2(1+m\bar{\gamma})}z} \end{aligned} \tag{7.40}$$

The CDF of z or $P\{\sum_{i=2}^{2} F_i < \lambda_f|H_1\}$ then becomes

$$P\{\sum_{i=1}^{2} F_i < \lambda_f\} = \begin{cases} 0 & \text{for } 0 < \lambda_f < 2\lambda_L \\ \int_{2\lambda_L}^{\lambda_f} \tilde{f}_z(z|H_1)\, dz & \text{for } 2\lambda_L < \lambda_f < \lambda_L + \lambda_U \\ P\{\sum_{i=1}^{2} F_i < \lambda_L + \lambda_U\} & \\ \quad + \int_{\lambda_L+\lambda_U}^{\lambda_f} \tilde{f}_z(z|H_1)\, dz & \text{for } \lambda_L + \lambda_U < \lambda_f < 2\lambda_U \\ 1 & \text{for } \lambda_f > 2\lambda_U. \end{cases} \tag{7.41}$$

And then for $2\lambda_L < z \leq \lambda_L + \lambda_U$, the CDF becomes

$$P\{\sum_{i=2}^{2} F_i < z\} = \frac{2(1+m\bar{\gamma})\left(2(1+m\bar{\gamma})e^{-\frac{\lambda_L}{(1+m\bar{\gamma})}} - e^{-\frac{z}{2(1+m\bar{\gamma})}}\left[2(1+m\bar{\gamma})+z-2\lambda_L\right]\right)}{A_1^2\,\beta_1^2} \tag{7.42}$$

and for $\lambda_L + \lambda_U < z \leq 2\lambda_U$

$$P\{\sum_{i=1}^{2} F_i < z\} = P\{\sum_{i=1}^{2} F_i < \lambda_L + \lambda_U\} + \frac{2(1+m\bar{\gamma})\left(e^{-\frac{z}{2(1+m\bar{\gamma})}}\left[2(1+m\bar{\gamma})+z-2\lambda_U\right] - e^{\frac{-\lambda_L-\lambda_U}{2(1+m\bar{\gamma})}}\left[2(1+m\bar{\gamma})+\lambda_L-\lambda_U\right]\right)}{A_1^2\,\beta_1^2} \tag{7.43}$$

Then, consider when PU is idle (H_0). Similarly to the analysis above on H_1, both PDF of y_{user1} and y_{user2} are truncated PDFs of (4.4) as

$$f_{trun,y}(y|H_0) = \begin{cases} {}^{f_y(y|H_0)}/_{\beta_0} & \text{, for } \lambda_L < y < \lambda_U \\ 0 & \text{, otherwise .} \end{cases} \tag{7.44}$$

or

$$f_{trun,y}(y|H_0) = \begin{cases} \dfrac{y^{m-1}e^{-y/2}}{A_0 \cdot \beta_0} & \text{, for } \lambda_L < y < \lambda_U \\ 0 & \text{, otherwise .} \end{cases} \tag{7.45}$$

given that

$$A_0 = \Gamma(m) \cdot 2^m. \tag{7.46}$$

Consequently, a PDF of z is obtained by integrating the PDF of both RVs such that

$$f_z(z|H_0) = \int_{-\infty}^{\infty} f_{trun,y}(z-y|H_0)\, f_{trun,y}(y|H_0)\, dy. \tag{7.47}$$

Based on the integration regions as in (7.37) and (7.38), when $2\lambda_L < z < \lambda_L + \lambda_U$, $f_z(z|H_0)$ is

$$\begin{aligned} f_z(z|H_0) &= \int_{\lambda_L}^{z-\lambda_L} f_{trun,y}(z-y|H_0)\, f_{trun,y}(y|H_0) dy \\ &= \frac{1}{A_0^2\,\beta_0^2} \int_{\lambda_L}^{z-\lambda_L} (z-y)^{m-1} e^{-(z-y)/2} y^{m-1} e^{-y/2} dy \\ &= \frac{1}{A_0^2\,\beta_0^2}\, e^{-z/2} \int_{\lambda_L}^{z-\lambda_L} \left(yz-y^2\right)^{m-1} dy \end{aligned} \tag{7.48}$$

and $f_z(z|H_0)$, when $\lambda_L + \lambda_U < z < 2\lambda_U$, is

$$\begin{aligned} f_z(z|H_0) &= \int_{z-\lambda_U}^{\lambda_U} f_{trun,y}(z-y|H_0)\, f_{trun,y}(y|H_0)dy \\ &= \frac{1}{A_0^2\,\beta_0^2}\, e^{-z/2} \int_{z-\lambda_U}^{\lambda_U} (yz - y^2)^{m-1} dy \end{aligned} \tag{7.49}$$

Both integration terms in (7.48) and (7.49) are complicated. Hence, an approximation on $P\{\sum_{i=1}^{2} F_i < z\}$ is considered as follows. A monotonically increasing linear equation is adopted to approximate CDF of z under this scenario such that

$$P\{\sum_{i=2}^{2} F_i < z\} = \begin{cases} 0 & \text{for } 0 < \lambda_f < 2\lambda_L \\ \dfrac{1}{2(\lambda_U - \lambda_L)}(z - 2\lambda_L) & \text{for } 2\lambda_L < z < 2\lambda_U \\ 1 & \text{for } \lambda_f > 2\lambda_U \ . \end{cases} \tag{7.50}$$

7.4 Simulation Results

In this section, the simulation results for the Double Threshold scheme are evaluated and compared to that of the OR-HDC and EGC-SDC scheme. Three spatially separated users are considered for cooperative spectrum sensing. The time-bandwidth product is set to 3 for each observation. The PU's SNR is 3dB and the channel is modelled as Rayleigh fading channel. Also, it is equally probable that the PU is active and idle.

7.4.1 Double Threshold Scheme

Fig. 7.5 shows the detection performance when λ_L and λ_U is 7.841 and 16.82 which respectively are the 75^{th} and 99^{th}-quantile of the distribution when PU is idle. It shows that the performance of this Double Threshold scheme is better than that of OR-HDC, and approaches that of EGC-SDC scheme. Moreover, the communication overhead between CR and the fusion center is reduced as only 29.5% of local observations are forwarded, whereas all of them need to be forwarded for EGC-SDC scheme.

Fig. 7.6 shows the detection performance when λ_L and λ_U is 5.348 and 16.82 which respectively are the 50^{th} and 99^{th}-quantile of the distribution when PU is idle. Moreover, Double Threshold scheme is better than that of OR-HDC and approaches that of EGC-SDC scheme. The communication overhead here is also reduced as only 47.8% of local observations are forwarded.

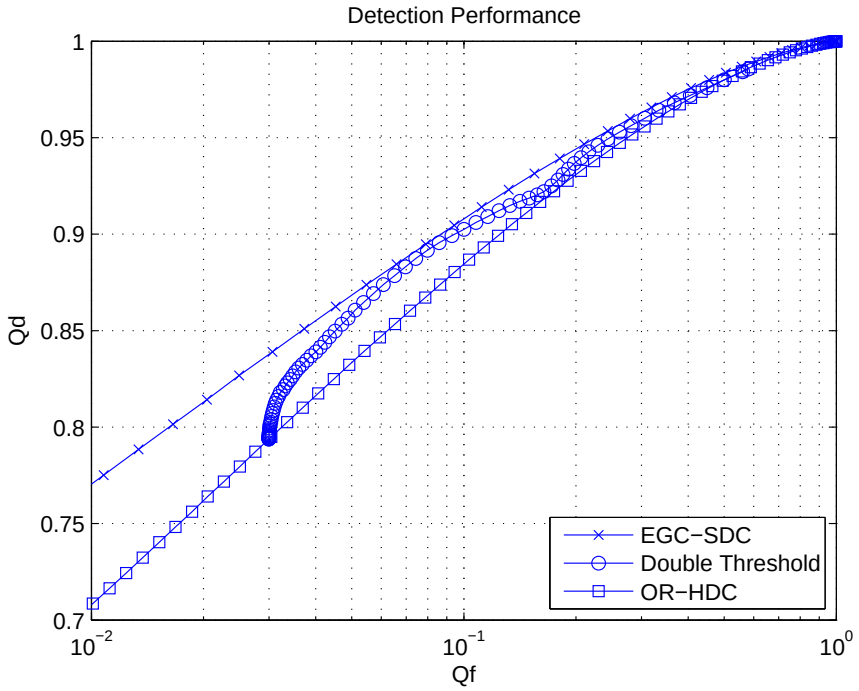

Figure 7.5: Detection performance for Double Threshold Scheme with $\lambda_L = 7.841$ and $\lambda_U = 16.82$

In addition, from Fig. 7.5 and 7.6, it can be seen that the detection performance of Double Threshold scheme are bound at a point where it adjoins the curve of OR-HDC scheme. This is due to the choice of the upper threshold, λ_U as analysed in the previous section. The lower bound on Q_f in both figures follows is $1-(1-0.01)^3 = 0.0297$, as the λ_U is set up as the 99^{th}-quantile of the distribution when PU is idle.

7.4.2 Double Threshold Scheme with Quantization

Here, quantization is applied to the forwarded local observations in Double Threshold scheme with λ_L and λ_U is set to 5.348 and 16.82 respectively. The rest of the system parameters are set exactly the same with previously presented results. Fig. 7.7 shows the detection performance when 2-bit and 3-bit quantization is applied to the uncertain area and compares them with the detection performance when the local observation is forwarded non-quantized. As the thresholds here are set the same with those of Fig. 7.6, 47.8% of local observations are forwarded similarly. However, the communication overhead is effectively reduced due to quantization. For instance, on average

$$2 + (2-1)\cdot(0.478) = 2.478 \approx 2.5 \text{ bits}$$

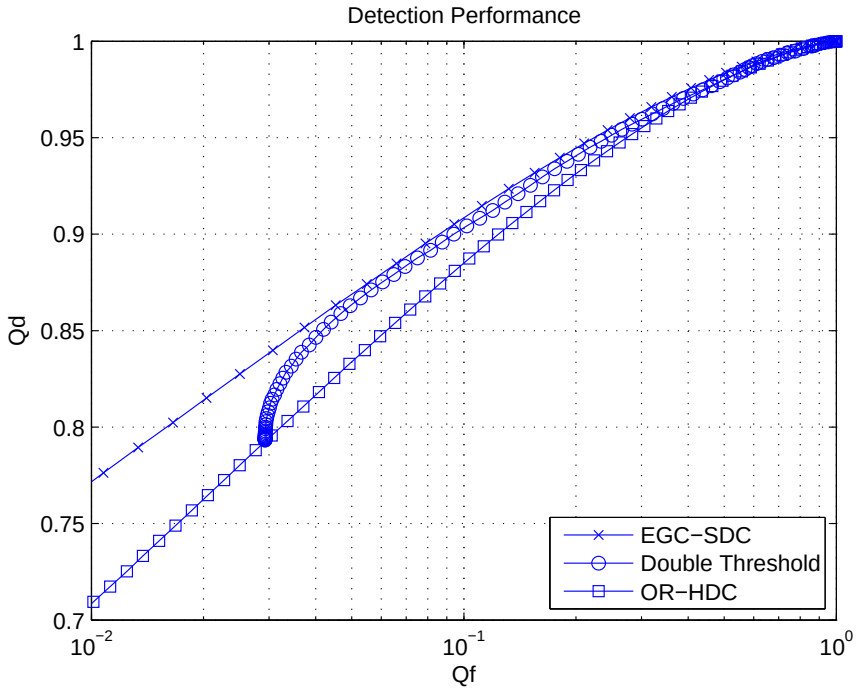

Figure 7.6: Detection performance for Double Threshold Scheme with $\lambda_L = 5.348$ and $\lambda_U = 16.82$

are forwarded for Double Threshold (2-bit) scheme and

$$2 + (3 - 1) \cdot (0.478) = 2.956 \approx 3 \text{ bits}$$

are forwarded for Double Threshold (3-bit) scheme compared to 16 bits for EGC-SDC.

7.4.3 Simulation Results for Double Threshold Analysis

In this section, the closed-form analysis for the Double Threshold scheme with two cooperating users, as provided in Section 7.3.5, is evaluated and compared with the simulation results. Fig. 7.8 and 7.9 show Q_f and Q_d for the Double Threshold scheme with two cooperating users with time-bandwidth product m=3, SNR= 3dB, λ_L and λ_U is 10 and 15 respectively. The simulation result shows that the analytical Q_f and Q_d matches with the simulation result, with slight error in Q_f due to an approximation in (7.50). As there are two cooperative users, the summation for the forwarded local observation can only be between 10 to 15 (when one user forwards its observation) and between 20 to 30 (the summation when two users forward their observation). Hence, a capped level for Q_f and Q_d occurs between the region when fusion threshold is between 15 and 20.

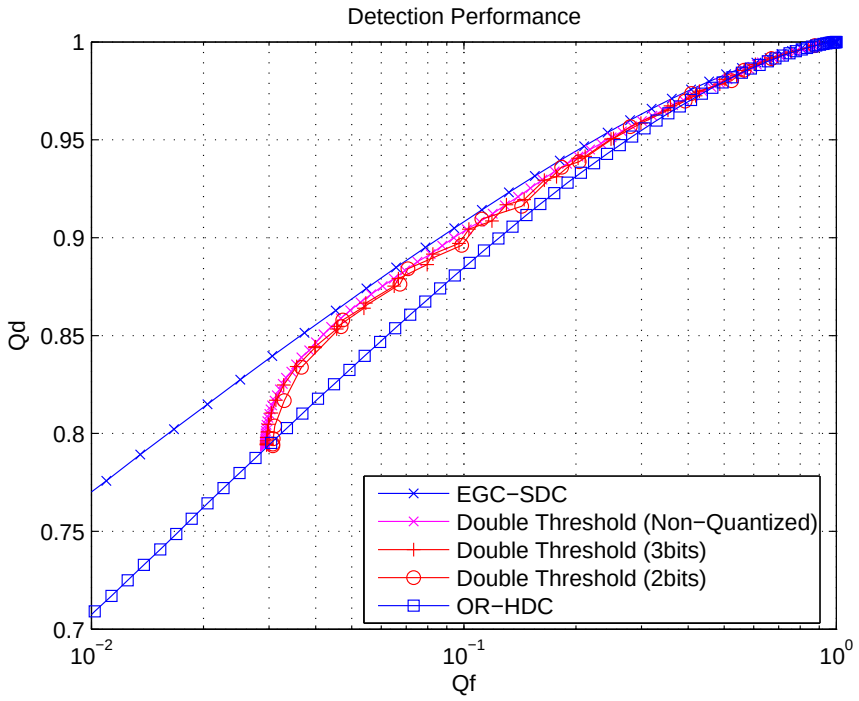

Figure 7.7: Detection performance for Double Threshold Scheme with two and three bit quantization and $\lambda_L = 5.348$ and $\lambda_U = 16.82$

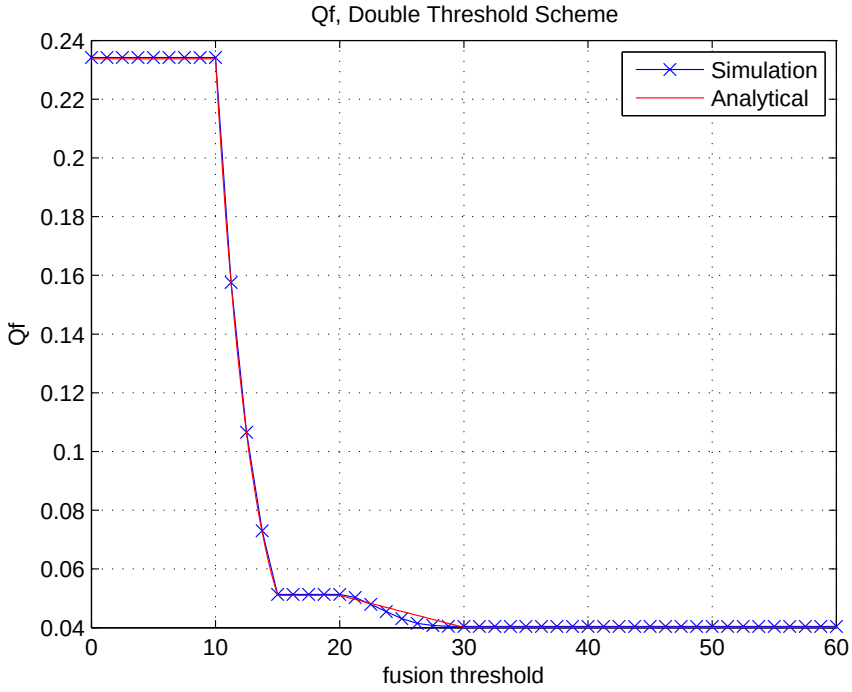

Figure 7.8: Double Threshold Scheme : Probability of False Alarm $\lambda_L = 10$ and $\lambda_U = 15$.

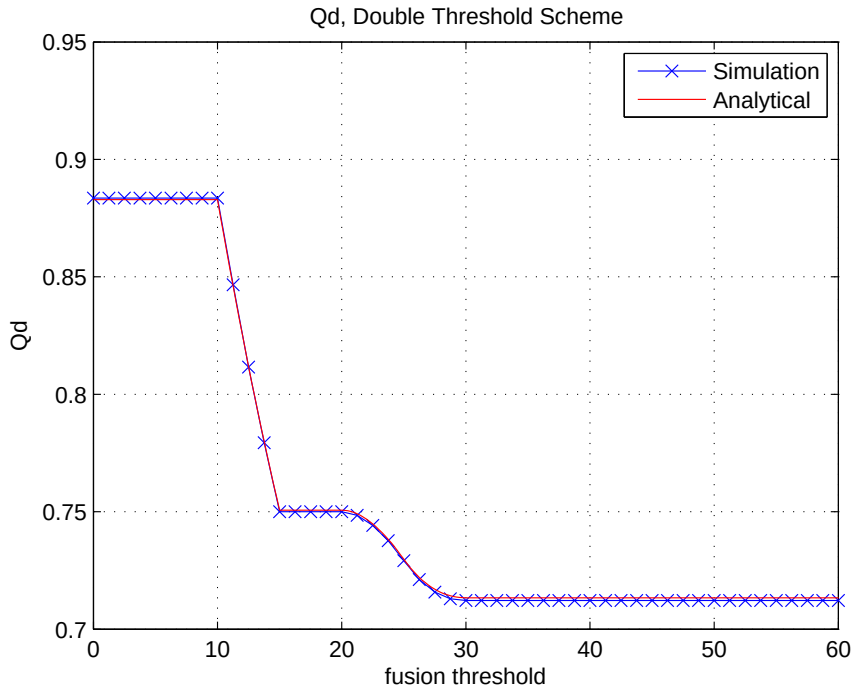

Figure 7.9: Double Threshold Scheme : Probability of Detection $\lambda_L = 10$ and $\lambda_U = 15$.

Fig. 7.10 and 7.11 show Q_f and Q_d for Double Threshold scheme with λ_L and λ_U is 7 and 17.5 respectively. The rest of the parameters are set similar to previous simulation results. Similar to the above, the simulation result shows that the analytical Q_f and Q_d matches with the simulation result, with an error in Q_f due to an approximation in (7.50).

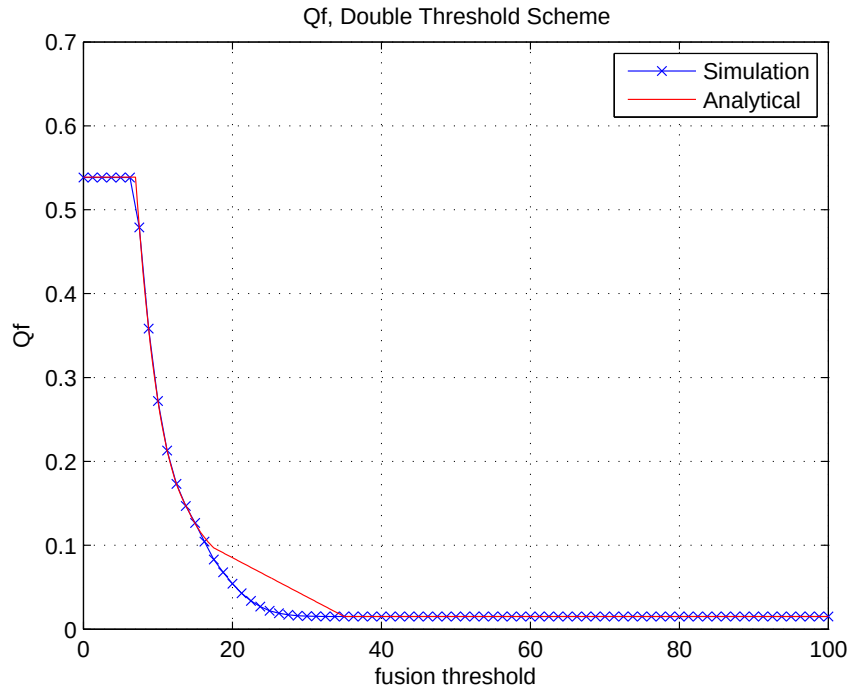

Figure 7.10: Double Threshold Scheme : Probability of False Alarm $\lambda_L = 7$ and $\lambda_U = 17.5$.

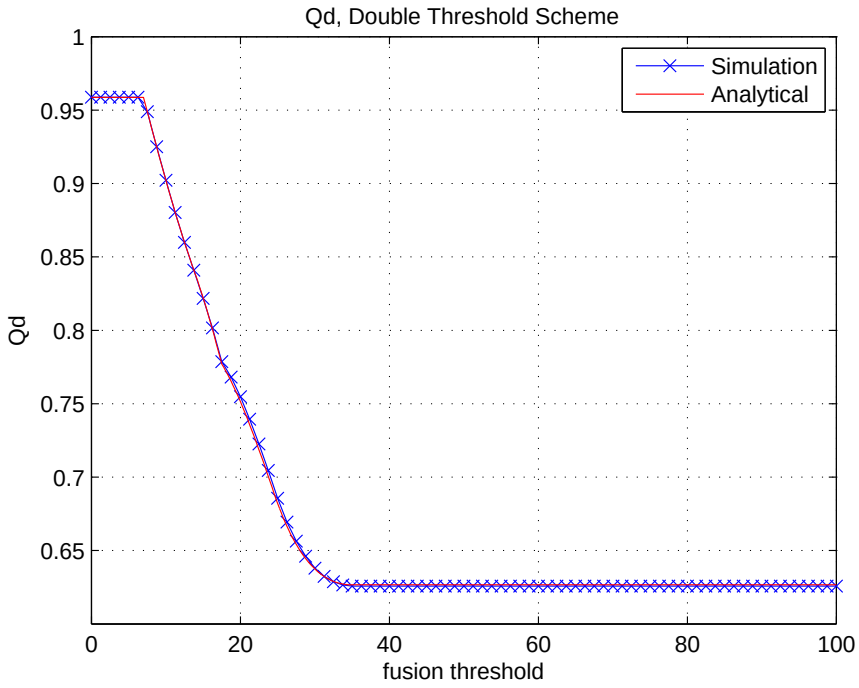

Figure 7.11: Double Threshold Scheme : Probability of Detection $\lambda_L = 7$ and $\lambda_U = 17.5$.

7.5 Summary

In this chapter, the Double Threshold cooperative spectrum sensing scheme was presented. By forwarding its local observation when CR is uncertain, the detection performance is improved. In order to reduce the communication bandwidth among CR users, quantization is applied to the forwarded local observations. Simulation results showed that the Double Threshold scheme improves the detection performance while requiring less communication bandwidth than the EGC-SDC scheme. In addition, the closed-form analysis for Q_f and Q_d for the Double Threshold scheme is provided in this chapter.

Chapter 8

Sequential Cooperative Spectrum Sensing

8.1 Introduction

In wireless communication simulation, the channel is usually assumed to be quasi-static. However, in reality, the channel is time-varying and there is a correlation between channel gain in consecutive time slots. The details on time-varying channel will be presented in Section 8.2.1. First, the detection performance for conventional OR-HDC scheme is considered in different channel types. Fig. 8.1 shows that the detection performance in quasi-static and correlated channel is exactly the same. Although there is a correlation in the channel for each successive energy detector observation, this energy detector technique does not make use of it.

In this chapter, the exploitation on the previous observation and channel correlation will be studied to show that relying on the previous observation could help improve the detection performance without taking more observation or using complicated techniques. Then, we present our previously proposed schemes and their related analysis. The rest of this chapter is organised as follows. First, Sequential cooperative spectrum sensing and its background are presented. Then, three sequential energy detection (SED) schemes, which we previously proposed in [91, 92], are presented. The three schemes are the Weighted SED scheme, which simply takes a fixed number of past observations, and another two adaptive schemes, namely Two-Stage SED and

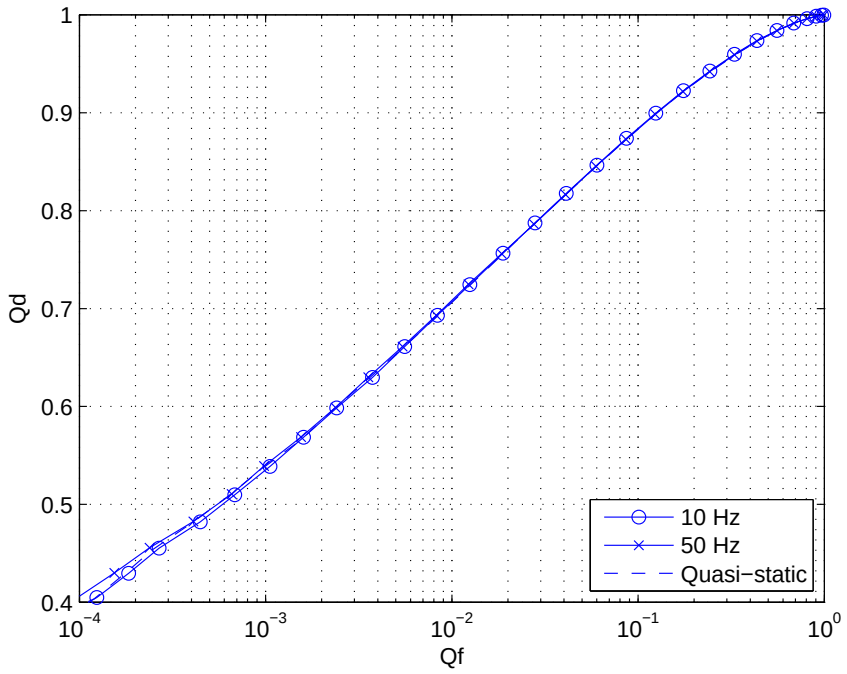

Figure 8.1: Cooperative detection performance for energy detection for correlated and quasi-static channel

Differential SED, which determine the number of past observations, based on its decision on PU's state. Finally, a closed-form analysis for the probability of false alarm and detection in the SED schemes are analyzed.

8.2 System Model

In this section, the system model for SED schemes are presented. First, the time varying channel as well as its simulation technique is considered. Then, the sensing procedures for sequential spectrum sensing is presented.

8.2.1 Time Varying Channel

Fig. 8.2 and Fig. 8.3 shows the real part of the channel gain in Rayleigh fading channel with Doppler frequency (f_d) of 10Hz and 50Hz respectively, while the sampling frequency f_s is set to 10^5 Hz. It can be seen that there is a correlation between channel gain between consecutive time slots. When f_d is low, the channel variation is less from time slot to the next time slot, compared to when f_d is high.

Further details on time-varying channel can be found in [93, 94].

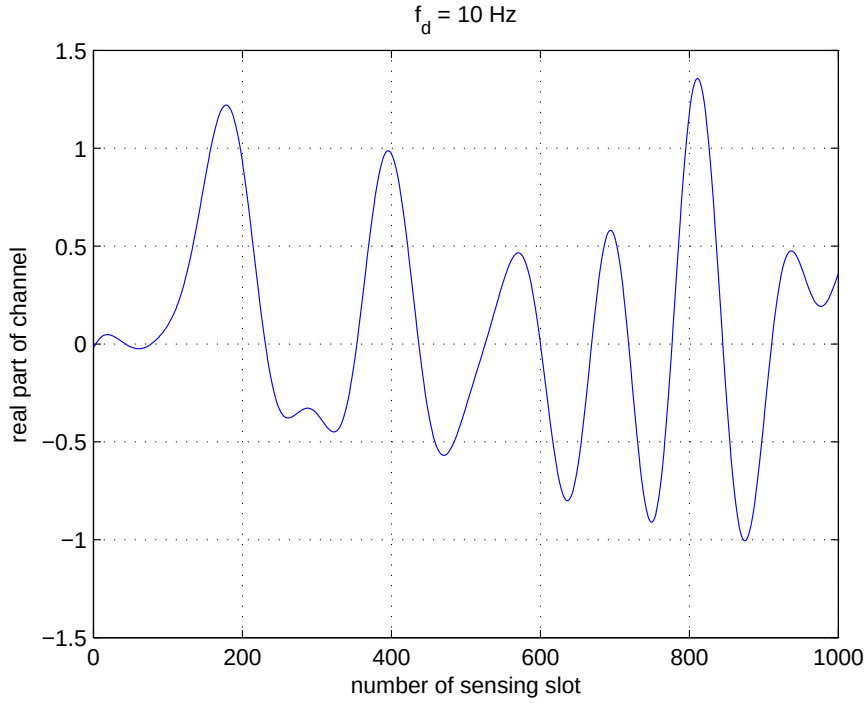

Figure 8.2: Real part of the channel gain in correlated channel with $f_d = 10$ Hz

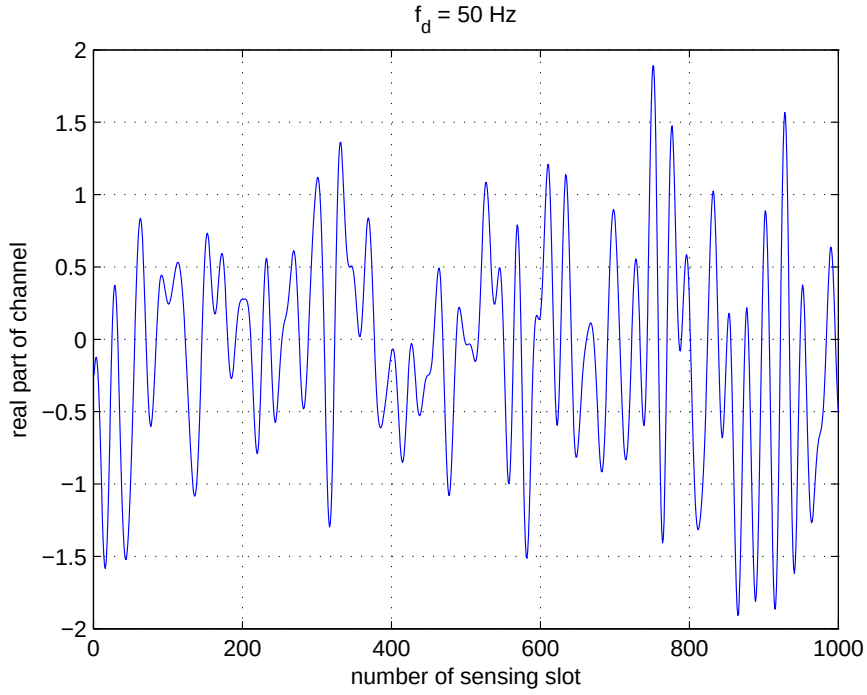

Figure 8.3: Real part of the channel gain in correlated channel with $f_d = 50$ Hz

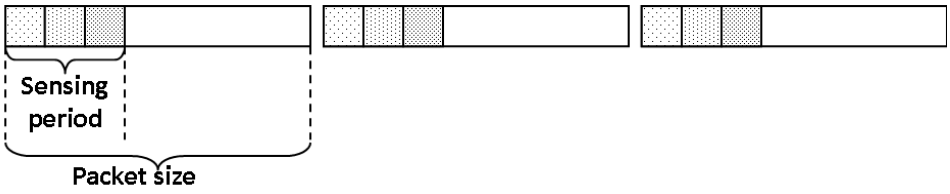

Figure 8.4: System model for correlated channel sensing framework

8.2.2 Sensing Procedures

The sequential sensing procedure is shown in Fig. 8.4. The sensing period occurs periodically at the beginning of each packet, followed by the data transmission part. The number of observation samples taken in the sensing period is defined by the time-bandwidth product.

8.2.3 Primary User activity

The PU activity is modelled according to a two-state Markov chain [95] as shown in Fig. 8.5. The parameter α and β represents the probability of PU changing its state from active (H_1) to idle (H_0) and vice versa, while the notation $1-\alpha$ and $1-\beta$ represents the probability of PU remains in active (H_1) and idle (H_0) state respectively.

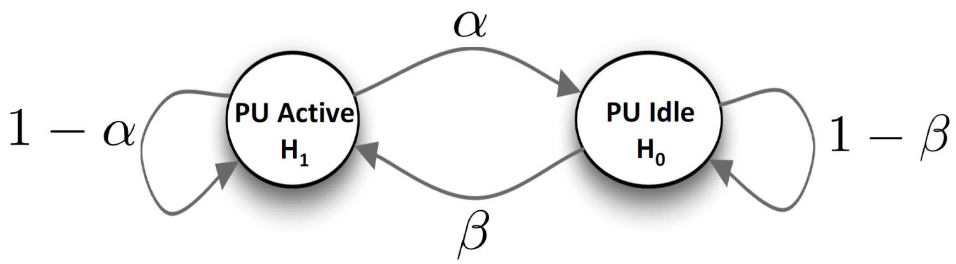

Figure 8.5: Two-state Markov chain on primary user's activity model

8.3 Weighted SED

In this section, a previously proposed cooperative spectrum sensing technique [91] that uses the previously received energy observations are presented. The Weighted SED scheme is designed to exploit channel correlation by utilizing observations from previous slots. The current and previous observations are weighted and aggregated. It employs the moving average model to combine the energy observations.

Then, the weighted output is compared to the threshold locally at the CR node. The local decision is then forwarded to the fusion center. At the fusion centre, OR-rule is used for global decision making due to its simplicity and PU's protection purpose. In other words, this approach makes use of soft combining for local decision and the OR-rule for global decision at the fusion center.

8.3.1 Sensing Procedures

The detailed sensing procedure for Weighted SED is as follows. First, the energy observations are weighted and aggregated with the moving average model at the k^{th} sensing slot such that

$$T_k = \mathbf{W}\mathbf{Y}_k = \sum_{i=0}^{N-1} w_i y_{k-(i+N-1)} \tag{8.1}$$

where T is the weighted sum energy, N is number of energy observations taken into weighting process, and $\mathbf{Y}_k$ is the local observation vector at the k^{th} sensing slot denoted as

$$\mathbf{Y}_k = \begin{bmatrix} y_{k-(N-1)} & y_{k-(N-2)} & \cdots & y_k \end{bmatrix}^T$$

where y_k is the current received signal and y_{k-i} is the observation from the i^{th} sensing slot before. $\mathbf{W}$ is the weighting vector such that

$$\mathbf{W} = \begin{bmatrix} w_0 & w_1 & \cdots & w_{N-1} \end{bmatrix}$$

where w_i is the i^{th} weighting factor. $\mathbf{W}$ is a normalized vector such that

$$(w_0 + w_1 + ... + w_{N-1}) = 1.$$

Then, the decision d_k is made by comparing T_k to the threshold λ.

$$d_k = \begin{cases} H_0 \text{ , if } T_k < \lambda \\ H_1 \text{ , otherwise} \end{cases}$$

Finally, the local decision d_k is sent to the fusion centre to make a final decision on PU's existence using the OR-rule.

Weight Computation

The weighting vector $\mathbf{W}$ is a key component of sequential cooperative sensing. Ideally, this vector should be optimized by minimizing the false alarm (P_f) and miss detection probability (P_m) [70]. The optimization criteria then becomes

$$\mathbf{W}^* = \arg\min_{\mathbf{W}} \ (P_f + P_m)$$

where P_f and P_d are the CCDF for weighted sum of N-RVs as

$$\begin{aligned} P_f &= P(T > \lambda | H_0) \\ &= P(w_0 y_{k-N+1} + w_1 y_{k-N+2} + ... + w_{N-1} y_k > \lambda | H_0) \end{aligned} \tag{8.2}$$

and

$$P_d = P(w_0 y_{k-N+1} + w_1 y_{k-N+2} + ... + w_{N-1} y_k > \lambda | H_1). \tag{8.3}$$

Hence optimizing $\mathbf{W}$ is complicated and the closed-form and optimal solution is difficult to obtain [41].

Sub-Optimal Weight Vector

Since the optimal solution is difficult to obtain, a sub-optimal weight calculation approach is proposed here. Consider an example of the PDF of received energy when PU is idle (H_0) and active (H_1) as shown in Fig. 4.1. The optimal detection approach is one that can jointly minimize the false alarm probability P_f and missed detection P_m, i.e., the shaded area in Fig. 4.1. Conventional approach is to determine the optimal detection threshold to minimize this area. With SED, we can include past observations to vary the PDF of the weighted sum energy such that the shaded area is minimized. This can be achieved, if possible, by separating the means of received energy, or minimizing the variance of the received energy in H_0 and H_1 case. However, we will show first that applying weighting will not be able to vary the mean by the following proposition.

Proposition 1. *For a normalized weight vector, the mean of the weighted sum energy equals to the mean of the local observation (i.e. $E[T] = E[Y]$) if the channel and PU activity is static*

Proof.

$$\begin{aligned} T_k =& \sum_{i=0}^{N-1} w_i y_{k-(i+N-1)} \\ =& w_0 \cdot y_{k-(N-1)} + ... + w_{N-1} \cdot y_k \\ E[T] =& w_0 \cdot E[Y_{N-1}] + ... + w_{N-1} \cdot E[Y_0] \end{aligned}$$

where Y_0 and Y_k are set of current received signal and that of the k^{th} sensing slot before. Since the channel and PU activity is static,

$$\begin{aligned} E[Y] =& E[Y_{N-1}] = ... = E[Y_0]. \\ \text{Hence, } E[T] =& (w_0 + w_1 + ... + w_{N-1}) \cdot E[Y] = E[Y]. \end{aligned}$$

□

The importance of this proposition is that the mean of the weighted sum energy will not be affected by the choice of the weighting vector $\mathbf{W}$, and is the same as the mean of a single observation. In other words, the separation between the mean of received energy in H_0 and H_1 case will not be affected by varying $\mathbf{W}$. Hence, to minimize the shaded area, the other option is to reduce the variance of these PDFs. The effect of variance on the distribution of received energy in H_0 and H_1 case is illustrated in Fig. 8.6. When more observations are taken, the variance for both received energy in two cases will be reduced. Hence, the separation between the distribution in H_0 and H_1 case is more evident and this leads to better detection performance. Proposition 2 shows that when equal weighting is applied in H_0 and H_1 case under quasi-static channel, variance of T equals to variance of Y divided by the number of total observations taken. Thus when N increases, the variance of T decreases linearly with it.

Proposition 2. *When equal weighting is applied, the variance decreases proportionally to the number of samples taken.*

Proof. First, the variance of T in correlated channel H_1 case is derived

$$Var(T) = Var\left(\sum_{i=0}^{N-1} w_i Y_{i+N-1}\right).$$

From the property for variance of the weighted sum of several random variables [96], it leads to

$$Var\left(T\right) = \sum_{i=0}^{N-1} w_i^2 \cdot Var\left(Y_{i+N-1}\right) + 2 \sum_{i,j;i<j} w_i w_j \cdot Cov\left(Y_{i+N-1}, Y_{j+N-1}\right) \tag{8.4}$$

For equal weighting, the weighting vector $\mathbf{W}$ is

$$\mathbf{W} = \begin{bmatrix} \frac{1}{N} & \frac{1}{N} & ... & \frac{1}{N} \end{bmatrix}$$

Thus,

$$Var\left(T\right) = \sum_{i=0}^{N-1} \left(\frac{1}{N}\right)^2 \cdot Var\left(Y_{i+N-1}\right) + 2 \sum_{i,j;i<j} \left(\frac{1}{N}\right)^2 \cdot Cov\left(Y_{i+N-1}, Y_{j+N-1}\right) \tag{8.5}$$

In quasi-static fading channel, observation in each frame is independent to its previous and next observation. Hence $Cov\left(Y_i, Y_j\right) = 0$ for all i and j. Then,

$$Var\left(T\right) = \left(\frac{1}{N}\right)^2 \cdot \sum_{i=0}^{N-1} Var\left(Y_{i+N-1}\right)$$

For each Y_{i+N-1}, its variance is the same such that $Var\left(Y\right) = Var\left(Y_{N-1}\right) = ... = Var\left(Y_0\right)$ which leads to

$$Var\left(T\right) = \frac{Var\left(Y\right)}{N}. \tag{8.6}$$

□

8.3.2 Weight Vector for Static PU Activity

As discussed above, the optimal weighting is one that can minimize the variances of received energy in T in H_0 and H_1 case. However, its complexity involves minimizing both distributions at the same time. Hence, we propose a sub-optimal approach to obtain the weighting vector by minimizing the variance of the received energy in H_0 or H_1 case separately. When the PU activity is static (i.e. the PU is either always on or always off), the following can be defined.

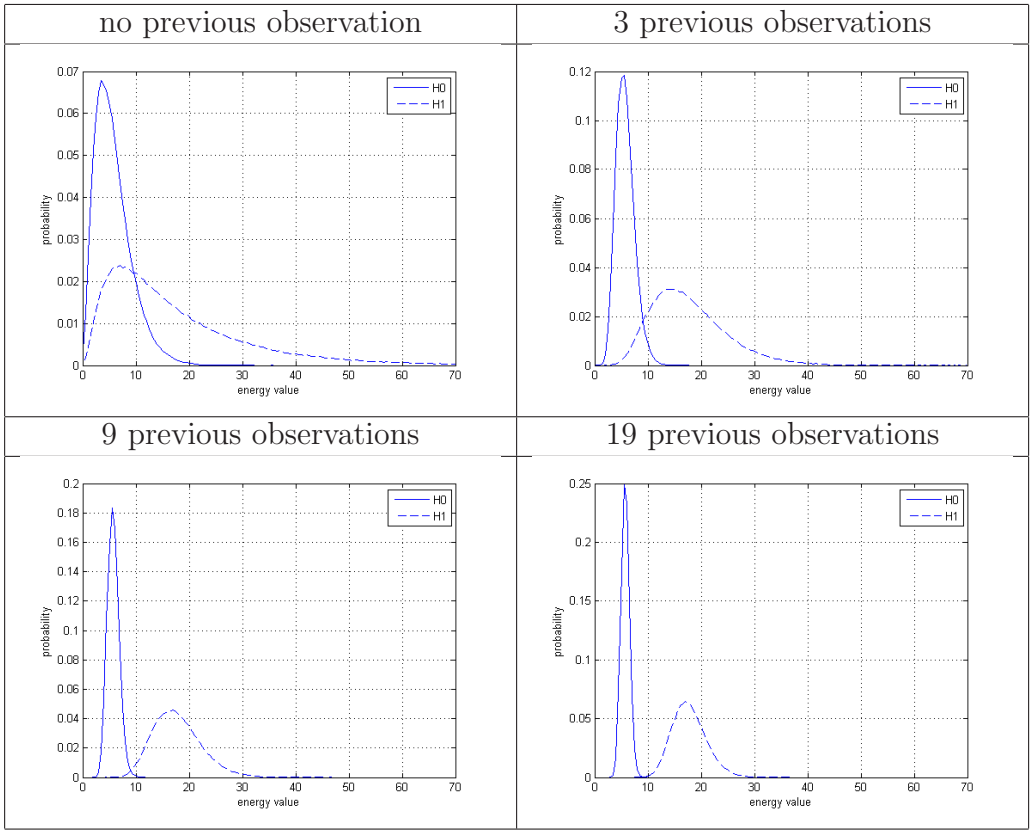

Figure 8.6: Energy distribution for weighted local observation with different number of previous observations taken

Proposition 3. *In quasi-static fading channel, the optimal weight vector that minimises the variance of H_0 and H_1 is the equal weighting.*

Proof. In quasi-static fading case, there is no correlation between each observation and hence (8.5) becomes

$$Var\,(T) = \sum_{i=0}^{N-1} w_i^2 \cdot Var\,(Y_{i+N-1}).$$

Since the PU activity is assumed to be static, the variance of the energy observations are identical. Thus the optimization criteria to minimize variance of T is

$$\begin{aligned} \text{Min} \quad & \sum_{i=1}^{N} w_i^2 \\ \text{s.t.}\ & (w_1 + w_2 + ... + w_N) = 1. \end{aligned}$$

By using standard Lagrange multiplier, the solution is

$$w_A = w_B = ... = w_N = \frac{1}{N}. \tag{8.7}$$

Hence, in quasi-static fading channel, equal weighting is optimal as it gives the lowest variance. □

Corollary 1. *In time-varying channel, the optimal weight vector that minimises the variance of H_0 is the equal weighting.*

Proof. As the primary user does not exist in H_0, the channel will not affect the received energy observation. Hence, the proof follows that of Proposition 3. □

Consequently, the remaining problem here is the optimization of weight vector for H_1 case in time varying channel. This involves the computation of the covariances between observations. A closed form solution for minimizing (8.5) could not be obtained and thus we resolved to computing it using numerical methods.

8.3.3 Weight Vector for Intermittent PU Activity

When PU activity is intermittent, the value of received energy value at the CR could change suddenly between observations. Hence, a practical approach is to rely more on the newer observations for detection. Thus, we propose the use of a simple exponential weighting, whereby each past observation is weighted less by a factor of $\frac{1}{e}$

$$\mathbf{W} = \frac{1}{K}\left[\begin{array}{cccc} e^1 & e^2 & \dots & e^N \end{array}\right]$$

where $K = \sum_{i=1}^{N} e^i$ is the normalisation factor.

8.3.4 Simulation Results

Simulation results, the more details of which will be discussed in Section 8.7, show that the proposed Weighted SED scheme can improve the detection performance by utilizing past observations. It provides significantly better detection performance than the conventional OR-rule energy detection scheme, when PU is static. However, when PU is intermittent, simulation result shows that the Weighted SED with equal weighting vector is worse due to PU activity, especially when it varies a lot. This is due to the heavy reliance on past observations which are already outdated, i.e. PU has already changed its state.

8.4 Two-Stage SED

As briefly discussed in the previous section, Weighted SED can improve the detection performance by utilizing past observations. However, when PU is intermittent and regularly changes its state, the detection performance is worsened as Weighted SED relies on the outdated past observations.

This section considers an adaptive technique which does not set a fixed number of previous observations but adaptively determines the number of past observation used for the weight combination. The fundamental concept is that if the PU activity has not changed, past observations should be used for weighting to improve performance. However, if the PU has changed its state, past observations should be discarded as they will lead to erroneous detection. Hence, the adaptive SED approaches will need to know when the PU has changed its activity. As CR users perform blind detection and can not precisely know PU's state, the CR's local observation will be used to perform an initial estimation. With the transition of PU's activity determined, the CR user then decides how many past observations it should rely on and take into the weighting process. The current and previous observations are then equally weighted before compared to the threshold locally at the CR node.

Here, a previously proposed scheme adaptive Two-Stage SED scheme [92] is discussed. While Differential SED scheme, which is slightly different to this scheme, is presented in the next section. The Two-Stage SED scheme consists of a two stage energy detection procedure. In the first stage, CR users perform simple single threshold energy detection to decide PU's existence. Based on this sensing decision, CR users estimate whether PU has changed its activity and decide how many past observations to be taken for equal weighting. If CR users think that PU does not change its state, it will include this energy observation value into weighting procedure. The second stage is then the previously mentioned Weighted SED to determine the existence of PU.

8.4.1 Two-Stage SED Sensing Procedures

The detailed sensing procedure for Two-Stage SED is as follows

1. First, CR users locally perform a conventional sensing by comparing the received energy observations to the first stage threshold λ_1.

2. Based on the sensing result in the first stage, CR users adaptively determine the number of past observations to be taken into the weight computation. If the past local decisions are the same as this initial detection (i.e., the PU presumably maintained its activity), they will be used for the weighting procedure. In other words, CR users ignore the previous observations once the sensing decision becomes different to the current one, as they think that PU has changed its state.

3. To avoid CR users relying on too many past observations and degrade the performance, we limit the number of past observations to be taken in to weight computation to a certain number.CR users then apply equal weighting to all energy observations that are taken into weight computation in the second stage. The weighted observations are then aggregated such that

$$T_k = \mathbf{W}\mathbf{Y}_k = \sum_{i=0}^{N-1} w_i y_{k-(i+N-1)} \tag{8.8}$$

where $\mathbf{W} = \begin{bmatrix} \frac{1}{N} & \frac{1}{N} & \cdots & \frac{1}{N} \end{bmatrix}$.

4. The local decision d_k is made by comparing T_k to the second stage threshold λ_2.

$$d_k = \begin{cases} H_0 \text{ , if } T_k < \lambda_2 \\ H_1 \text{ , otherwise} \end{cases}$$

5. Finally, the local decision d_k is sent to the fusion centre to make a final decision on PU's existence using the OR-rule.

Simulation results for this Two-Stage SED will be shown in Section 8.7.2.

8.5 Differential SED

The Two-Stage SED performs an instantaneous sensing decision and compares with previous decisions to determine the number of observations included. Here, we consider another approach called the Differential SED. In slow fading channel, the channel gains for consecutive sensing slots do not vary much. Hence, the received energy values for those consecutive sensing slots will be similar as well, provided that the PU does not change its state. On the contrary, when PU changes its state, the difference

between consecutive observations would be high. In this scheme, CR users estimate the PU's state based on this difference. If the difference between two consecutive energy observations is less than a certain threshold, the CR system will consider that the state of PU remains unchanged. As a result, it uses this new energy observation and weighted with past observations to perform detection. On the other hand, if the difference between consecutive observations are larger than the threshold, the CR system will consider that the PU has changed its state. Hence, all previous observations will be discarded and the detection will be based only on this new observation.

The detailed sensing procedure for Differential SED is as follows

1. First, each CR users locally calculates the difference between two consecutive energy observations.

2. If this difference is less than the variable threshold, λ_d. The previously received energy observations will be taken into weight computation. In other words, CR users ignore the previous observation once the difference is greater than λ_d, as they think that PU has changed its state.

3. Similarly to the Two-Stage SED, in order to avoid CR users relying on too many past observations, we limit the number of past observations to be taken in to weight computation to a certain number. CR users then apply equal weighting to all energy observations that are taken into weight computation. The weighted observations are then aggregated as given in (8.8).

4. Then, the rest of the sensing procedures follows the previously proposed Two-Stage SED scheme.

Simulation results for this Differential SED will be shown in Section 8.7.3.

8.6 SED Analysis

In this section, the Weighted SED and Two-Stage SED scheme are analysed. Also, the generic form for probability of false alarm and detection in both schemes is presented. As the global decision in cooperative spectrum sensing is made using the OR-rule from local decisions, i.e. OR-HDC decision combining rule is used at the fusion center, Q_f

and Q_d has a one-to-one relationship to P_f and P_d as shown in (4.19). Hence, later on in this section, the analysis can be simplified by only considering the P_f and P_d in a single user case.

8.6.1 Primary User activity model

In this part, the probability of PU's transition, either changing state or remaining in the same state, is analysed. The two-stage markov chain PU's activity model was shown in Fig.8.5. In order to evaluate P_f and P_d for the proposed schemes, the probabilities related to PU activity needs to be analysed. Let $P(H_i)$ denotes the probability that PU is in H_i state and $P(H_i \rightarrow H_j)$ denotes the probability that PU was in H_i state and is in H_j state in the next sensing slot. For example, $P(H_0 \rightarrow H_0)$ means that PU remains idle and unchanged from previous to current sensing slot. The probabilities related to the PU's state and transition are defined as follows [97].

$$\begin{aligned}
P(H_0) &= \frac{\alpha}{(\alpha+\beta)} \\
P(H_1) &= \frac{\beta}{(\alpha+\beta)} \\
P(H_0 \rightarrow H_0) &= (1-\beta)\cdot P(H_0) \\
&= \frac{\alpha\cdot(1-\beta)}{\alpha+\beta} \\
P(H_0 \rightarrow H_1) &= \beta \cdot P(H_0) \\
&= \frac{\alpha\beta}{\alpha+\beta} \\
P(H_1 \rightarrow H_0) &= \alpha \cdot P(H_1) \\
&= \frac{\alpha\beta}{\alpha+\beta} \\
P(H_1 \rightarrow H_1) &= (1-\alpha)\cdot P(H_1) \\
&= \frac{(1-\alpha)\cdot\beta}{\alpha+\beta}.
\end{aligned} \tag{8.9}$$

In addition, the PU's state in each sensing slot is analyzed here because the proposed techniques do not only consider the current sensing slot, but also the previous slots. Let $\mathbf{S}$ be a set of PU's state in the current and previous time-slots, such that $\mathbf{S} = [s_0, s_1, s_2, ..., s_{2^N-1}]$. $\mathbf{S}_{idle}$ and $\mathbf{S}_{active}$ defines a subset of $\mathbf{S}$ where the PU is respectively idle and active in the current sensing-slot, regardless of its state in previous

Table 8.1: $\mathbf{S}$: Set of PU's state

	PU's State		One Previous Slot	Current Slot
$\mathbf{S}_{idle}$	s_0		H_0	H_0
	s_2		H_1	H_0
$\mathbf{S}_{active}$	s_1		H_0	H_1
	s_3		H_1	H_1

slots. Relationship between each element of $\mathbf{S}_{idle}$, $\mathbf{S}_{active}$ and each PU's state is shown in Table 8.1, assuming that two energy observations are weighted. Furthermore, the probabilities on PU's transition are shown in (8.10), where $P(s_i|H_l)$ is the conditional probability that PU belongs to s_i state given that it is in H_l state in the current sensing slot.

$$\begin{aligned} P(s_0|H_0) &= P(H_0 \rightarrow H_0|H_0) \\ &= {}^{P(H_0\rightarrow H_0)}/_{P(H_0)} \\ &= (1-\beta) \end{aligned}$$

and similarly

$$\begin{aligned} P(s_1|H_1) &= \alpha \\ P(s_2|H_0) &= \beta \\ P(s_3|H_1) &= (1-\alpha). \end{aligned} \tag{8.10}$$

8.6.2 Weighted SED

Here, we analyse the probability of false alarm and detection for Weighted SED scheme, where a fixed number of local observations from energy detector are taken into weighting process as in (8.1). The probability of false alarm and the probability of detection can be formulated as a summation of the probability that CR user makes an H_1 decision in each PU's state (s_i).

$$\begin{aligned} P_{f,WS}(\lambda) &= \sum_{\forall s_i \in \mathbf{S}_{idle}} P(\, T > \lambda |\, s_i) \cdot P(s_i) \\ P_{d,WS}(\lambda) &= \sum_{\forall s_i \in \mathbf{S}_{active}} P(\, T > \lambda |\, s_i) \cdot P(s_i). \end{aligned} \tag{8.11}$$

This generic form can be used to formulate these probabilities with any number of local observations. Here, for illustration purposes, we consider taking only two

observations in the weighting process. According to the transitional probability in (8.10), $P_{f,WS}$ and $P_{d,WS}$ from (8.11) can be expanded into

$$\begin{aligned} P_{f,WS}(\lambda) &= (1-\beta)\cdot P(T>\lambda \,|\, s_0) \\ &\quad + \beta \cdot P(T>\lambda \,|\, s_2) \end{aligned}$$

$$\begin{aligned} P_{d,WS}(\lambda) &= \alpha \cdot P(T>\lambda \,|\, s_1) \\ &\quad + (1-\alpha)\cdot P(T>\lambda \,|\, s_3). \end{aligned} \tag{8.12}$$

In order to obtain these probabilities, the weighted sum of observations under different PU's state needs to be evaluated. For instance, in the s_1 case where PU's state has changed from idle to active, obtaining $P(T>\lambda \,|\, s_1)$ needs an integration for PDF for T, which is difficult to find as follows.

$$\begin{aligned} P(T>\lambda \,|\, s_1) &= \int_{\lambda}^{\infty}\int_{0}^{t} f(y_1|H_0)\cdot f(y_2|H_1)\, dy_2\, dt \\ &= \int_{\lambda}^{\infty}\int_{0}^{t} f(2t-y_2|H_0)\cdot f(y_2|H_1)\, dy_2\, dt \end{aligned} \tag{8.13}$$

where $t=\frac{1}{2}(y_1+y_2)$, a weighted sum of received energy from previous and current sensing slot. For this reason, we resolve this complexity by numerically evaluating these terms using computer simulation. Due to mathematical difficulty to obtain the exact closed-form for $P_{f,WS}$ and $P_{d,WS}$, we present an approximated version here. The term $P(T>\lambda \,|\, s_i)$ are highly dependent on PU's state as the received energy follows different PDF when PU is idle and active. Hence, we need to consider this probability case by case.

First, consider s_0 case where PU is idle (H_0) in both current and previous sensing slots.

$$\begin{aligned} P(T>\lambda \,|\, s_0) &= P\left(\frac{(y_1+y_2)}{2}>\lambda\right) \\ &= P\Big(y_1+y_2>2\lambda\Big). \end{aligned} \tag{8.14}$$

Both y_1 and y_2 follow central Chi-Squared distribution with $2m$ degree of freedom as shown in (4.4). From this, y_1+y_2 which is a summation of two RVs also follows Chi-squared distribution with $4m$ degree of freedom. Hence, $P(T>\lambda \,|\, s_0)$ is approximated

as the CCDF in (2.28)

$$P(T > \lambda \,|\, s_0) \approx \frac{\Gamma(2m, \lambda)}{\Gamma(2m)}. \tag{8.15}$$

Then, for s_1 case, PU is idle in previous sensing slot and then becomes active in current slot. The received energy y_1, y_2 follows $f(y|H_0)$ and $f(y|H_1)$ as in (4.4) and (4.10) respectively. However, it was shown in (8.13) that the closed form is difficult to obtain. Here, we adopt the central limit theorem and approximate that y_1, y_2 follows Gaussian distribution [98] where

$$y_1 \sim \mathcal{N}\left(2m, 4m\right)$$

and

$$y_2 \sim \mathcal{N}\left(2m(1+\bar{\gamma}), 4m(1+\bar{\gamma})^2\right).$$

From this, $y_1 + y_2$ which can be approximated as derived in (2.39) as

$$y_1 + y_2 \sim \mathcal{N}\left(2m(2+\bar{\gamma}), 4m + 4m(1+\bar{\gamma})^2\right).$$

Hence, $P(T > \lambda \,|\, s_1)$ can be approximated as CCDF for Gaussian distribution in (2.24)

$$\begin{aligned} P(T > \lambda \,|\, s_1) &\approx \frac{1}{2} \operatorname{erfc}\left(\frac{2\lambda - 2m(2+\bar{\gamma})}{\sqrt{2 \cdot (4m + 4m(1+\bar{\gamma})^2)}}\right) \\ &\approx \frac{1}{2} \operatorname{erfc}\left(\frac{\lambda - m(2+\bar{\gamma})}{\sqrt{2 \cdot (m + m(1+\bar{\gamma})^2)}}\right). \end{aligned} \tag{8.16}$$

Then, the approximation for the case of s_2 is similar to the above case for s_1 because PU is active in one slot and idle in the other slot. Hence, $P(T > \lambda \,|\, s_2)$ also follows (8.16).

Finally, PU is active in both current and previous sensing slots for s_3 case. Considering that Doppler frequency and channel variation is low, the channel gain for y_1 and y_2 would approximately be the same. It is approximated that $y_1 + y_2$ follows (4.10) with extended time-bandwidth product of $2m$. Hence, $P(T > \lambda \,|\, s_3)$ can be approximated as a modified version of probability of detection in (4.11), with time-bandwidth product of $2m$ and detection threshold of 2λ.

Table 8.2: **D** : Set of CR's decision

CR's Decision		One Previous Slot	Current Slot
d_0		H_0	H_0
d_1		H_0	H_1
d_2		H_1	H_0
d_3		H_1	H_1

8.6.3 Two-Stage SED

In this section, we analyse the probability of false alarm and detection for Two-Stage SED scheme, $P_{f,TS}$ and $P_{d,TS}$. In this scheme, CR users adaptively determine the number of past observations based on the sensing result in the first stage. Hence, in addition to considering a set of PU's state (**S**), like in the Weighted SED scheme, the CR's first-stage decision also needs to be considered. Let **D** be a set of CR's decision from the first stage in the current and previous time-slots, such that $\mathbf{D} = [d_0, d_1, d_2, ..., d_{2^N-1}]$. Relationship between each element of **D** and the CR's first-stage decision is shown in Table 8.2, assuming that a maximum of two energy observations are considered. First, the conditional probability related to CR making the decision, when PU is idle and active is defined here. Let $P(H_i|H_j)$ be the probability that CR makes its first stage H_i decision when PU is in H_j state.

$$\begin{aligned} F &= P(H_1|H_0) \\ &= P_f(\lambda_1) \\ D &= P(H_1|H_1) \\ &= P_d(\lambda_1). \end{aligned} \tag{8.17}$$

P_f and P_d for Two-Stage SED scheme can be formulated in a generic form as a summation of the probability that CR makes each first-stage decision (d_i) in each PU's state (s_i), as

$$\begin{aligned} P_{f,TS}(\lambda_2) &= \sum_{\forall s_i \in \mathbf{S}_{idle}, \forall d_j \in \mathbf{D}} P(T > \lambda_2 | s_i, d_j) \cdot P(s_i, d_j) \\ P_{d,TS}(\lambda_2) &= \sum_{\forall s_i \in \mathbf{S}_{active}, \forall d_j \in \mathbf{D}} P(T > \lambda_2 | s_i, d_j) \cdot P(s_i, d_j) \end{aligned} \tag{8.18}$$

where λ_2 is the detection threshold in the second stage. Similarly to the analysis for Weighted-SED scheme, this generic form can be used to formulate the probability

of false alarm and detection with any number of local observations. However, the complexity increases with the number of local observations.

For instance, assuming that a maximum of two observations are allowed in the second stage, $P_{f,TS}$ and $P_{d,TS}$ can be expanded as follows, according to the probability of PU's transition in (8.10) and the probability related to the first-stage detection in (8.17).

$$\begin{aligned}
P_{f,TS}(\lambda_2) = {} & (1-F)\cdot(1-F)\cdot(1-\beta)\cdot P(T>\lambda_2|s_0,d_0) \\
& + (1-F)\cdot F\cdot(1-\beta)\cdot P(T>\lambda_2|s_0,d_1) \\
& + F\cdot(1-F)\cdot(1-\beta)\cdot P(T>\lambda_2|s_0,d_2) \\
& + F\cdot F\cdot(1-\beta)\cdot P(T>\lambda_2|s_0,d_3) \\
& + (1-D)\cdot(1-F)\cdot\beta\cdot P(T>\lambda_2|s_2,d_0) \\
& + (1-D)\cdot F\cdot\beta\cdot P(T>\lambda_2|s_2,d_1) \\
& + D\cdot(1-F)\cdot\beta\cdot P(T>\lambda_2|s_2,d_2) \\
& + D\cdot F\cdot\beta\cdot P(T>\lambda_2|s_2,d_3).
\end{aligned}$$

$$\begin{aligned}
P_{d,TS}(\lambda_2) = {} & (1-F)\cdot(1-D)\cdot\alpha\cdot P(T>\lambda_2|s_1,d_0) \\
& + (1-F)\cdot D\cdot\alpha\cdot P(T>\lambda_2|s_1,d_1) \\
& + F\cdot(1-D)\cdot\alpha\cdot P(T>\lambda_2|s_1,d_2) \\
& + F\cdot D\cdot\alpha\cdot P(T>\lambda_2|s_1,d_3) \\
& + (1-D)\cdot(1-D)\cdot(1-\alpha)\cdot P(T>\lambda_2|s_3,d_0) \\
& + (1-D)\cdot D\cdot(1-\alpha)\cdot P(T>\lambda_2|s_3,d_1) \\
& + D\cdot(1-D)\cdot(1-\alpha)\cdot P(T>\lambda_2|s_3,d_2) \\
& + D\cdot D\cdot(1-\alpha)\cdot P(T>\lambda_2|s_3,d_3). \qquad (8.19)
\end{aligned}$$

The $P_{f,TS}$ and $P_{d,TS}$ shown above is in a fullly-expanded generic form and it can be categorized into three special cases depending on the value of first-stage and second-stage threshold (λ_1 and λ_2).

λ_2 is less than λ_1

Consider the term $P(T > \lambda_2|s_i, d_1)$ from (8.19). As CR's decision d_1 is different between previous and current sensing slot, only then observation from the current slot

is taken into second stage. Due to the CR's first-stage decision H_1 for current sensing slot, it deduces that the observation is larger than λ_1. Consequently, it means that T is larger than λ_1. Hence, $P(T > \lambda_2|s_i, d_1)$ is always 1 here as λ_2 is less than λ_1.

Similarly to above for the term $P(T > \lambda_2|s_i, d_3)$, two observations are taken into weighting process here. Due to CR's decision H_1 for both previous and current sensing slot, this also deduces that both observations are larger than λ_1. As T is a weighted summation from both observations, T here is also larger than λ_1. Hence, $P(T > \lambda_2|s_i, d_3)$ is also always 1 here as λ_2 is less than λ_1.

P_f and P_d from (8.19) can be shortened into (8.20).

$$\begin{aligned}
P_{f,TS}(\lambda_2) = {} & F + (1-F)\cdot(1-F)\cdot(1-\beta)\cdot P(T > \lambda_2|s_0, d_0) \\
& + F\cdot(1-F)\cdot(1-\beta)\cdot P(T > \lambda_2|s_0, d_2) \\
& + (1-D)\cdot(1-F)\cdot\beta\cdot P(T > \lambda_2|s_2, d_0) \\
& + D\cdot(1-F)\cdot\beta\cdot P(T > \lambda_2|s_2, d_2) \\
P_{d,TS}(\lambda_2) = {} & D + (1-F)\cdot(1-D)\cdot\alpha\cdot P(T > \lambda_2|s_1, d_0) \\
& + F\cdot(1-D)\cdot\alpha\cdot P(T > \lambda_2|s_1, d_2) \\
& + (1-D)\cdot(1-D)\cdot(1-\alpha)\cdot P(T > \lambda_2|s_3, d_0) \\
& + D\cdot(1-D)\cdot(1-\alpha)\cdot P(T > \lambda_2|s_3, d_2). \qquad (8.20)
\end{aligned}$$

Then, to obtain the closed-form for the probability terms, consider CR's decision d_2 where the decision from the previous and current sensing slot is different. Hence, only energy observation from the current slot is taken into weighting process such that $T = Y$. With the first-stage decision of H_0, this deduces that T follows truncated distribution, following either H_0 or H_1 but only restricted from 0 to λ_1. Consider $P(T > \lambda_2|s_i, d_2)$ which is defined by the probability that T is larger than λ_2. Consequently, $P(T > \lambda_2|s_i, d_2)$ term in (8.20) analytically becomes

$$\begin{aligned}
P(T > \lambda_2|s_i \in \mathbf{S}_{idle}, d_2) &= \frac{P_f(\lambda_2) - P_f(\lambda_1)}{1 - P_f(\lambda_1)} \\
P(T > \lambda_2|s_i \in \mathbf{S}_{active}, d_2) &= \frac{P_d(\lambda_2) - P_d(\lambda_1)}{1 - P_d(\lambda_1)}. \qquad (8.21)
\end{aligned}$$

Next, consider $P(T > \lambda_2|s_i, d_0)$ where CR's decision is d_0 and the decision from the previous and current sensing slot is similar and two observations are taken into weighting process. Here, T follows a joint distribution, based on s_i. For example, in the

s_1, d_0 case, T is a weighted summation from the two observations which respectively follows truncated H_0 in previous slot and truncated H_1 in current sensing slot. Because T follows a distribution from summation of two truncated distributions, it is difficult to analytically obtain the term $P(T > \lambda_2|s_i, d_0)$, as it involves various integrations of PDF for different truncated distributions as follows.

for $0 < t < \frac{\lambda_1}{2}$,

$$\begin{aligned} f_t(t|s_1, d_0) &= \int_0^{2t} f(y_1|H_0) \cdot f(y_2|H_1)\, dy_2 \\ &= \int_0^{2t} f(2t - y_2|H_0) \cdot f(y_2|H_1)\, dy_2 \end{aligned}$$

for $\frac{\lambda_1}{2} < t < \lambda_1$,

$$f_t(t|s_1, d_0) = \int_{2t-\lambda_1}^{\lambda_1} f(2t - y_2|H_0) \cdot f(y_2|H_1)\, dy_2$$

and for otherwise,

$$f_t(t|s_1, d_0) = 0. \tag{8.22}$$

Then, to find the probability that T is greater than λ_2, we need

$$P(T > \lambda_2) = \int_{\lambda_2}^{\infty} f_t(t)\, dt. \tag{8.23}$$

For this reason, it makes the analysis mathematically difficult and we resolve this complexity by numerically evaluating these terms using computer simulation. Later on, the approximated version of these terms will be discussed in Section 8.6.4.

λ_2 equals to λ_1

Here when λ_2 equals to λ_1, the terms $P(T > \lambda_2|s_i, d_1)$ and $P(T > \lambda_2|s_i, d_3)$ from (8.19) are always 1, as mentioned above. Contrarily, for the terms $P(T > \lambda_2|s_i, d_0)$ and $P(T > \lambda_2|s_i, d_2)$, the observations here, for both previous and current sensing slot, are less than λ_1. When λ_2 equals to λ_1, we can deduce that the terms $P(T > \lambda_2|s_i, d_0)$ and $P(T > \lambda_2|s_i, d_2)$ are always 0. Consequently, $P_{f,TS}$ and $P_{d,TS}$ can be shortened to

$$\begin{aligned} P_{f,TS}(\lambda_2) &= F \\ &= P_f(\lambda_1) \\ P_{d,TS}(\lambda_2) &= D \\ &= P_d(\lambda_1). \end{aligned} \tag{8.24}$$

The relationship in this special case explains why there is a dip on the Receiver Operating Characteristic (ROC) curve, where the detection performance for Two-Stage SED is exactly the same as conventional scheme, as shown in Fig. 8.9.

λ_2 is larger than λ_1

Similarly to above, when λ_2 is larger than λ_1, the terms $P(T > \lambda_2|s_i, d_0)$ and $P(T > \lambda_2|s_i, d_2)$ are always 0, as the observations are always lower than λ_1 and λ_2.

Consequently, $P_{f,TS}$ and $P_{d,TS}$ become

$$\begin{aligned}
P_{f,TS}(\lambda_2) = &(1-F)\cdot F\cdot(1-\beta)\cdot P(T>\lambda_2|s_0,d_1)\\
&+ F\cdot F\cdot(1-\beta)\cdot P(T>\lambda_2|s_0,d_3)\\
&+ (1-D)\cdot F\cdot\beta\cdot P(T>\lambda_2|s_2,d_1)\\
&+ D\cdot F\cdot\beta\cdot P(T>\lambda_2|s_2,d_3)\\
P_{d,TS}(\lambda_2) = &(1-F)\cdot D\cdot\alpha\cdot P(T>\lambda_2|s_1,d_1)\\
&+ F\cdot D\cdot\alpha\cdot P(T>\lambda_2|s_1,d_3)\\
&+ (1-D)\cdot D\cdot(1-\alpha)\cdot P(T>\lambda_2|s_3,d_1)\\
&+ D\cdot D\cdot(1-\alpha)\cdot P(T>\lambda_2|s_3,d_3). \qquad (8.25)
\end{aligned}$$

Here, when CR's decision is d_1, the analysis is similar to (8.21) and its consideration on CR's decision d_2 above. For the CR's decision d_1 here, where the decision from the previous and current sensing slot is also different, $P(T > \lambda_2|s_i, d_1)$ terms in (8.20) analytically becomes

$$\begin{aligned}
P(T>\lambda_2|s_i\in\mathbf{S}_{idle},d_1) &= \frac{P_f(\lambda_2)}{P_f(\lambda_1)}\\
P(T>\lambda_2|s_i\in\mathbf{S}_{active},d_1) &= \frac{P_d(\lambda_2)}{P_d(\lambda_1)}. \qquad (8.26)
\end{aligned}$$

Finally, when CR's decision is d_3, two observations are weighted. As T follows a joint distribution from two truncated distributions, it is difficult to analytically obtain the term $P(T > \lambda_2|s_i, d_3)$. We also resolve it by numerically evaluating these probability terms.

8.6.4 Two-Stage SED Approximation

Due to mathematical difficulty to obtain the exact closed-form for some terms in $P_{f,TS}$ and $P_{d,TS}$, we present an approximation to these terms where two obseravations are in the weighting process. Here, we adopt Gaussian distribution for the approximation, similarly to the Weighted SED scheme above. Although T is the summation of two RVs which follow truncated distribution, for simplicity, we do not consider truncation but consider approximation to T as a summation of two Gaussian RVs. However, truncation is considered when evaluating the term $P(T > \lambda_2|s_i, d_i)$. When λ_2 is less than λ_1,

$$P(T > \lambda_2|s_i, d_i) \approx \frac{\text{CCDF}(\lambda_2) - \text{CCDF}(\lambda_1)}{1 - \text{CCDF}(\lambda_1)} \tag{8.27}$$

given that CCDF(.) is a CCDF function for a Gaussian distribution as shown in (2.24). And when λ_2 is larger than λ_1,

$$P(T > \lambda_2|s_i, d_i) \approx \frac{\text{CCDF}(\lambda_2)}{\text{CCDF}(\lambda_1)}. \tag{8.28}$$

For instance, in s_1 and λ_2 is larger than λ_1 case, T can be approximated to follow

$$\mathcal{N}\left(m(2+\bar{\gamma}), m + m(1+\bar{\gamma})^2\right).$$

Then,

$$\begin{aligned} P(T > \lambda_2|s_1, d_3) &\approx \frac{\text{CCDF}(\lambda_2)}{\text{CCDF}(\lambda_1)} \\ &\approx \frac{\text{erfc}\left(\frac{\lambda_2 - m(2+\bar{\gamma})}{\sqrt{2\cdot(m+m(1+\bar{\gamma})^2)}}\right)}{\text{erfc}\left(\frac{\lambda_1 - m(2+\bar{\gamma})}{\sqrt{2\cdot(m+m(1+\bar{\gamma})^2)}}\right)}. \end{aligned} \tag{8.29}$$

8.6.5 Differential SED

Similar to the Two-Stage SED scheme, Differential SED scheme also adaptively determines the number of local observations. Hence, to consider $P_{f,Diff}$ and $P_{d,Diff}$ for this Differential SED, the probability that the difference between two consecutive observations is less than λ_d is needed, such that

$$P(\delta_k < \lambda_d)$$

where $\delta_k = |y_k - y_{k-1}|$, i.e. the difference between two consecutive observations.

Table 8.3: $\mathbf{C}$: Set of condition towards number of local observations in Differential SED

		Condition	N
c_1		$\delta_k > \lambda_d$	1
c_2		$\delta_k < \lambda_d$ and $\delta_{k-1} > \lambda_d$	2
c_3		$\delta_k < \lambda_d$ and $\delta_{k-1} < \lambda_d$ and $\delta_{k-2} > \lambda_d$	3
c_3		$\delta_k < \lambda_d$ and $\delta_{k-1} < \lambda_d$ and $\delta_{k-2} < \lambda_d$	4

First, the probability that defines how many past observations are taken into weighting process needs to be considered. Table 8.3 shows $\mathbf{C}$, a set of different conditions towards number of local observations which are taken into weighting process in Differential SED, assuming that it is in the k^{th} sensing-slot and a maximum of four observations, i.e. three past observations, are allowed in the weighting process and N represents number of local observations in the weighting process.

Then, $P_{f,Diff}$ and $P_{d,Diff}$ for this Differential SED scheme can be defined as

$$P_{f,Diff}(\lambda_2) = \sum_{\forall s_i \in \mathbf{S}_{idle}, \forall c_j \in \mathbf{C}} P(T > \lambda_2 | s_i, c_j) \cdot P(s_i, c_j)$$
$$P_{d,Diff}(\lambda_2) = \sum_{\forall s_i \in \mathbf{S}_{active}, \forall c_j \in \mathbf{C}} P(T > \lambda_2 | s_i, c_j) \cdot P(s_i, c_j). \quad (8.30)$$

However, to track this probability $P(s_i, c_j)$, it involves two or more random variables, each of which is either H_0 or H_1-distributed, and its difference. The analysis, therefore, becomes very difficult and, to the author's best knowledge, is mathematically un-trackable. For this reason, we do not further analyze the P_f and P_d for Differential SED in this thesis.

8.7 Simulation Results

In this section, three SED schemes are evaluated using computer simulation with the following parameters. Three spatially separated users are considered for cooperative sensing. The time-bandwidth product is set to 3 for each observation. Each packet has length of 100 symbols and the sampling frequency is 100 kHz. The PU's SNR is 3dB and the channel is modelled as a time-varying Rayleigh fading channel with Doppler frequency of 50 Hz. For the two adaptive schemes, we set a maximum of three previous observations in the weighting process. Some parameters, which are specific to any particular scheme, are mentioned within its own part.

8.7.1 Weighted SED

As shown in Section 8.3, when the PU activity is static, equal weighting is the optimal weight for the H_0 case, but not for the H_1 case. Hence we first evaluate the performance for optimal weighting under the two cases. Then, the intermittent PU activity is modelled and the detection performance of the proposed Weighted SED with equal and exponential weighting is evaluated.

Optimal H_0 and H_1 weighting vector

To evaluate the weight vector for static PU activity, PU is modelled such that it is either always on or always off. The equal weighting $\mathbf{W} = [\ 0.25 \quad 0.25 \quad 0.25 \quad 0.25\ ]$ is optimal when three previous observations are taken. However for the H_1 case, we found by numerical methods that the set of optimal weighting vector which minimizes the variance of H_1 is $\mathbf{W} = [\ 0.334 \quad 0.166 \quad 0.166 \quad 0.334\ ]$.

The detection performance for the Weighted SED scheme in 50 Hz correlated channel with the optimized weight vectors is shown in Fig.8.7, where Q_f and Q_d represent the probability of false alarm and detection for cooperative spectrum sensing. We model that it is equally probable for PU to be idle and active. The results show that the Weighted SED provides significantly better detection performance than the conventional cooperative OR-rule energy detection scheme. This is due to the use of past observations that are available locally. The equal weighting is shown to outperform the weighting that minimizes the variance in H_1 case. Moreover, the advantage of using equal weighting is that it is SNR and channel correlation independent, while the optimization by search algorithm for minimum variance in H_1 case is dependent upon the SNR and channel correlation.

Then, intermittent PU activity is introduced and the detection performance from equal and exponential weighting vector are considered in Fig. 8.8. Similar to the above, we consider three past observations for Weighted SED scheme. The PU activity factor α and β are both set equal to 0.001 and 0.1 for the case that PU seldom and regularly changes its state respectively. First, we investigate the detection performance for the proposed Weighted SED scheme on equal weighting. Simulation result shows that the PU activity affects the detection performance. When PU movement is low in the α and β equal to 0.001 case, the proposed Weighted SED scheme with equal weighting

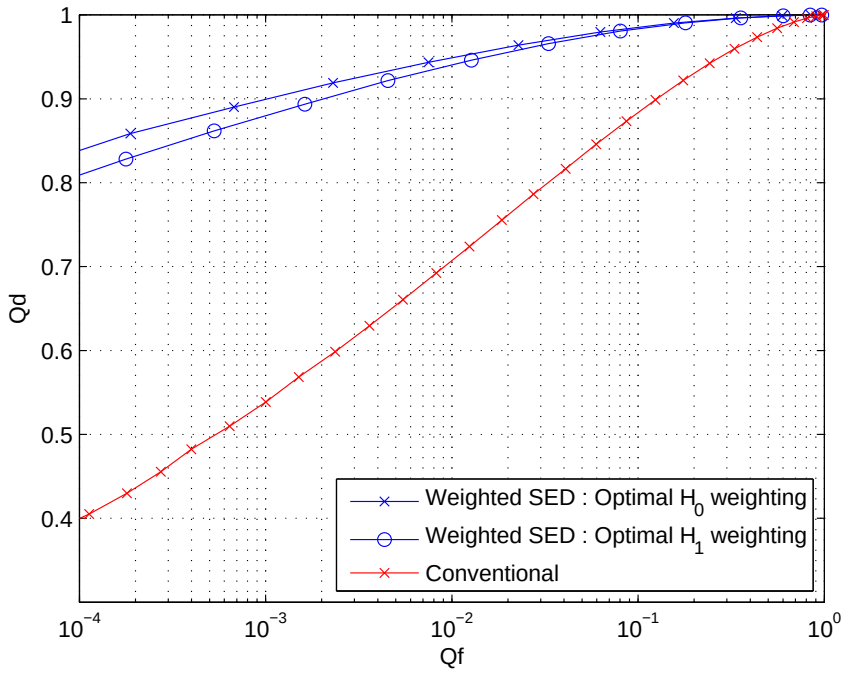

Figure 8.7: Detection performance for Weighted SED scheme with three previous observations on optimal H_0 and optimal H_1 weighting vector, when PU is static

is better than the conventional technique in high false alarm region, but still worse than the conventional technique in low false alarm region. However, when α and β are equal to 0.1, the detection performance is worsened and it is even worse than the conventional energy detection technique which does not take any previous observation. This is because when the PU activity varies a lot, equal weighting relied too heavily on past observation that is already outdated. Hence, it is better to simply use the current observation. Then, the detection performance for the proposed Weighted SED scheme on exponential weighting is investigated. The PU activity is set similarly to the previous one with equal weighting. The result shows that the proposed exponential weighting provides an improvement on detection performance when α and β equal to 0.1, the proposed exponential weighting improves the detection performance in the high false alarm area above the conventional technique. By applying exponential weighting, the more recent observations get higher weighting than the older observation, while the equal weighting one gives the same weight for every observation. When PU changes its activity between idle and active, previous observations in further time slot can be outdated and affect the sum T, which then also affect sensing result and the detection performance.

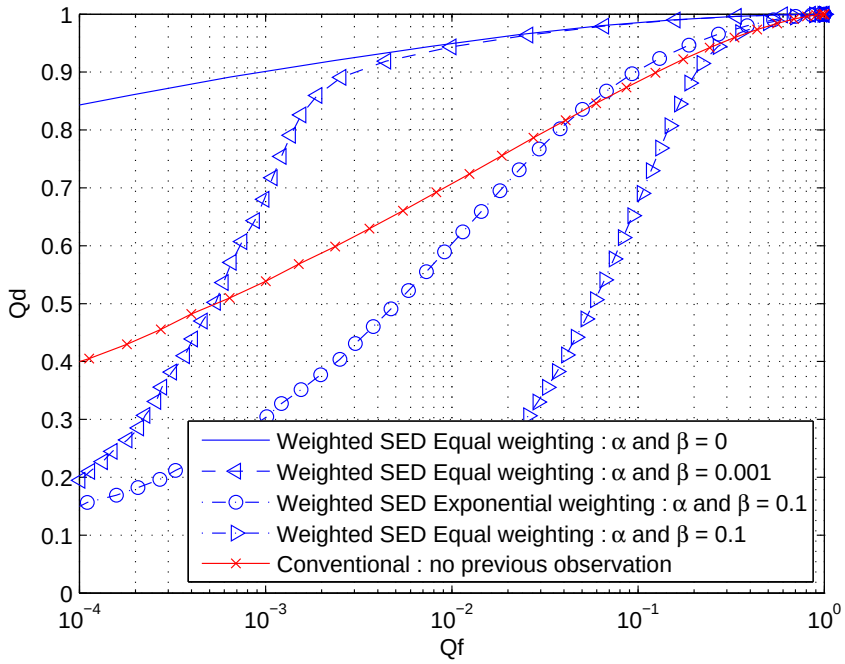

Figure 8.8: Detection performance for Weighted SED scheme with static and intermittent PU activity in 50 Hz correlated channel

8.7.2 Two-Stage SED

Here, we evaluate the detection performance for the proposed Two-Stage SED scheme, where a maximum of three previous observations are taken. Other simulation parameters are set up similarly to the Weighted SED scheme above. The PU activity is modelled with high variation such that α and β is 0.1. The detection performance for the proposed Two-Stage SED is evalutaed and compared to the Weighted SED scheme on equal weighting with one previous observation, which has best performance and the conventional scheme. The weighted SED with one previous observation has the best detection performance due to its reliance on past observations to improve the performance, but not too much that the performance will be affected in the case that PU has changed its state. The detection performance for this scheme is shown in Fig. 8.9.

Simulation results show that the detection performance is improved in the high probability of detection area, in which the spectrum sensing procedure is expected to operate. In this scheme, there is a dip on the ROC curve, at that point the detection performance is the same as conventional scheme. This occurs when the value of two thresholds (λ_1 and λ_2) are the same. The reason for this behavior was analytically

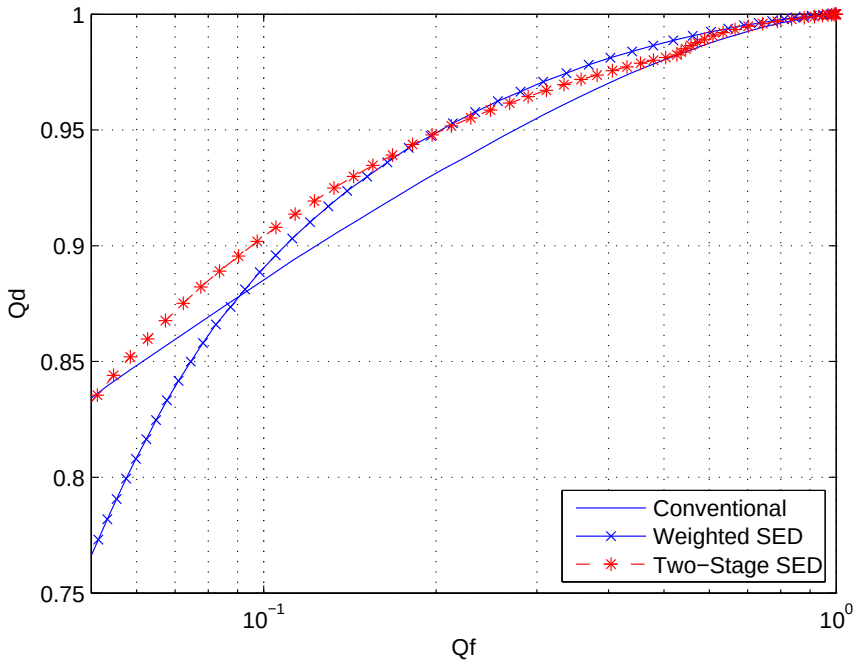

Figure 8.9: Detection performance for the Two-Stage SED scheme in 50 Hz correlated channel case

explained in Section 8.6.3. Besides, in terms of the sensing requirement under this simulation settings, the Two-Stage SED can meet the IEEE 802.22 WRAN spectrum sensing requirement on the probability of false alarm (10%) and detection (90%) [99], while the conventional and Weighted SED scheme can not.

8.7.3 Differential SED

In this scheme, simulation parameters are set up as similar to the Two-Stage SED, i.e. a maximum of three previous observations are taken with time-bandwidth of 3. The detection performance for the Differential SED is shown in Fig. 8.10. This scheme can provide an improvement on detection performance in high probability of detection area, but without a performance dip as occurred in the Two-Stage SED scheme. It also outperforms both the Weighted SED and the conventional scheme. Moreover, similarly to the Two-Stage SED, the Differential SED can also meet the IEEE 802.22 spectrum sensing requirement, while Weighted SED and conventional scheme fail to do so.

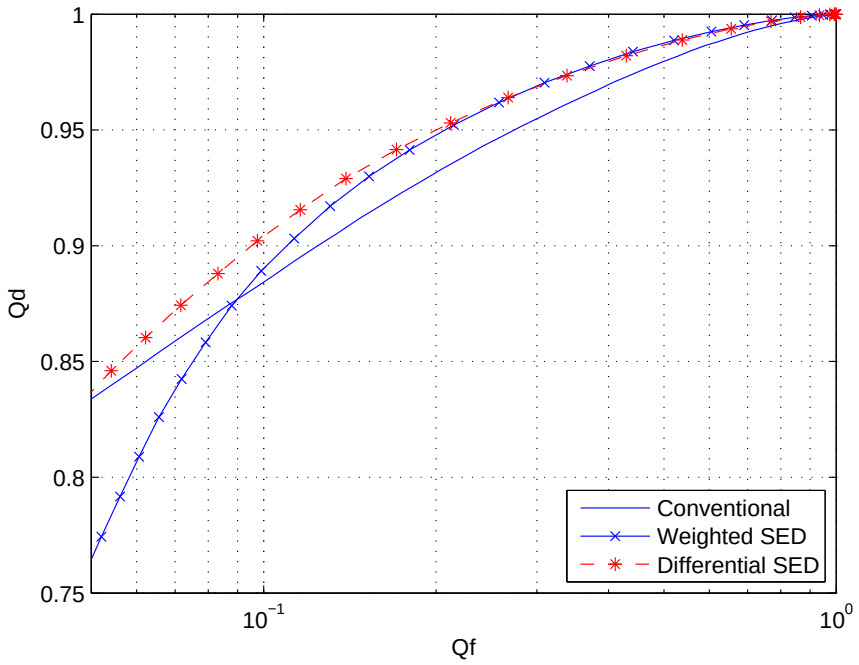

Figure 8.10: Detection performance for the Differential SED scheme in 50 Hz correlated channel case

8.7.4 SNR requirement for IEEE 802.22 standard

In this part, both adaptive schemes are evaluated in terms of the minimum required SNR to achieve the IEEE 802.22 target Q_f and Q_d in different scenarios of PU activity. The simulation parameters are set up similarly to the previous part. The two schemes are evaluated and compared with the conventional single threshold scheme.

Fig. 8.11 shows a minimum SNR for achieving the target of 90% probability of detection and 10% probability of false alarm under different PU activity. Simulation result, shown in Fig. 8.11, shows that the weighted SED provides an advantage over the conventional scheme when PU activity is low. However, in the case that PU activity is high, where PU frequently changes its state, its performance degrades as Weighted SED still relies on the previous observation which is already outdated.

In addition, the result shows that the Two-Stage SED outperforms the Weighted SED and conventional scheme. In case when PU activity is low, high performance gain can be achieved. For instance, when α and β is 0.01, SNR needs to be at least 3.35 dB for the conventional scheme to achieve the detection performance target, while it is only 0 dB for the Two-Stage SED and Differential SED. Furthermore, in case when PU activity is high such as α and β is 0.1, only 2.6 and 2.85 dB of SNR is required

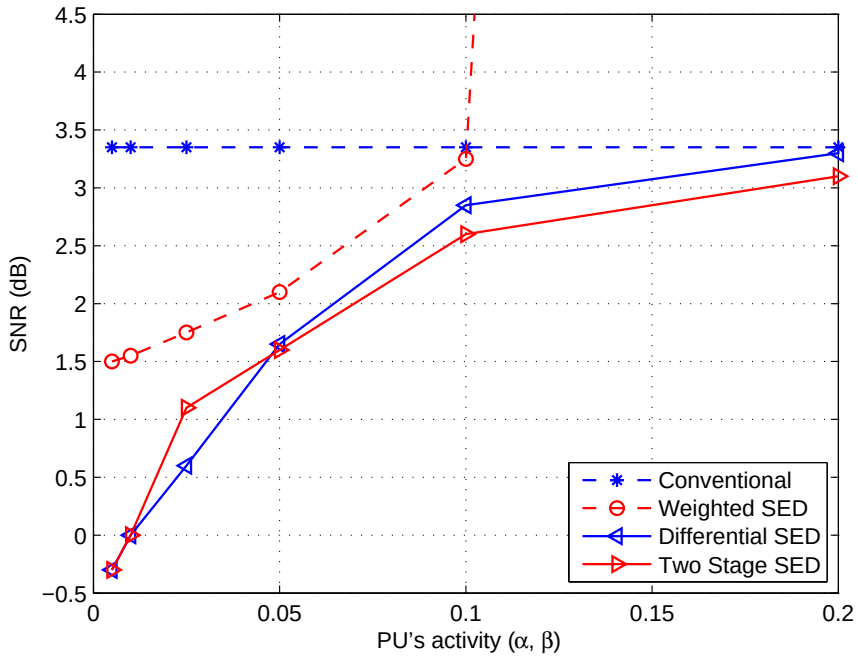

Figure 8.11: Minimum required SNR for target probability of detection and false alarm

respectively for the Two-Stage SED and Differential SED to acheive the detection target, while conventional scheme requires 3.35 dB.

8.7.5 Analysis for probability of false alarm and detection

Here, we show the probability of false alarm and detection, which is obtained from the generic form, discussed in Section 8.6.2. First, we consider the Weighted SED. Then, the adaptive Two-Stage SED scheme is considered.

Weighted SED

Fig. 8.12 show the analytical result and its approximation on P_f and P_d for equal weighting Weighted SED scheme with two local observations in the weighting process and compare them with P_f and P_d obtained entirely from the simulation. The other simulation parameters are set as similar in the previous section. PU acitivity is modelled intermittent with α and β set to 0.1. The results show that both the probabilities obtained numerically closely match with those obtained entirely from the simulation. In addition, the approximation is also shown to be accurate.

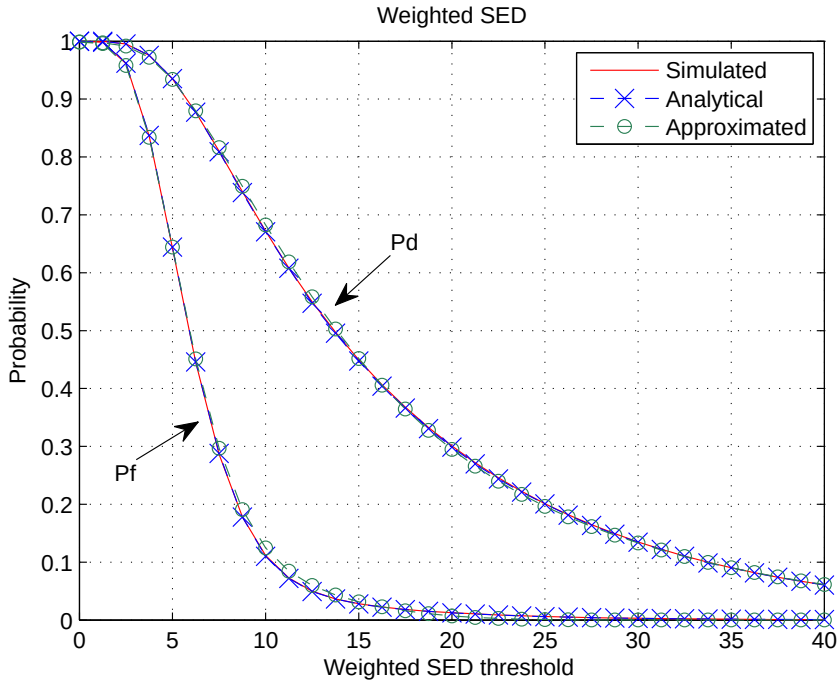

Figure 8.12: Probability of false alarm and detection in Weighted SED scheme

Two-Stage SED

We consider $P_{f,TS}$ and $P_{d,TS}$ for Two-Stage SED scheme. Unlike the Weighted SED scheme where only PU's state is considered, the analysis here considers both PU's state and CR's decision in the first-stage sensing.

Fig. 8.13 show P_f and P_d in Two-Stage SED scheme with a maximum of two local observations in the weighting process and compare them with P_f and P_d obtained entirely from the simulation. We set the first stage threshold to 8 and the other simulation parameters are set as similar in the previous results. The results show that both probability of false alarm and detection obtained from the analysis match with those entirely from simulation and the analysis is accurate. In addition, the approximation is also shown to be accurate in high P_d region, within which the CR system is expected work on.

8.8 Summary

In this chapter, three sequential cooperative spectrum sensing techniques are presented. By taking energy observations in previous sensing slots, these schemes can

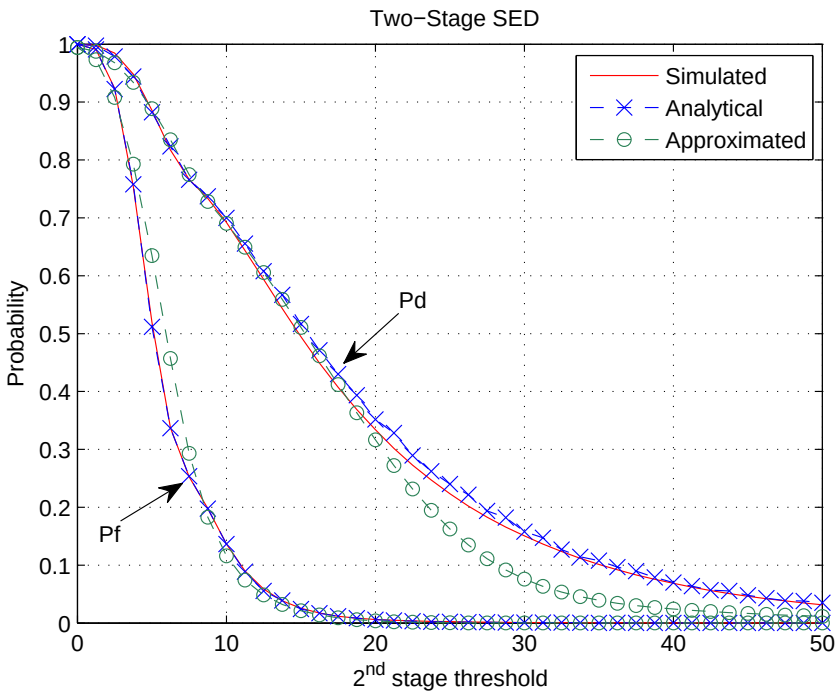

Figure 8.13: Probability of false alarm and detection in Two-Stage SED scheme

exploit the time varying nature of the channel. Simulation results show that these Weighted SED, Two-Stage SED and Differential SED can improve the detection performance. Especially in the Two-Stage SED and Differential SED, by adaptively relying on the past observations upon the CR's decision on the PU's state, further improvement on detection performance can be achieved. Moreover, both schemes are shown to provide a performance gain on minimum required SNR to achive the IEEE 802.22 standard of 10% false alarm and 90% detection. When PU activity is low, a significant gain can be achieved by using the adaptive schemes. Effectively this allows the CR system to work in scenarios that conventional techniques can not accommodate the requirements.

Furthermore, a detailed analysis on the probability of false alarm and detection in Weighted SED and Two-Stage SED schemes are derived. The approximated version for these SED schemes is also given and shown to match with the simulated result. In addition, this analysis can help further optimize the cooperative spectrum sensing performance.

Chapter 9

Conclusions and Future Works

9.1 Conclusions

In this thesis, various techniques for cooperative spectrum sensing for CR have been extensively studied. First, the background theory and related statistics for CR spectrum sensing is summarized. By forwarding CR's local observations to the fusion center, an EGC-SDC cooperative spectrum sensing scheme can improve the detection performance. However, this scheme requires large communication overhead from the CR users and the fusion center. To reduce the overhead, a Quantized cooperative spectrum sensing scheme quantizes its local observations and forwards to the fusion center to make the final decision. Alternatively, Double Threshold cooperative spectrum sensing technique only forwards CR's local observation when CR user is not certain about its observation and cannot make its own decision. Quantization is also applied to this scheme to further reduce the communication overhead.

In addition, the other aspects of improving the detection performance are studied in Sequential Energy Detector, where CR users periodically sense the spectrum. By relying on the previous observations, the detection performance is improved in the Weighted SED scheme. However, relying on fixed number of observations can deteriorate the sensing performance when PU is highly intermittent as the previous observations are outdated. Two adaptive schemes, which aim to detect when PU changes its state and adapt its sensing parameter accordingly, are proposed. It was shown that the adaptive schemes can improve the detection performance as well as enable the CR to work within IEEE802.22 WRAN standard under lower minimum

SNR requirement than that of the conventional OR-HDC scheme.

Moreover, the closed-form analysis for various spectrum sensing schemes are investigated. The derivation for probability of detection and false alarm in EGC-SDC, Double Threshold, Weighted SED and Two-Stage SED scheme are also presented. We also provided an approximation for P_f and P_d under Weighted SED and Two-Stage SED scheme.

9.2 Future Works

In this section, we list the following possible future works

1. **Closed-form analysis for Probability of Detection and False alarm**

   In order to optimize the sensing parameters at CR users, it is vital that the closed-form for P_f and P_d is available. In this work, we showed that closed-form derivation is possible and can be approximated. However, it comes with high computational complexity. If an exact closed-form is available with low complexity, the optimization for Quantized, Double Threshold and Sequential cooperative spectrum sensing schemes may be derivable.

2. **Quantized Cooperative Spectrum Sensing**

   There are various quantization schemes apart from ones that are studied in this thesis, for instance, an iterative Linde-Buzo-Gray algorithm. The challenge here is how to choose an appropriate scheme which has low complexity burden on CR system and provides better detection performance.

References

[1] Y. K. Kim and R. Prasad, *4G roadmap and emerging communication technologies*. Artech House, 2006.

[2] U. S. Jha and R. Prasad, *OFDM towards fixed and mobile broadband wireless access*. Artech House, Inc., 2007.

[3] A. Osseiran, J. F. Monserrat, and W. Mohr, *Mobile and Wireless Communications for IMT-advanced and Beyond*. Wiley, 2011.

[4] E. Dahlman, S. Parkvall, and J. Skold, *4G: LTE/LTE-Advanced for Mobile Broadband: LTE/LTE-Advanced for Mobile Broadband*. Academic Press, 2011.

[5] T. Janevski, "5g mobile phone concept," in *Consumer Communications and Networking Conference, 2009. CCNC 2009. 6th IEEE*. IEEE, 2009, pp. 1–2.

[6] J. Mitola III and G. Q. Maguire Jr, "Cognitive radio: making software radios more personal," *Personal Communications, IEEE*, vol. 6, no. 4, pp. 13–18, 1999.

[7] I. Akyildiz, W. Lee, M. Vuran, and S. Mohanty, "Next generation/dynamic spectrum access/cognitive radio wireless networks: a survey," *Computer Networks*, vol. 50, no. 13, pp. 2127–2159, 2006.

[8] G. Ganesan and Y. Li, "Cooperative spectrum sensing in cognitive radio, part i: Two user networks," *Wireless Communications, IEEE Transactions on*, vol. 6, no. 6, pp. 2204–2213, 2007.

[9] J. Mitola III, "Software radios: Survey, critical evaluation and future directions," *IEEE Aerospace and Electronic Systems Magazine*, vol. 8, no. 4, pp. 25–36, 1993.

[10] K. Seshukumar, R. Saravanan *et al.*, "Spectrum sensing review in cognitive radio," in *Emerging Trends in VLSI, Embedded System, Nano Electronics and Telecommunication System (ICEVENT), 2013 International Conference on*. IEEE, 2013, pp. 1–4.

[11] M. Lopez-Benitez and F. Casadevall, "Improved energy detection spectrum sensing for cognitive radio," *Communications, IET*, vol. 6, no. 8, pp. 785–796, 2012.

[12] D. Tse and P. Viswanath, *Fundamentals of wireless communication*. Cambridge university press, 2005.

[13] T. Rappaport, *Wireless communications: principles and practice*. Publishing House of Electronics Industry, 2004.

[14] A. Goldsmith, *Wireless communications*. Cambridge university press, 2005.

[15] V. Erceg, L. J. Greenstein, S. Y. Tjandra, S. R. Parkoff, A. Gupta, B. Kulic, A. A. Julius, and R. Bianchi, "An empirically based path loss model for wireless channels in suburban environments," *Selected Areas in Communications, IEEE Journal on*, vol. 17, no. 7, pp. 1205–1211, 1999.

[16] M. K. Simon and M.-S. Alouini, *Digital communication over fading channels*. Wiley-Interscience, 2005, vol. 95.

[17] N. C. Beaulieu and K. T. Hemachandra, "New simple solutions for the bivariate rician pdf and cdf," in *Wireless Communications and Networking Conference (WCNC), 2010 IEEE*. IEEE, 2010, pp. 1–4.

[18] F. F. Digham, M.-S. Alouini, and M. K. Simon, "On the energy detection of unknown signals over fading channels," *Communications, IEEE Transactions on*, vol. 55, no. 1, pp. 21–24, 2007.

[19] G. Williams, "Quantising for minimum error with particular reference to speech," *Electronics Letters*, vol. 3, p. 134, 1967.

[20] J. Max, "Quantizing for minimum distortion," *Information Theory, IRE Transactions on*, vol. 6, no. 1, pp. 7–12, 1960.

[21] M. Paez and T. Glisson, "Minimum mean-squared-error quantization in speech PCM and DPCM systems," *Communications, IEEE Transactions on [legacy, pre-1988]*, vol. 20, no. 2, pp. 225–230, 1972.

[22] M. Basseville and A. Benveniste, "Desgin and comparative study of some sequential jump detection algorithms for digital signals," *Acoustics, Speech and Signal Processing, IEEE Transactions on*, vol. 31, no. 3, pp. 521–535, 1983.

[23] V. Andrejev, "Optimization of autoregressive models of interfering radio-reflections," *Radioelectronics and Communications Systems*, vol. 51, no. 7, pp. 377–380, 2008.

[24] J. Proakis and D. Manolakis, *Digital Signal Processsing*. Prentice Hall, 1996.

[25] A. C. Rencher and W. F. Christensen, *Methods of multivariate analysis*. Wiley, 2012, vol. 709.

[26] G. Schay, *Introduction to probability with statistical applications*. Birkhäuser, 2007.

[27] C. M. Grinstead and J. L. Snell, *Introduction to probability*. American Mathematical Soc., 1998.

[28] B. Wang and K. Liu, "Advances in cognitive radio networks: A survey," *Selected Topics in Signal Processing, IEEE Journal of*, vol. 5, no. 1, pp. 5–23, 2011.

[29] S. Shobana, R. Saravanan, and R. Muthaiah, "Matched filter based spectrum sensing on cognitive radio for ofdm wlans," *International Journal of Engineering and Technology*, vol. 5, 2013.

[30] G. Huang and J. K. Tugnait, "On cyclostationarity based spectrum sensing under uncertain gaussian noise," 2013.

[31] P. J. Kolodzy, "Interference temperature: a metric for dynamic spectrum utilization," *International Journal of Network Management*, vol. 16, no. 2, pp. 103–113, 2006.

[32] M. Naraghi-Pour and T. Ikuma, "Autocorrelation-based spectrum sensing for cognitive radios," *Vehicular Technology, IEEE Transactions on*, vol. 59, no. 2, pp. 718–733, 2010.

[33] T. Yucek and H. Arslan, "A survey of spectrum sensing algorithms for cognitive radio applications," *IEEE Communications Surveys & Tutorials*, vol. 11, no. 1, pp. 116–130, 2009.

[34] K. Ben Letaief and W. Zhang, "Cooperative communications for cognitive radio networks," *Proceedings of the IEEE*, vol. 97, no. 5, pp. 878–893, 2009.

[35] S. Haykin, D. J. Thomson, and J. H. Reed, "Spectrum sensing for cognitive radio," *Proceedings of the IEEE*, vol. 97, no. 5, pp. 849–877, 2009.

[36] R. R. Tenney and N. R. Sandell, "Detection with distributed sensors," *Aerospace and Electronic Systems, IEEE Transactions on*, no. 4, pp. 501–510, 1981.

[37] R. Montgomery and D. Ghosh, "Control with distributed sensing and processing," in *American Control Conference, 1991*, 1991, pp. 1429–1430.

[38] M. Basseville, I. V. Nikiforov *et al.*, *Detection of abrupt changes: theory and application*. Prentice Hall Englewood Cliffs, 1993, vol. 104.

[39] G. Ganesan and L. Ye, "Cooperative spectrum sensing in cognitive radio, part ii: Multiuser networks," *Wireless Communications, IEEE Transactions on*, vol. 6, no. 6, pp. 2214–2222, 2007.

[40] A. Ghasemi and E. S. Sousa, "Collaborative spectrum sensing for opportunistic access in fading environments," in *New Frontiers in Dynamic Spectrum Access Networks, 2005. DySPAN 2005. 2005 First IEEE International Symposium on*. IEEE, 2005, pp. 131–136.

[41] F. Digham, M. Alouini, and M. Simon, "On the energy detection of unknown signals over fading channels," in *Communications, 2003. ICC'03. IEEE International Conference on*, vol. 5. Ieee, 2003, pp. 3575–3579.

[42] A. Ghasemi and E. Sousa, "Opportunistic spectrum access in fading channels through collaborative sensing," *Journal of Communications*, vol. 2, no. 2, p. 71, 2007.

[43] A. Singh, M. R. Bhatnagar, and R. K. Mallik, "Cooperative spectrum sensing in multiple antenna based cognitive radio network using an improved energy detector," *Communications Letters, IEEE*, vol. 16, no. 1, pp. 64–67, 2012.

[44] Z. Quan, S. Cui, and A. H. Sayed, "Optimal linear cooperation for spectrum sensing in cognitive radio networks," *Selected Topics in Signal Processing, IEEE Journal of*, vol. 2, no. 1, pp. 28–40, 2008.

[45] M. Xiao and M. Skoglund, "Multiple-user cooperative communications based on linear network coding," *Communications, IEEE Transactions on*, vol. 58, no. 12, pp. 3345–3351, 2010.

[46] T. Harrold, P. Faris, and M. Beach, "Distributed spectrum detection algorithms for cognitive radio," in *Cognitive Radio and Software Defined Radios: Technologies and Techniques, 2008 IET Seminar on*. IET, 2008, pp. 1–5.

[47] E. C. Peh, Y.-C. Liang, Y. L. Guan, and Y. Zeng, "Cooperative spectrum sensing in cognitive radio networks with weighted decision fusion schemes," *Wireless Communications, IEEE Transactions on*, vol. 9, no. 12, pp. 3838–3847, 2010.

[48] K. Po and J.-i. Takada, "Signal detection for analog and digital tv signals for cognitive radio," *IEIC Technical Report (Institute of Electronics, Information and Communication Engineers)*, vol. 106, no. 395, pp. 91–95, 2006.

[49] A. Taherpour, M. Nasiri-Kenari, and S. Gazor, "Multiple antenna spectrum sensing in cognitive radios," *Wireless Communications, IEEE Transactions on*, vol. 9, no. 2, pp. 814–823, 2010.

[50] E. Axell and E. G. Larsson, "Optimal and sub-optimal spectrum sensing of ofdm signals in known and unknown noise variance," *Selected Areas in Communications, IEEE Journal on*, vol. 29, no. 2, pp. 290–304, 2011.

[51] J. Font-Segura and X. Wang, "Glrt-based spectrum sensing for cognitive radio with prior information," *Communications, IEEE Transactions on*, vol. 58, no. 7, pp. 2137–2146, 2010.

[52] H. Li, H. Dai, and C. Li, "Collaborative quickest spectrum sensing via random broadcast in cognitive radio systems," *Wireless Communications, IEEE Transactions on*, vol. 9, no. 7, pp. 2338–2348, 2010.

[53] N. Moayeri and H. Guo, "How often and how long should a cognitive radio sense the spectrum?" in *New Frontiers in Dynamic Spectrum, 2010 IEEE Symposium on*. IEEE, 2010, pp. 1–10.

[54] Q. Zou, S. Zheng, and A. H. Sayed, "Cooperative sensing via sequential detection," *Signal Processing, IEEE Transactions on*, vol. 58, no. 12, pp. 6266–6283, 2010.

[55] J. Ma, X. Zhou, and G. Li, "Probability-based periodic spectrum sensing during secondary communication," *Communications, IEEE Transactions on*, vol. 58, no. 4, pp. 1291–1301, 2010.

[56] S.-J. Kim, G. Li, and G. B. Giannakis, "Minimum-delay spectrum sensing for multi-band cognitive radios," in *Global Telecommunications Conference (GLOBECOM 2010), 2010 IEEE*. IEEE, 2010, pp. 1–5.

[57] K. W. Choi, "Adaptive sensing technique to maximize spectrum utilization in cognitive radio," *Vehicular Technology, IEEE Transactions on*, vol. 59, no. 2, pp. 992–998, 2010.

[58] M. Matsui, K. Akabane, H. Shiba, and K. Uehara, "Prototype of a cognitive radio system with cooperative sensing and interference alerting," in *Cognitive Radio Oriented Wireless Networks and Communications, 2008. CrownCom 2008. 3rd International Conference on*. IEEE, 2008, pp. 1–6.

[59] H. Li, "Cooperative spectrum sensing via belief propagation in spectrum-heterogeneous cognitive radio systems," in *Wireless Communications and Networking Conference (WCNC), 2010 IEEE*. IEEE, 2010, pp. 1–6.

[60] P. Marques, J. Bastos, and A. Gameiro, "Sensing umts bands using cyclostationary features and cooperation between opportunistic terminals," in *Cognitive Radio Oriented Wireless Networks and Communications, 2008. CrownCom 2008. 3rd International Conference on.* IEEE, 2008, pp. 1–5.

[61] V. Kuppusamy and R. Mahapatra, "Primary user detection in ofdm based mimo cognitive radio," in *Cognitive Radio Oriented Wireless Networks and Communications, 2008. CrownCom 2008. 3rd International Conference on.* IEEE, 2008, pp. 1–5.

[62] T. C. Aysal, S. Kandeepan, and R. Piesiewicz, "Cooperative spectrum sensing over imperfect channels," in *GLOBECOM Workshops, 2008 IEEE.* IEEE, 2008, pp. 1–5.

[63] B. Wild and K. Ramchandran, "Detecting primary receivers for cognitive radio applications," in *New Frontiers in Dynamic Spectrum Access Networks, 2005. DySPAN 2005. 2005 First IEEE International Symposium on.* IEEE, 2005, pp. 124–130.

[64] S. Zarrin and T. J. Lim, "Cooperative spectrum sensing in cognitive radios with incomplete likelihood functions," *Signal Processing, IEEE Transactions on*, vol. 58, no. 6, pp. 3272–3281, 2010.

[65] N. T. Khajavi and S.-S. Sadough, "Improved spectrum sensing and achieved throughputs in cognitive radio networks," in *Wireless Advanced (WiAD), 2010 6th Conference on.* IEEE, 2010, pp. 1–6.

[66] X. Zhou, J. Ma, G. Li, Y. Kwon, and A. C. Soong, "Probability-based combination for cooperative spectrum sensing," *Communications, IEEE Transactions on*, vol. 58, no. 2, pp. 463–466, 2010.

[67] S. P. Herath, N. Rajatheva, and P. Saengudomlert, "Primary and cognitive user cooperative spectrum sensing in ofdma air interface," in *Vehicular Technology Conference (VTC 2010-Spring), 2010 IEEE 71st.* IEEE, 2010, pp. 1–5.

[68] H. Urkowitz, "Energy detection of unknown deterministic signals," in *Proceedings of the IEEE*, vol. 55, no. 4, pp. 523–531, 1967.

[69] I. Gradshteyn, I. Ryzhik, A. Jeffrey, and D. Zwillinger, *Table of integrals, series, and products*. Academic press, 2007.

[70] W. Zhang, R. Mallik, and K. Letaief, "Optimization of cooperative spectrum sensing with energy detection in cognitive radio networks," *IEEE Transactions on Wireless Communications*, vol. 8, no. 12, pp. 5761–5766, 2009.

[71] Z. Quan, S. Cui, H. Poor, and A. Sayed, "Collaborative wideband sensing for cognitive radios," *Signal Processing Magazine, IEEE*, vol. 25, no. 6, pp. 60–73, 2008.

[72] N. L. Johnson, S. Kotz, and N. Balakrishnan, *Continuous Multivariate Distributions, volume 1, Models and Applications*. New York: John Wiley & Sons, 2002.

[73] P. Dharmawansa, N. Rajatheva, and K. AHMED, "On the distribution of the sum of nakagami-m random variables," *IEEE transactions on communications*, vol. 55, no. 7, pp. 1407–1416, 2007.

[74] S. P. Herath and N. Rajatheva, "Analysis of equal gain combining in energy detection for cognitive radio over nakagami channels," in *Global Telecommunications Conference, 2008. IEEE GLOBECOM 2008. IEEE*. IEEE, 2008, pp. 1–5.

[75] M. Mustonen, M. Matinmikko, and A. Mammela, "Cooperative spectrum sensing using quantized soft decision combining," in *Cognitive Radio Oriented Wireless Networks and Communications, 2009. CROWNCOM'09. 4th International Conference on*. IEEE, 2009, pp. 1–5.

[76] H. Chen, C. Tse, and F. Zhao, "Optimal quantisation bit budget for a spectrum sensing scheme in bandwidth-constrained cognitive sensor networks," *IET wireless sensor systems*, vol. 1, no. 3, pp. 144–150, 2011.

[77] S. Koivu, H. Saarnisaari, and M. Juntti, "Quantization and dynamic range effects on the energy detection," in *Proceedings of the 6th Nordic signal processing symposium, NORSIG*. Citeseer, 2004, pp. 9–11.

[78] Y. Tani and T. Saba, "Quantization scheme for energy detector of soft decision cooperative spectrum sensing in cognitive radio," in *GLOBECOM Workshops (GC Wkshps), 2010 IEEE*. IEEE, 2010, pp. 69–73.

[79] R. S. Blum, "Distributed detection for diversity reception of fading signals in noise," *Information Theory, IEEE Transactions on*, vol. 45, no. 1, pp. 158–164, 1999.

[80] S. Chaudhari, J. Lunden, V. Koivunen, and H. V. Poor, "Cooperative sensing with imperfect reporting channels: Hard decisions or soft decisions?" *Signal Processing, IEEE Transactions on*, vol. 60, no. 1, pp. 18–28, 2012.

[81] S. Chaudhari and V. Koivunen, "Effect of quantization and channel errors on collaborative spectrum sensing," in *Signals, Systems and Computers, 2009 Conference Record of the Forty-Third Asilomar Conference on*. IEEE, 2009, pp. 528–533.

[82] C. Sun, W. Zhang, and K. Letaief, "Cooperative spectrum sensing for cognitive radios under bandwidth constraints," in *Wireless Communications and Networking Conference, 2007. WCNC 2007. IEEE*. IEEE, 2007, pp. 1–5.

[83] X. Zheng, L. Cui, J. Chen, Q. Wu, and J. Wang, "Cooperative spectrum sensing in cognitive radio systems," in *Image and Signal Processing, 2008. CISP'08. Congress on*, vol. 5. IEEE, 2008, pp. 262–266.

[84] L. Ling, C. Yan, and Z. Hongbo, "A new cooperative spectrum sensing algorithm in cognitive networks," in *Wireless Communications, Networking and Mobile Computing, 2009. WiCom'09. 5th International Conference on*. IEEE, 2009, pp. 1–4.

[85] S. K. Srivastava and A. Banerjee, "n-ratiologic based cooperative spectrum sensing using double threshold energy detection," in *Cognitive Radio Oriented Wireless Networks and Communications, 2009. CROWNCOM'09. 4th International Conference on*. IEEE, 2009, pp. 1–6.

[86] L. Duan, L. Zhang, Y. Chu, and S. Liu, "Cooperative spectrum sensing with double threshold detection based on reputation in cognitive radio," in *Wireless*

Communications, Networking and Mobile Computing, 2009. WiCom'09. 5th International Conference on. IEEE, 2009, pp. 1–4.

[87] J. Zhu, Z. Xu, F. Wang, B. Huang, and B. Zhang, "Double threshold energy detection of cooperative spectrum sensing in cognitive radio," in *Cognitive Radio Oriented Wireless Networks and Communications, 2008. CrownCom 2008. 3rd International Conference on*, may 2008, pp. 1 –5.

[88] W. Han, J. Li, Z. Li, J. Yao, and D. Chen, "Double thresholds for judgment in cognitive spectrum sensing," in *Personal, Indoor and Mobile Radio Communications, 2008. PIMRC 2008. IEEE 19th International Symposium on.* IEEE, 2008, pp. 1–5.

[89] S. Xu, Y. Shang, and H. Wang, "Double thresholds based cooperative spectrum sensing against untrusted secondary users in cognitive radio networks," in *Vehicular Technology Conference, 2009. VTC Spring 2009. IEEE 69th.* IEEE, 2009, pp. 1–5.

[90] "IEEE standard for floating-point arithmetic," *IEEE Std 754-2008*, pp. 1 –58, 2008.

[91] W. Prawatmuang and D. K. C. So, "Sequential cooperative spectrum sensing technique for cognitive radio system in correlated channel," in *Proc. IEEE Vehicular Technology Conference (VTC Spring)*, 2012.

[92] ——, "Adaptive sequential cooperative spectrum sensing technique in time varying channel," in *Proc. IEEE International Symposium on Personal, Indoor and Mobile Radio Communications (PIMRC'12)*, 2012.

[93] G. Matz and F. Hlawatsch, "Time-varying communication channels: Fundamentals, recent developments, and open problems," in *Proc. European Signal Processing Conference (EUSIPCO 2006), Firenze, Italy*, 2006.

[94] C.-D. Iskander and H.-T. Multisystems, "A matlab-based object-oriented approach to multipath fading channel simulation," *MATLAB White Paper*, 2008.

[95] M. Khoshkholgh, K. Navaie, and H. Yanikomeroglu, "On the impact of the primary network activity on the achievable capacity of spectrum sharing over fading channels," *IEEE Transactions on Wireless Communications*, vol. 8, no. 4, pp. 2100–2111, 2009.

[96] K. Subrahmaniam and K. Kocherlakota, *A primer in probability.* CRC, 1990, vol. 111.

[97] O. Ibe, *Markov processes for stochastic modeling.* Academic press, 2008.

[98] D. Cabric, A. Tkachenko, and R. W. Brodersen, "Experimental study of spectrum sensing based on energy detection and network cooperation," in *Proceedings of the first international workshop on Technology and policy for accessing spectrum.* ACM, 2006, p. 12.

[99] C. Stevenson, G. Chouinard, Z. Lei, W. Hu, S. Shellhammer, and W. Caldwell, "IEEE 802.22: The first cognitive radio wireless regional area network standard," *IEEE Communications Magazine*, vol. 47, no. 1, pp. 130–138, 2009.